Radioecological Assessment after Potential Accidents with the Russian Nuclear Submarines K-27 and K-159 in the Arctic Marine Environment

⫼⫼⫼ DSA

Norwegian Radiation and
Nuclear Safety Authority

Abstract
The report has considered potential accidents related to the Russian nuclear submarines K-27 and K-159. The radiological assessment is based on a wide set of radionuclides.

Resymé
I rapporten blir det vurdert potensielle ulykker knyttet til de russiske atomubåtene K-27 og K-159. Den radiologiske evalueringer er basert på et bredt sett av radionuklider.

Head of project: Iosjpe Mikhail.
Approved:

Kristin Frogg, acting director, Department of Nuclear Safety and Environmental Radioactivity

Radioecological Assessment after Potential Accidents with the Russian Nuclear Submarines K-27 and K-159 in the Arctic Marine Environment

Content

Abbreviation list

Acronym	Full version
ARCTICMAR	Arctic and North Seas Marine Model
CF	Concentration factor
CR	Concentration ratio
FAO	Food and Agriculture Organisation of the United Nations and World Health Organisation
IAEA	International Atomic Energy Agency
IASAP	International Arctic Seas Assessment Project
KS	The Kara Sea
NAOSIM	North Atlantic/Arctic coupled Ocean Sea Ice Model
NRPA	Norwegian Radiation Protection Authority (Now DSA - Norwegian Radiation and Nuclear Safety Authority)
NS	Nuclear Submarine
SB	The Stepovogo Bay
UNSCEAR	United Nations Scientific Committee on the Effects of Atomic Radiation

1   Introduction

The Arctic is a vulnerable region with regards to potential impacts from radioactive contamination. In light of this, the Norwegian Government's Nuclear Arctic Plan, launched in 1995, is directed, among other things, towards reducing the risk of nuclear accidents and radioactive pollution. Within this program, and in connection with the EC-funded project "Feasibility Study" (Contract NSI 2014 / 354026), four reports have been prepared (Hosseini et al., 2015, 2016, 2017; Brown and Hosseini, 2019) with the main purpose to evaluate the impacts of possible releases linked to a continuation of existing practices, i.e. leaving sources in situ, or potential management operations, including recovery and transport, for Russian submarines K-27 and K-159. Brown and Hosseini, (2019) include also radioecological analysis for some other potential releases of radionuclides from dumped radiactive objects, dumped by the former Soviet Union in the Russian Arctic.

The above reports provide detailed information on evaluation of inventory, assumptions about potential release scenarios and results of radioecological assessment. The present report provides additional information, which is a supplement for previous results concerning radioecological assessment after potential releases of radioniclides into marine environment.

The need for this study is based mainly on three points, which will arguably lead to an improvement in the radioecological assessments performed in previous studies (Hosseini et al., 2015, 2016, 2017; Brown and Hosseini, 2019). This includes:

(i)   some new assumptions for the release scenarios for nuclear submarines K-27 and K-159,

(ii) including water-sediment interactions within the processes considered in modelling distribution of radionuclides in the marine environment and

(iii) including a wide set of radionuclides in radioecological assessment of the potential release scenarios in comparison with previous studies.

The present study is based on the application of ARCTICMAR model, which is described below.

2 The ARCTICMAR model (the NRPA box modelling approach)

The present model uses a modified approach for compartmental modelling (Iosjpe et al., 2002, 2009; Iosjpe, 2006), which allows the study of dispersion of radionuclides over time (non-instantaneous mixing in the oceanic space). The box structures for surface, mid-depth and deep-water layers have been developed based on the description of polar, Atlantic and deep waters in the Arctic Ocean and the Northern Seas and site-specific information for the boxes generated from the 3D hydrodynamic model NAOSIM (Karcher and Harms, 2000; Karcher et al., 2017). The model contains 345 water and sediment compartments. The surface structure of the model is presented in Figure 1.
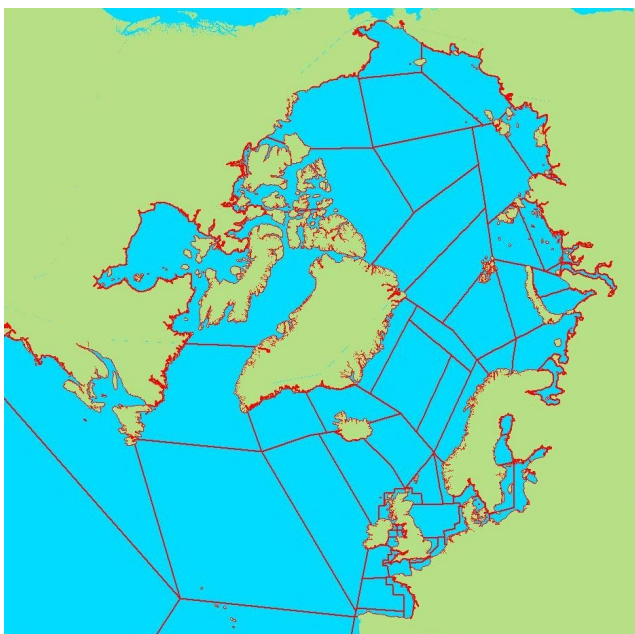
Figure 1. The structure of the surface water boxes for the NRPA box model (ARCTICMAR).

The box model includes the processes of advection of radioactivity between compartments, sedimentation, diffusion of radioactivity through pore water in sediments, particle mixing, pore water mixing and a burial process of radioactivity in deep sediment layers. Radioactive decay is calculated for all compartments. Accumulation of contamination by biota is further calculated from radionuclide concentrations in filtered seawater in different water regions. Doses to humans are calculated on the basis of given seafood consumptions, based on available data for seafood catches and assumptions about human diet in the respective areas. Dose rates to biota are derived on the basis of calculated radionuclide concentrations in marine organisms, water and sediment, using dose conversion factors. The model structure is presented in Figure 2.
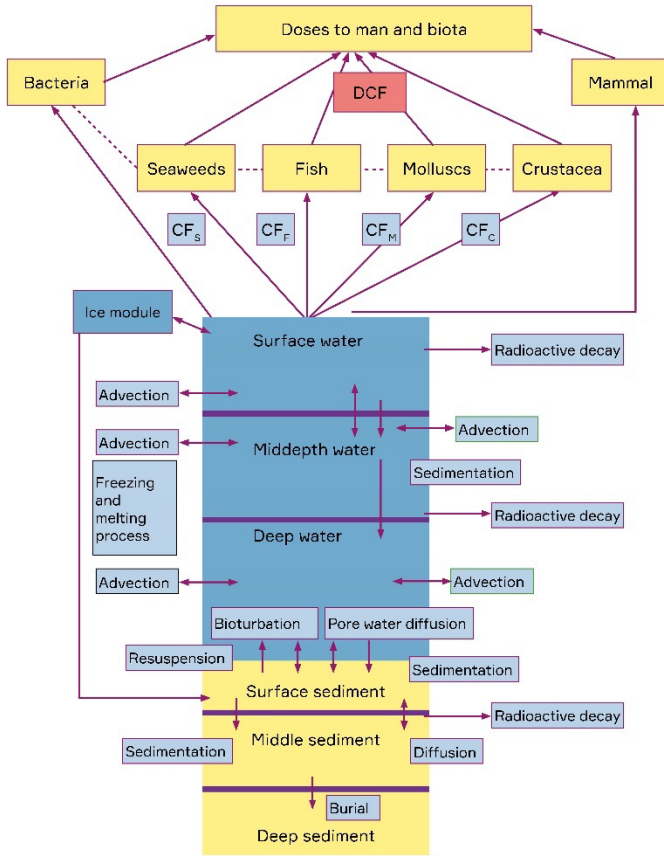
Figure 2. A schematic structure of the processes involved in modelling.

2.1 Main equations for the dispersion of radionuclides in the oceanic space

The equations of the transfer of radionuclides between the boxes are of the form:

$$\frac{dA_i}{dt} = \sum_{j=1}^{n} k_{ji} A_j \gamma[t \geq (T_j + w_{ji})] - \sum_{j=1}^{n} k_{ij} A_i \gamma[t \geq (T_i + w_{ij})] - k_i A_i \gamma(t \geq T_i) + Q_i, t \geq T_i$$

(1)

$$A_i = 0, t < T_i$$

where $k_{ii}=0$ for all *i*, A_i and A_j are activities (Bq) at time *t* in boxes i and *j*; k_{ij} and k_{ji} are rates of transfer (y⁻¹) between boxes *i* and *j*; k_i is an effective rate of transfer of activity (y⁻¹) from box *i* taking into account loss of material from the compartment without transfer to another, for example radioactive decay; Q_i is a source of input into box *i* (Bq y⁻¹); n is the number of boxes in the system, T_i is the time of availability for box *i* (the first times when box *i* is open for dispersion of radionuclides) and γ is an unit function:

$$\gamma(t \geq T_i) = \begin{cases} 1, t \geq T_i \\ 0, t < T_i \end{cases}.$$

The times of availability T_i

$$T_i = \min_{\mu_m(v_0,v_i)\in M_i} \sum_{j,k} w_{jk} \qquad (2)$$

are calculated as a minimized sum of the weights for all paths $\mu_m(v_0,...,v_i)$ from the initial box (v_0) with discharge of radionuclides to the box i on the oriented graph $G=(V, E)$ with a set V of nodes v_j correspondent to boxes and a set E of arcs e_{jk} correspondent to the transfer possibility between the boxes j and k (graph elements as well as available paths are illustrated by Figure 3). Every arc e_{jk} has a weight w_{jk} which is defined as the time required before the transfer of radionuclides from box j to box k can begin (without any way through other boxes). Weight, w_{jk}, is considered as a discrete function F of the water fluxes f_{jk}, f_{kj} between boxes j and k, geographical information g_{jk} and expert evaluation X_{jk}. M_i is a set of feasible paths from the initial box (v_0) to the box i (v_i).

The traditional box modelling is a particular case of the present approach when all times of availability in (1) are zero: $\{T_i\} = 0, i = 1,...,n.$

$$M_i = \begin{cases} \mu_1(v_0,v_j,v_i) \\ \mu_2(v_0,v_k,v_i) \\ \mu_3(v_0,v_j,v_k,v_i) \\ \mu_4(v_0,v_k,v_j,v_i) \end{cases}$$

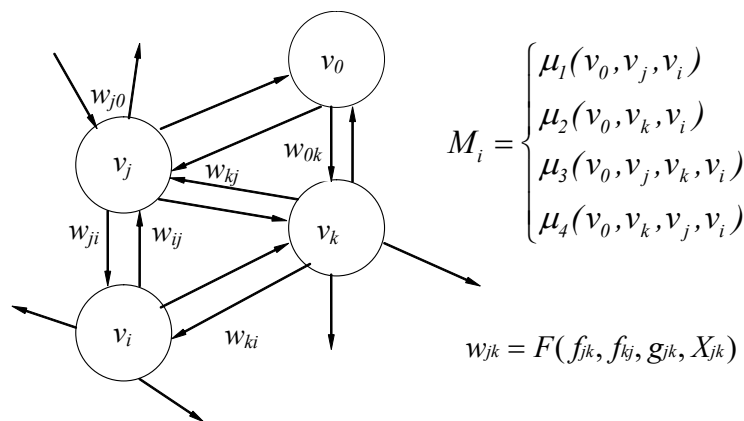$$w_{jk} = F(f_{jk}, f_{kj}, g_{jk}, X_{jk})$$

Figure 3. Graph elements.

Expressions for the transfer rates of radioactivity between the bottom water and sediment compartments will be useful in the present analysis (the transfer rates are shown in Figure 4):

$$k_{WS} = \frac{SR \cdot k_d}{d \cdot (1 + k_d \cdot SSL)} + \frac{D}{d \cdot h_S (1 + k_d \cdot SSL)} + \frac{R_T \cdot \omega \cdot h_S}{d \cdot (1 + k_d \cdot SSL)} +$$

$$+ \frac{R_W \cdot \rho \cdot k_d \cdot (1 - \omega)}{d \cdot (1 + k_d \cdot SSL)}$$

$$k_{SW} = \frac{D}{h_S^2 \cdot [\omega + k_d \cdot \rho \cdot (1 - \omega)]} + \frac{R_T \cdot \omega}{\omega + k_d \cdot \rho \cdot (1 - \omega)} + \frac{R_W \cdot \rho \cdot k_d \cdot (1 - \omega)}{h_S \cdot [\omega + k_d \cdot \rho \cdot (1 - \omega)]}$$

$$(4)$$

$$k_{SM} = \frac{D \cdot \omega}{h_S^2 \cdot [\omega + k_d \cdot \rho \cdot (1 - \omega)]} + \frac{k_d \cdot SR}{h_S \cdot [\omega + k_d \cdot \rho \cdot (1 - \omega)]}$$

$$k_{MS} = \frac{D \cdot \omega}{h_S \cdot h_{SM} \cdot [\omega + k_d \cdot \rho \cdot (1 - \omega)]}$$

$$k_{MD} = \frac{k_d \cdot SR}{h_{SM} \cdot [\omega + k_d \cdot \rho \cdot (1 - \omega)]} .$$

Here k_{WS} is composed of expressions describing the transfer of activity by sedimentation, molecular diffusion, pore water mixing and particle mixing, respectively. Similarly, k_{SW} is composed of expressions describing the transfer of radioactivity by molecular diffusion, pore water mixing and particle mixing. k_{SM} is composed of expressions describing the transfer of radioactivity by sedimentation and molecular diffusion. k_{MS} corresponds to the transfer by molecular diffusion. Finally, k_{MD} corresponds to the transfer of radioactivity by sedimentation. R_W (m y^{-1}) is the sediment reworking rate; R_T (y^{-1}) is the pore-water turnover rate; k_d (m^3 t^{-1}) is the sediment distribution coefficient; SSL (t m^{-3}) is the suspended sediment load in the water column; SR (t m^{-2} y^{-1}) is the sedimentation rate; D (m^2 y^{-1}) is the molecular diffusion coefficient, h_S (m) and h_{SM} (m) are the surface and middle sediment thickness respectively; ω is the porosity of the bottom sediment; ρ (t m^{-3}) is the density of the sediment material and d is the depth of the water column.
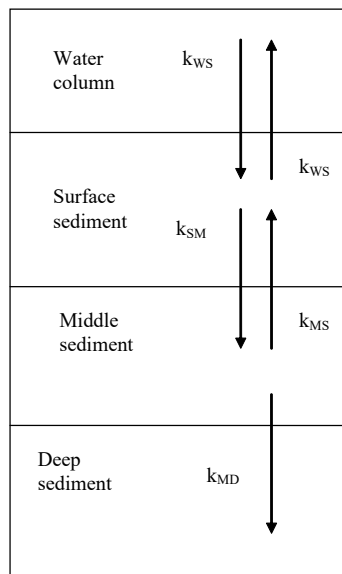

Figure 4. Generic vertical structure of the water-sediment compartments.

The ARCTICMAR model has previously been employed successfully in a number of applications. Results of simulations have been compaered with experimental data, where data have been available (Iosjpe et al., 2009; Iosjpe, 2011; Iosjpe and Liland, 2012; Periánez et al., 2016).

Concentrations of the radionuclides in marine organisms can be calculated from radionuclide concentrations in filtered seawater and the concentrations factors as shown in Figure 2. More detailed information concerninig the bioaccumulation processes in biota makes it possible to use a kinetic modelling. Figure 5 shows the schematic of the biokinetic models, which was selected as a basis for the present study (Hosseini et al., 2016, 2017; IAEA 1998; Iosjpe et al., 2016). The model has been chosen after an analysis of existing models (Thomann, 1981; Heling et al., 2002; Brown et al., 2004; Vives i Batlle et al., 2008; Maderich et al., 2013). The following reference organisms are selected for the radioecological analyse in the present report: fish, crustaceans, molluscs, sea mammals and sea-birds.
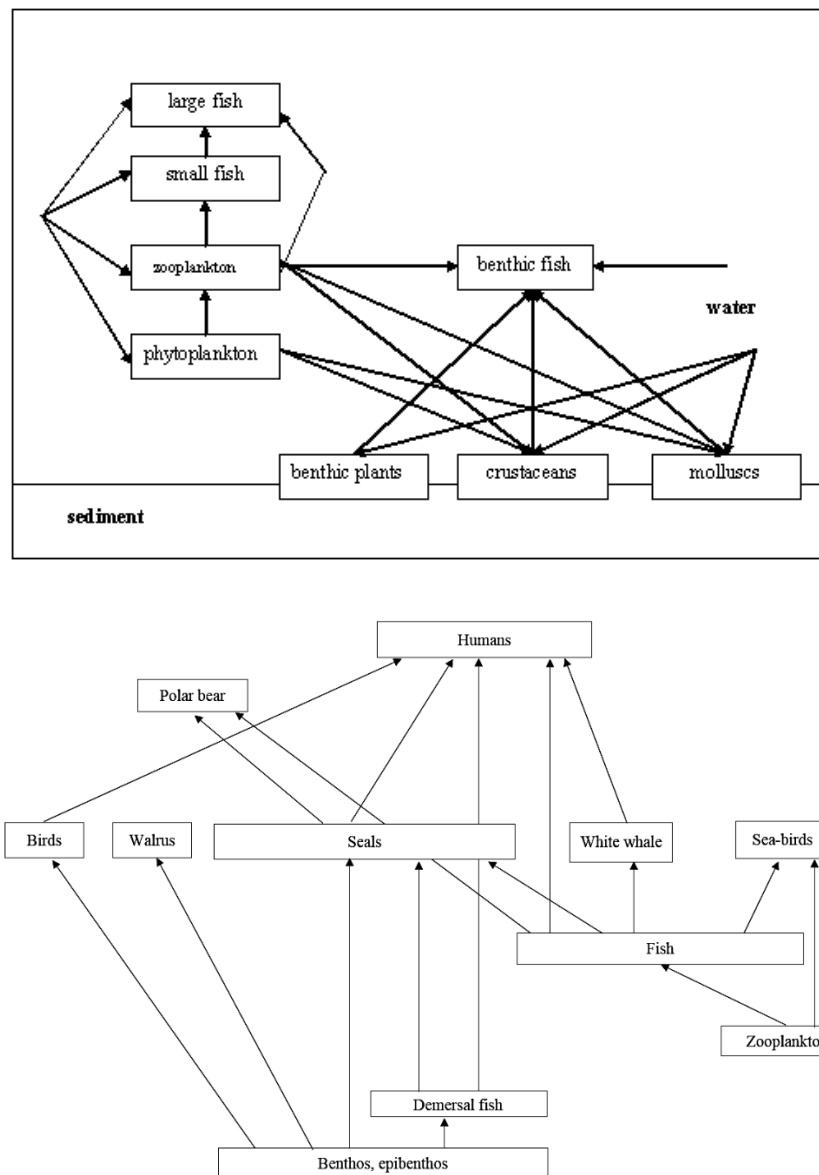

Figure 5. Schematic of the biokinetic models.

The system of equations for the biokinetic model can be described by the following expressions:

(5)

$$\frac{dC_i^{(tl)}}{dt} = AE_i \cdot IR_i \cdot C_{i-1}^{(tl)} + k_{u,i} \cdot C_w - C_i^{(tl)} \cdot k_{e,i}$$

Here $C^{(tl)}_i$ and $C^{(tl)}_{i-1}$ – concentrations of radionuclide in trophic levels "*i*" and "*i-1*"; C_W – concentration of radionuclide in water column; AE_i – the assimilation efficiency for trophic level "*i*", IR_i – ingestion per unit mass for trophic level "*i*"; $k_{u,i}$ – rate of the direct uptake of activity from water column for trophic level "i"; $k_{e,i}$ – the excretion rate for trophic level "i". Where the consumption for species in trophic levels "*i*" includes "*m*" different species in trophic levels "*i-1*", parameter $C^{(tl)}_{i-1}$ can be described as

$$C^{(tl)}_{i-1} = \sum_{j=1}^{m} w_j \cdot C^{(tl)}_{i-1,j}$$

Here the consumption for species in trophic level "*i*" includes *m* species in trophic levels

"*i-1*" with concentration of radionuclide in species j (j=1,...,m) of $C^{(tl)}_{i-1,j}$; w_j is a fraction of species *j* of all m species, where

$$\sum_{j=1}^{m} w_j = 1$$

It is important to note that knowledge about biokinetic coefficients based on habitat, ingestion of food, diet and excretion of activity for studied species are crucial information for biokinetic modelling.

2.2 Dose assessment for humans

The internal dose *D* can be determined using the following expression:

$$D = \sum_{j=1}^{m} DCF_j \sum_{l=1}^{k} \phi_l \cdot CF_{lj} \sum_{i=1}^{n} A_{il} \int_0^T C_{ij}(t)dt \tag{6}$$

where [0, T] is the time interval for dose assessment; DCF_j is the dose conversion factor for radionuclide *j* (j = 1,2,..., m); CF_{lj} is the concentration factor for radionuclide *j* in seafood of type *l* (*l* = 1,2,..., k); A_{il} is consumption of seafood of type *l* in the model compartment *i*; (*i* = 1,2,...,n) for the critical group for the doses to critical group and catch of seafood for collective doses, if necessary; C_{ij} is the concentration of radionuclide *j* in filtered seawater in model compartment *i*; and φ_l is equal 1 for the doses to the critical group and φ_l is the edible fraction for seafood of type i (50% for fish, 35% for crustaceans and 15% for molluscs (CEC, 1990; EC, 2000; IASAP, 2003) for the collective doses, if necessary.

The individual dose rate for the external exposure can be estimated with the following expresson (Iosjpe et al., 2009). Methodology is similar to EC (1994):

$$DR_{ext} = F_W^{(O)} \cdot \sum_i DCF_i^{(ext,w)} \overline{C}_i^{(bulk,w)} + F_S^{(O)} \cdot f_S \sum_i DCF_i^{(ext,s)} \cdot \overline{C}_i^{(bulk,s)} \tag{7}$$

where $\overline{C}_i^{(bulk,w)}$ is the average bulk concentration of radionuclide *i* in the water column with regards to both water and sediment phases; $\overline{C}_i^{(bulk,s)}$ is the average bulk concentration of the sediment phase in the actual sea area; $DCF_i^{(ext,w)}$ and $DCF_i^{(ext,s)}$ are the dose conversion factors for external exposure of radionuclide *i*, for water immersion and contaminated ground surface,

respectively; $F_W^{(O)}$ and $F_S^{(O)}$ are the occupancy factors for "swimming" and the "beach sediment" pathways (in the following calculations it is assumed that both factors are of 0.5); f_S is a part of the sediment concentration, which is considered as beach concentration (following (IASAP, 2003), it is assumed that f_S is 0.1).

In the present study, the doses to man are calculated only for ingestion because the comparison of the contribution to human doses from this pathway against external exposure indicates a clear domination of the former (EC, 1994; IASAP, 2003, Iosjpe et al., 2009).

2.3 Dose assessment for biota

The ARCTICMAR model uses the following expressions for internal and external dose rates for biota (Brown and Hosseini, 2019; Hosseini et al., 2016, 2017, Iosjpe et al., 2009).

The basic underlying equations (Equations 8 and 9) utilise activity concentration data in order to derive internal (D_{int}) and external (D_{ext}) absorbed dose-rates (in units of µGy h^{-1}). The total absorbed dose-rate is the sum of these components, through the application of dose conversion coefficients (DCCs).

$$\dot{D}_{int}^b = \sum_i C_i^b * DCC_{int,i}^b \qquad (8)$$

where:

C_i^b is the average concentration of radionuclide i in the reference organism b (Bq kg^{-1} fresh weight),

$DCC_{int,i}^b$ is the radionuclide-specific dose conversion coefficient (DCC) for internal exposure defined as the ratio between the average activity concentration of radionuclide i in the organism j and the dose rate to the organism b (µGy h^{-1} per Bq kg^{-1} fresh weight).

$$\dot{D}_{ext}^b = \sum_z v_z \sum_i C_{zi}^{ref} * DCC_{ext,zi}^b \qquad (9)$$

where v_z is the occupancy factor, i.e. fraction of the time that the organism b spends at a specified position z in its habitat, C_{zi}^{ref} is the average concentration of radionuclide i in the reference media of a given location z (Bq kg^{-1} fresh weight (water) or dry weight (sediment) or Bq l^{-1} (water)), $DCC^j_{ext,zi}$ is the dose conversion coefficient for external exposure defined as the ratio between the average activity concentration of radionuclide i in the reference media corresponding to the location z and the dose rate to organism b (µGy h^{-1} per Bq kg^{-1} fresh weight or Bq l^{-1}).

Weighted total dose rates (in µGy h^{-1}) are derived through the application of weighting factors (dimensionless) for alpha, low beta and high beta-gamma radiation.

$$DCC_{int} = wf_{low\beta} \cdot DCC_{int,low\beta} + wf_{\beta+\gamma} \cdot DCC_{int,\beta+\gamma} + wf_\alpha \cdot DCC_{int,\alpha}$$

$$(10)$$

$$DCC_{ext} = wf_{low\beta} \cdot DCC_{ext,low\beta} + wf_{\beta+\gamma} \cdot DCC_{ext,\beta+\gamma}$$

Here wf are weighting factors for various components of radiation (low β, β + γ and α), DCC are dose conversion coefficients in μGy h^{-1} per Bq l^{-1} or Bq kg^{-1}. Default radiation weighting factors of 10 for alpha radiation, 1 for low energy beta and 1 for (high energy) beta and gamma radiation are applied in this assessment in line with those applied in UNSCEAR (2008).

3 Radioecological assessment after potential accidents with the nuclear submarine K-27

3.1 Locations of the potential accidents with the NS K-27

In conjunction with previous reports (Hosseini et al., 2015, 2016, 2017; Brown and Hosseini, 2019), the locations of the potential accidents with NS K-27 are chosen as the Stepovogo Bay, within the southern area of the Kara Sea, and in Gremikha Bay, within the southern part of the Barents Sea. Both locations are shown in Figure 6.
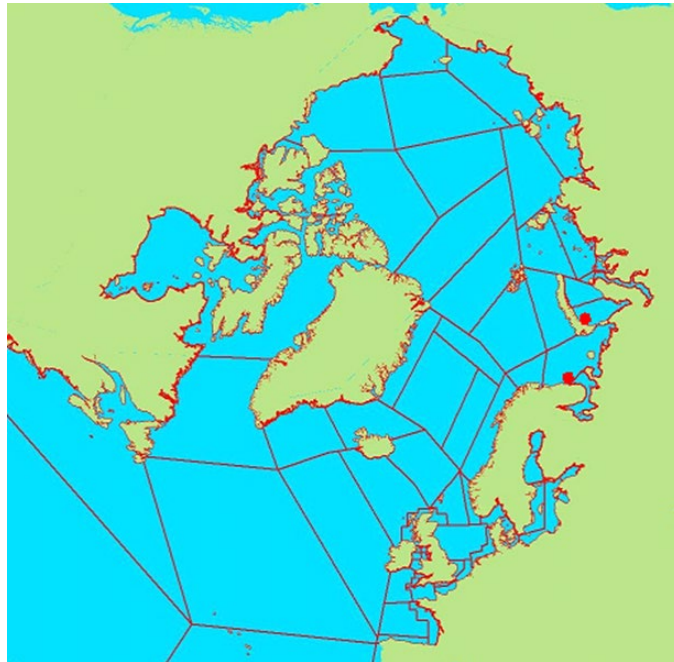

Figure 6. Locations (denoted by red circles) of potential accidents with the nuclear submarine K-27.

3.2 Inventory and release scenarios for NS K-27.

Estimation of radionuclide inventories, as well as assumptions about potential scenarios have been under permanent development during the Feasibility project (Hosseini et al., 2015, 2016, 2017; Brown and Hosseini, 2019).

The present study is based on the radionuclide inventories and assumptions about radionuclide releases presented by Hosseini et al. (2015) with refinements from Brown and Hosseini (2019).

Because some radionuclides, with their provenance in a criticality event, have a very short physical half-life or very low inventory, they can be safely discounted. The following radionuclides have therefore been selected for consideration in the present study, including their potential bioaccumulation: Am-241, Am-242m, Co-60, Cs-137, Eu-152, Eu-155, Fe-55, I-129, Nb-93m, Ni-59, Ni-63, Np-237, Pm-147, Pu-238, Pu-239, Pu-240, Pu-241, Se-79, Sm-151, Sn-121m, Sn-126, Sr-90, U-234, U-236, Zr-93.

For the worst-case scenario, a release pattern, divided into two fractions, was assumed: (i) an instantaneous release of radionuclides and (ii) a slow long-term release similar to models applied in simulating the dissolution of the uranium oxide matrix. This is in line with similar scenarios

described, for example, for sunken vessels with spent fuel on board (Reistad, 2008; Iosjpe et al., 2009; Iosjpe and Liland, 2012).

It should be noted that the release of fuel corrosion products depends on many factors (fuel matrix construction, seawater temperature, type and extent of damage of the submarine core during the accident etc.). Therefore, the annual corrosion rate can differ widely (for example, 0.001% and 1% according to Yefimov (1994) and White Book-2000 (2005), respectively. A corrosion rate of 1% has been chosen here in accordance with (Brown & Hosseini 2019), based on an assumption about a maximal continual leakage of 0.8 TBq per year for Cs-137. This is because a leakage of 0.8 TBq is in good agreement with an assumption for the corrosion rate of approximately 1% from a Cs-137 inventory of $8\cdot10^{12}$ Bq (Hosseini et al.,2015). Additionally, the instantaneous maximal release of 6 TBq for Cs-137 is considered for comparison with previous studies.

Instant and continious releases, which are used in the present report are shown in Figures 7 and 8.
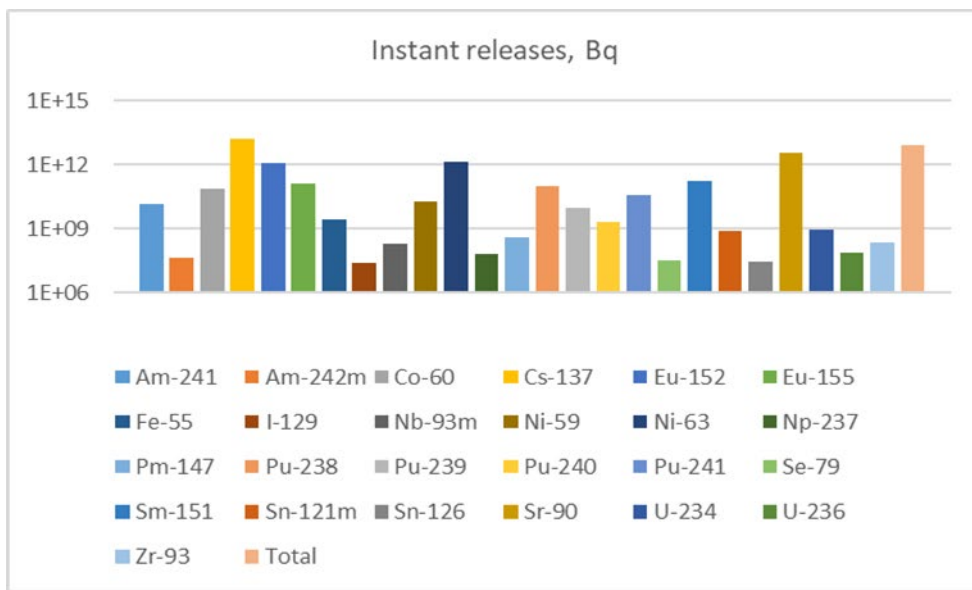

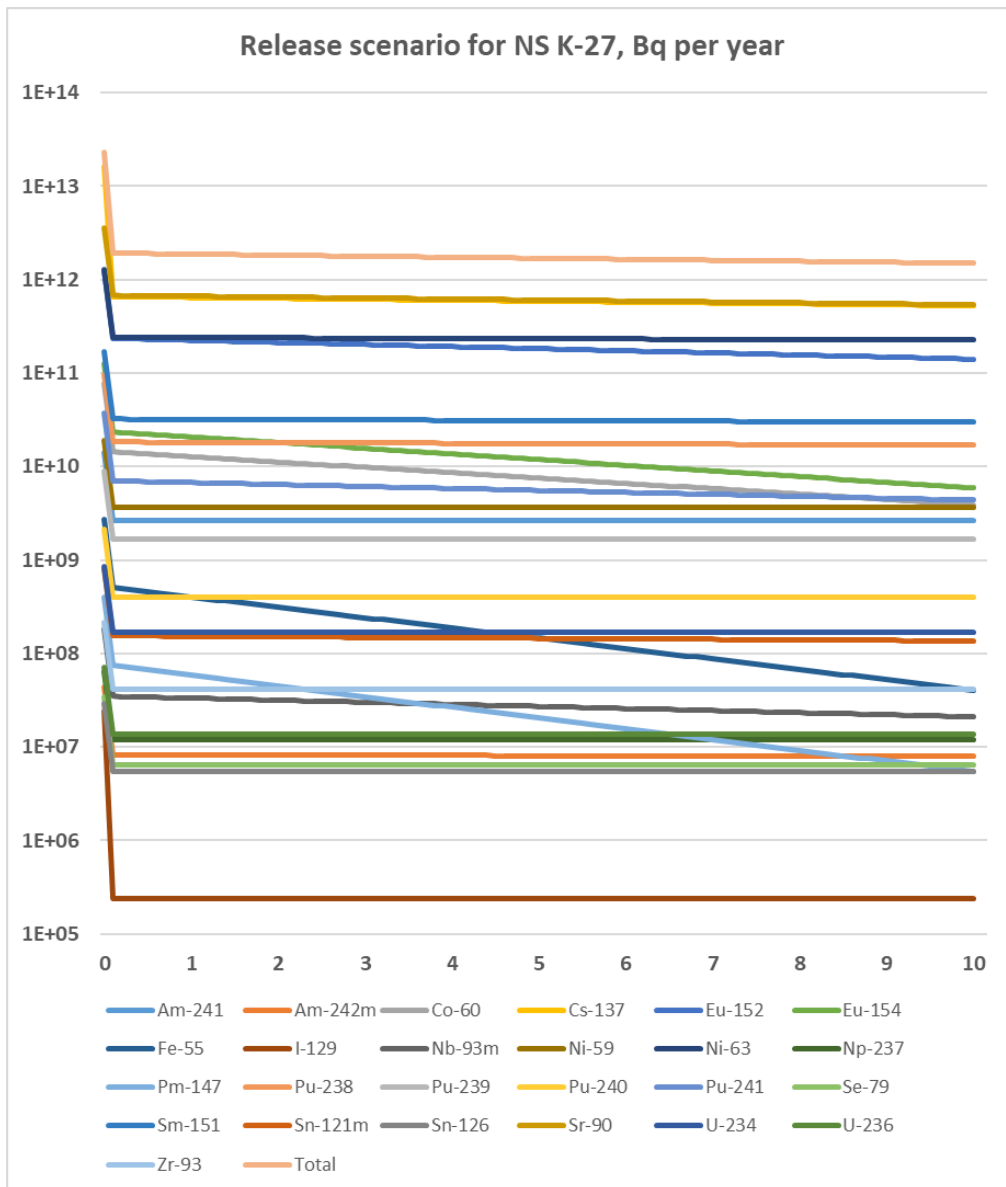Figure 7. Instantaneous releases of radionuclides after potential accident with NS K-27.

Figure 8. Instantaneous plus contionious releases of radionuclides from NS K-27 after the potential accident. Simulations are presented within time interval [0, 10] years.

3.3   Consequences after potential accidents with the nuclear submarine K-27

3.3.1   Consequences for the Stepovogo Bay region

3.3.1.1   Concentrations of radionuclides in water column

Results of calculations presented in Figure 9 demonstrate the five most significant radionuclides for contamination of the water column in the Stepovogo Bay. Total concentration is dominated by Cs-137 and Sr-90. The concentration in the water column decreases after dilution in the Kara Sea, which is shown in Figure 10.
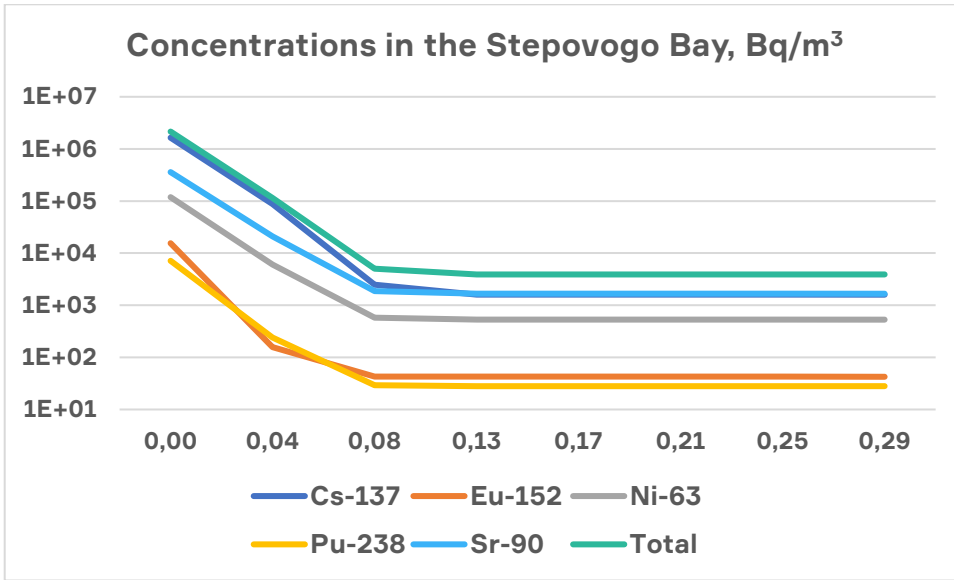
Figure 9. Dynamic of concentration in filtered water of radionuclides in the Stepovogo Bay during the first three months. Release had started at a time of zero. Simulations are presented within the time interval [0, 0.29] year.
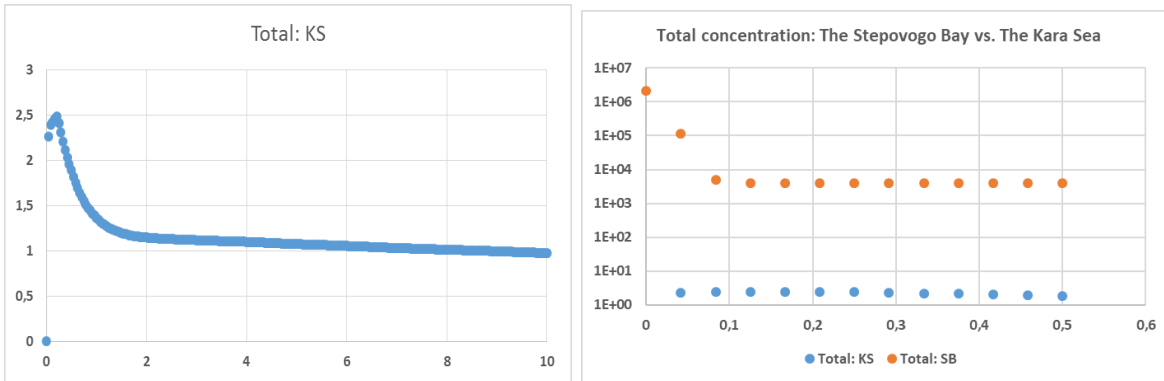

Figure 10. The total concentration in the Southwestern part of Kara Sea (KS) and comparison of the total concentrations in the Stepovogo Bay (SB) with the west-south part of the KS. Concentrations are presented in Bq/m³, Simulations are presented within time intervals [0, 10] years for the KS and [0, 0.6] year for the SB.

3.3.1.2 Concentrations of radionuclides in sediment

Results of calculations presented in Figure 11 demonstrate the five most significant radionuclides for contamination of the sediment in the Stepovogo Bay. Total concentration is dominated by Eu-152, mainly because of a combination of relatively high release of Eu-152 and high value for the sediment distribution coefficient for this radionuclide.
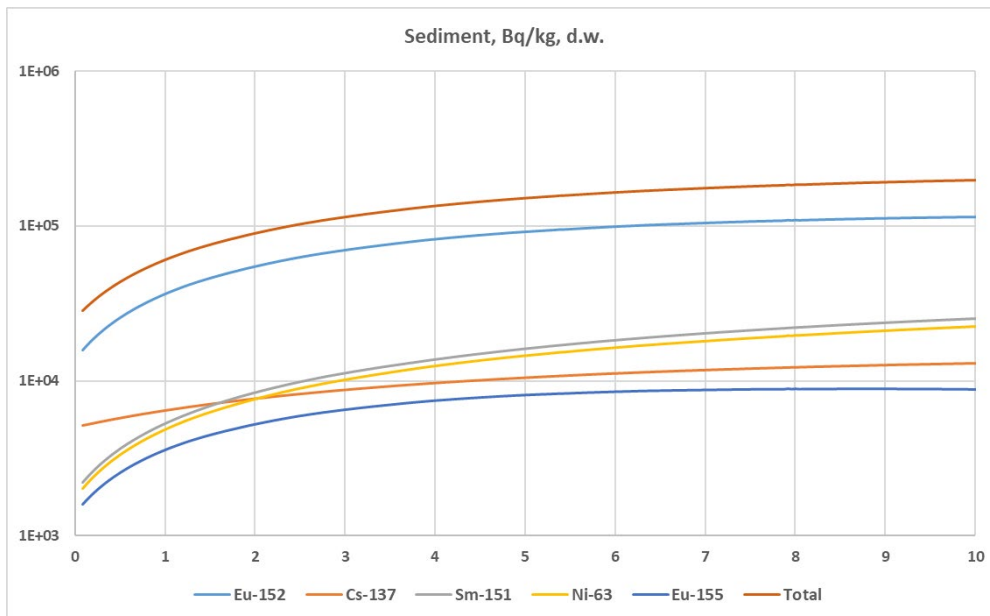
Figure 11. Dynamic of concentration of radionuclides in sediment of the Stepovogo Bay. Simulations are presented within time interval [0, 10] years.

3.3.1.3.   About methodology for calculating the concentration of radionuclides in seafood and selected marine organisms.

Results of simulations show that the use of kinetic modelling of the bioaccumulation process can be very important for consequences after an accidental release of radionuclides. The biokinetic sub-model has been tested by applying it to the consequences after the Chernobyl accident in the Gulf of Finland (Iosjpe et al., 2016). Comparison with experimental data (HELCOM, 1995; EC, 2000) demonstrates that the kinetic modelling of the bioaccumulation processes provides a more correct description of the concentration of radionuclides in biota. It is important to stress that coefficients for the kinetic sub-model for the bioaccumulation process for this study have been taken from (Thomann, 1981). Therefore, the testing of the kinetic approach with data after the Chernobyl accident (1986) has to be considered as a validation of the kinetic sub-model.

Figures 12 and 13 shows comparison of consequences for the present study for Cs-137 for the bioaccumulation process through (i) the concentration in filtered water and the concentration factor for Cs-137 and (ii) kinetic submodel for bioaccumulation process. Figure 12 shows comparison for these two approaches for the concentration in fish for the Stepovogo Bay. Figure 13 shows that significant differences in Figure 12 lead to the significant differences for annual doses to the humans during at least ten years. Therefore, considering the more realistic determinations provided, it is important to use the kinetic submodel for the description of the bioaccumulation of radionuclides in biota. Nonetheless, it is necessary to stress that knowledge about biokinetic coefficients based on the habitat, ingestion of food, diet and excretion of activity, which is crucial information for biokinetic modelling, is not well known for many radionuclides.

The approach where (i) kinetic sub-models for definition of the bioaccumulation process will be used for the radionuclides with known kinetic parameters and (ii) the concentration factor/ratio will be used for estimation of the concentration in biota for the remaining radionuclides provides one solution to the objective of providing a comprehensive abalysis.

However, such an approach can distort reality significantly, as it is shown in Figure 14.

According to recomendations from the "Food and Agriculture Organisation of the United Nations and World Health Organisation (FAO)" (CAC, 2006), radionuclides can be separated into groups, dependent mainly on their potential to be hazardous to humans, and their concentration. Concentrations in fish for radionuclides in Group 3 are shown in Figure 14, where Cs-137 has been derived using the kinetic approach, and other radionuclides using the concentration factor approach. Given its relatively elevated levels in seawater, Cs-137 should strongly dominate the concentration, but during the initial period of the bioaccumulation process, the impact of Cs-137 is negligibale in comparison with other radionuclides. This discrepancy corresponds to the fact during the period when releases of radionuclides start, the concentration in biota is zero (as for Cs-137 in Figure 14), but according to the present release scenarios the concentration ratio approach provides maximal concentration in biota. Therefore, in the present study, the following two phases for determination of the bioaccumulation process will be used: (i) definition of most significant radionuclides for a bioaccumulation process through concentration factor/ratio approach and (ii) definition of parameters for kinetic sub-models for radionuclides selected in phase (i).
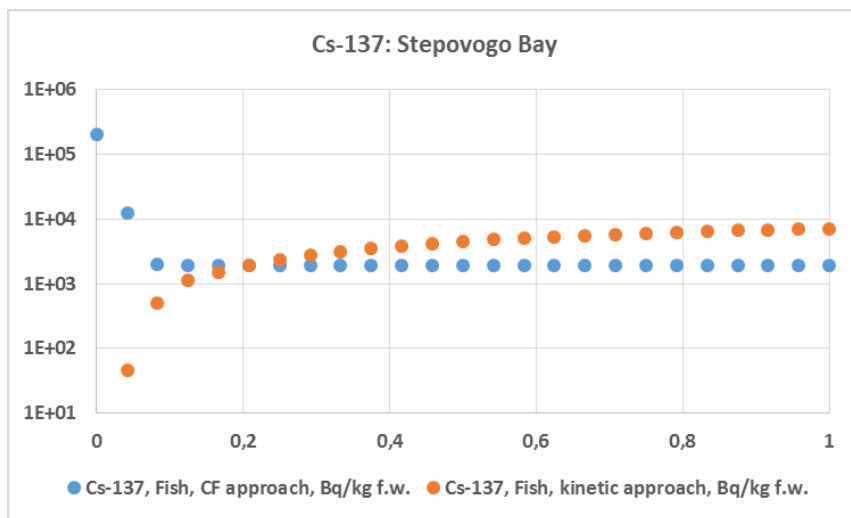

Figure 12. Dynamic of concentration of radionuclides in the Stepovogo Bay during the first year. Release had started in time of zero. Simulations are presented within time interval [0, 1] year.
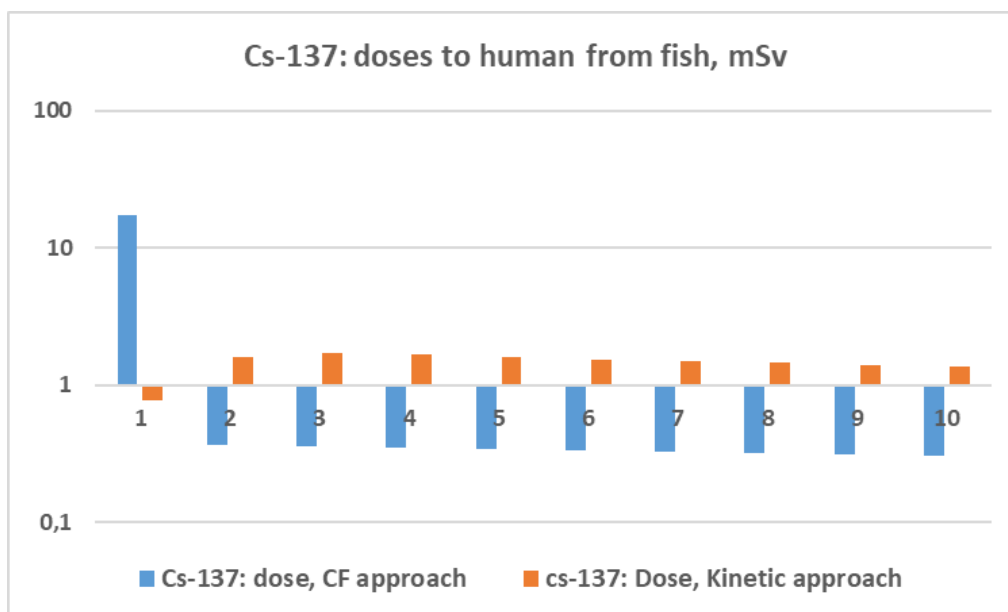

Figure 13. Dynamic of doses for the critical group through ingestion of the sea food in the Stepovogo Bay during ten years (in mSv). Release had started at time=zero. Simulations are presented within time interval [0, 10] years.
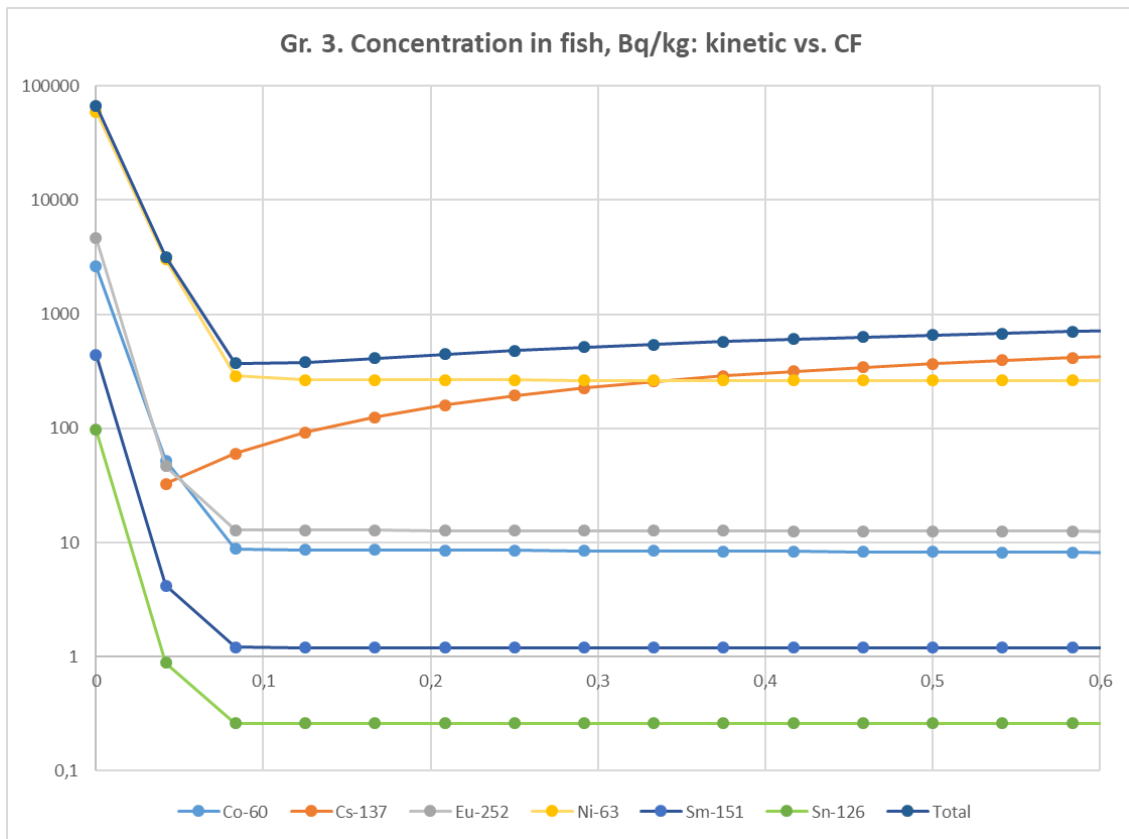
Figure 14. Concentration of radionuclides in fish for the group 3, where the kinetic approach is used for the bioaccumulation process for Cs-137 concentration ratios for other radionuclides. Simulations are presented within time interval [0, 0.6] year.

3.3.1.4. Definition of most significant radionuclides for a bioaccumulation process through concentration factor/ratio approach.

Examples of some typical radionuclides for each group according to FAO/WHO (CAC, 2006) are presented in Table 1.

Table 1. Examples of FAO/WHO international guideline levels for radionuclides in food.

Example radionuclides		Levels (Bq/kg)	
		Infant foods	Other foods
Group 1	^{238}Pu, ^{239}Pu, ^{241}Am	1	10
Group 2	^{90}Sr, ^{106}Ru, ^{129}I	100	100
Group 3	^{60}Co, ^{134}Cs, ^{137}Cs	1000	1000
Group 4	^{3}H, ^{14}C, ^{99}Tc	1000	10 000

It is important to note that the concentration factors used for calculating dose rates to biota (Hosseini et al., 2008) can differ significantly from IAEA recommendations (IAEA, 2004). This is largely because concentration factors given in ERICA database (Hosseini et al., 2008) are calculated for the whole organism, whereas IAEA concentration factors are often defined only for edible parts of the organism i.e., which has a potential consequence for dose assessments to man. Examples of differences between concentration factors from the IAEA recommendations

and the ERICA database for some radionuclides are shown in Table 2. In the present report, dose rates to man will be calculated on the basis of concentration factors from the IAEA recommendations. For the calculations of dose rates to biota a conservative approach was chosen using concentration factors from the ERICA database, when these concentration factors were higher than the corresponding concentration factors from IAEA recommendations.

Table 2. Comparison of concentration factors for selected radionuclides.

Organism	Element	IAEA, 2004	Hosseini et al., 2008
Fish	Co	$7 \cdot 10^2$	$5.6 \cdot 10^3$
Fish	Pu	100	$3.5 \cdot 10^3$
Fish	Sr	$3 \cdot 10^0$	$2.3 \cdot 10^{1*}$
Crustaceans	Am	$4 \cdot 10^2$	$1.3 \cdot 10^3$
Crustaceans	Sr	$5 \cdot 10^0$	$1.3 \cdot 10^1$
Crustaceans	Tc	$1 \cdot 10^3$	$1.7 \cdot 10^4$
Molluscs	Ru	$5 \cdot 10^2$	$1.6 \cdot 10^3$

* Whole body

Some examples for the concentration of radionuclides for all four groups are shown in Figures 15-18 for selected biota. Simulations have been performed for ten years after the potential accident.
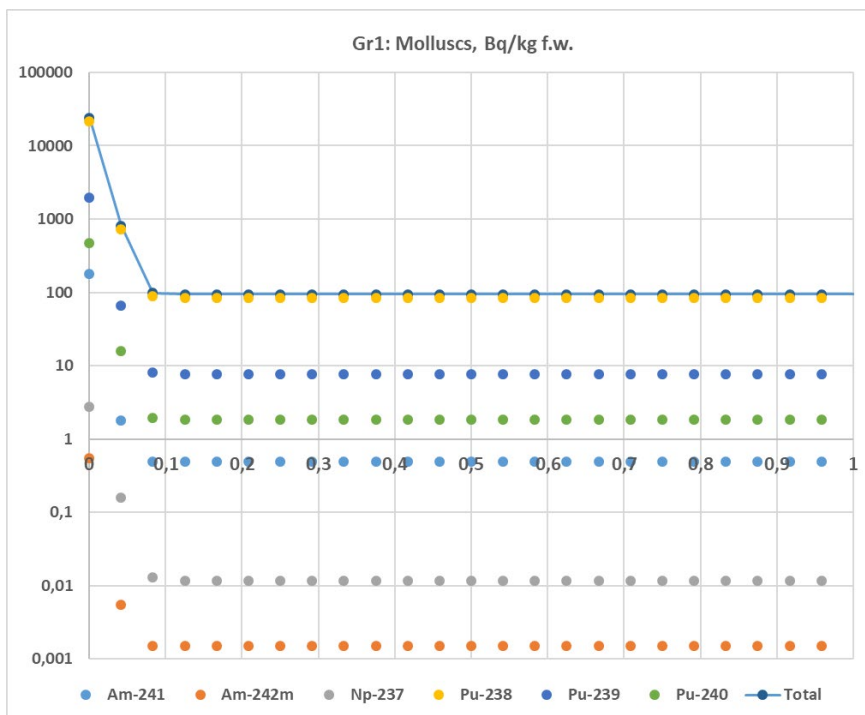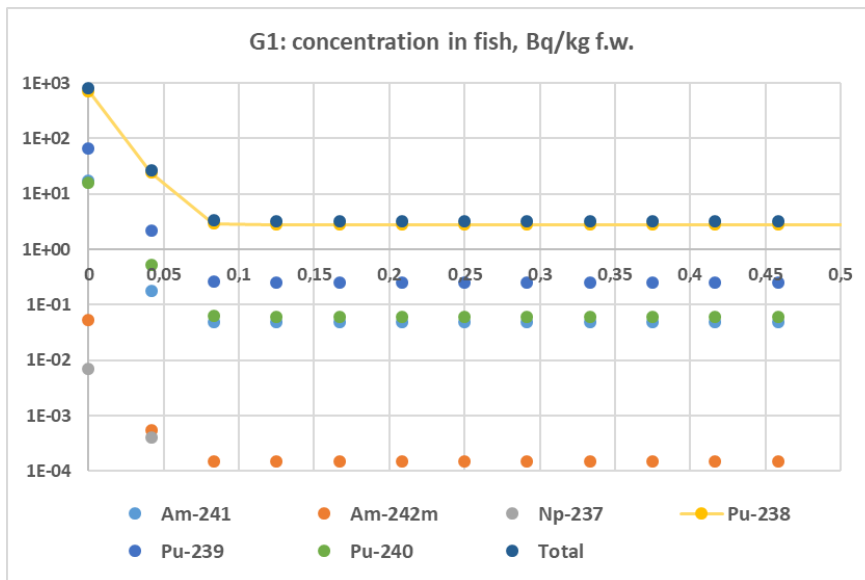
Figure 15. Concentration of radionuclides in fish (top) and molluscs (bottom) from radionuclides from the group 1. Simulations are presented within time intervals [0, 0.5] year (top) and [0, 1] year (bottom).
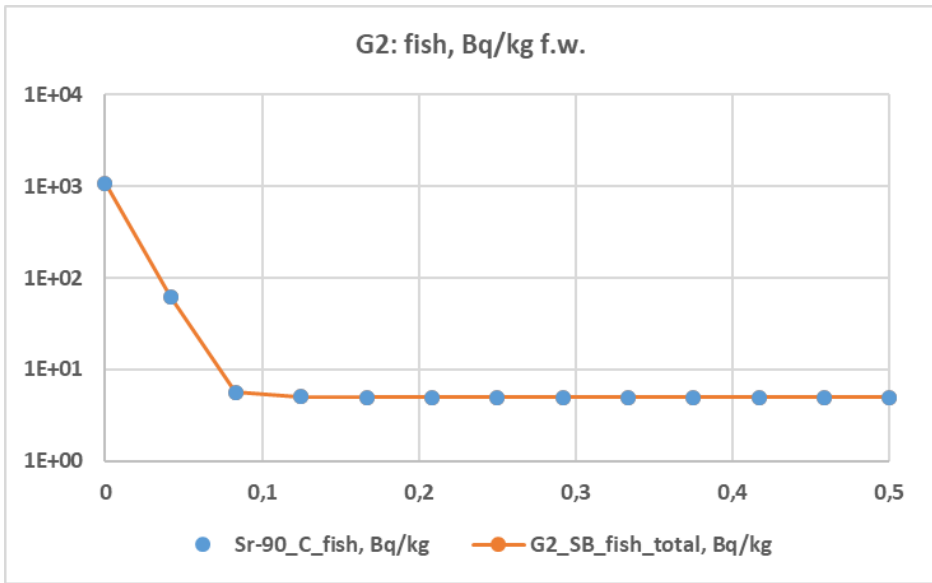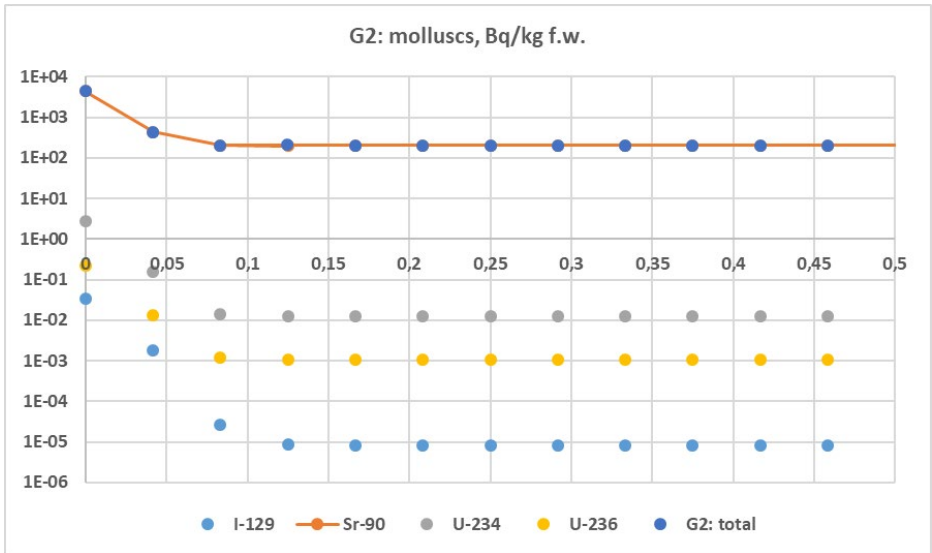
Figure 16. Concentration of radionuclides in molluscs (top) and fish (bottom) (group 2). Simulations are presented within time interval [0, 0.5] year.
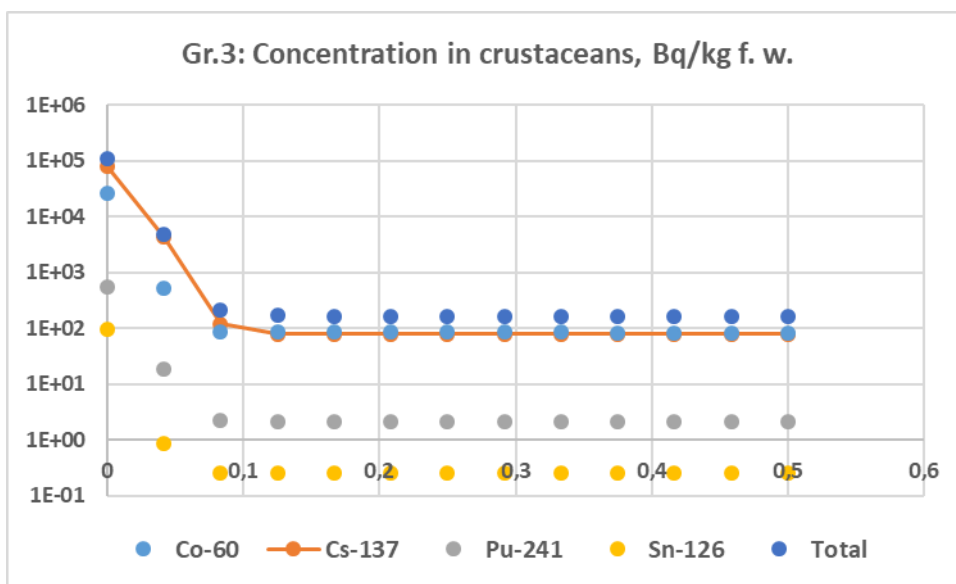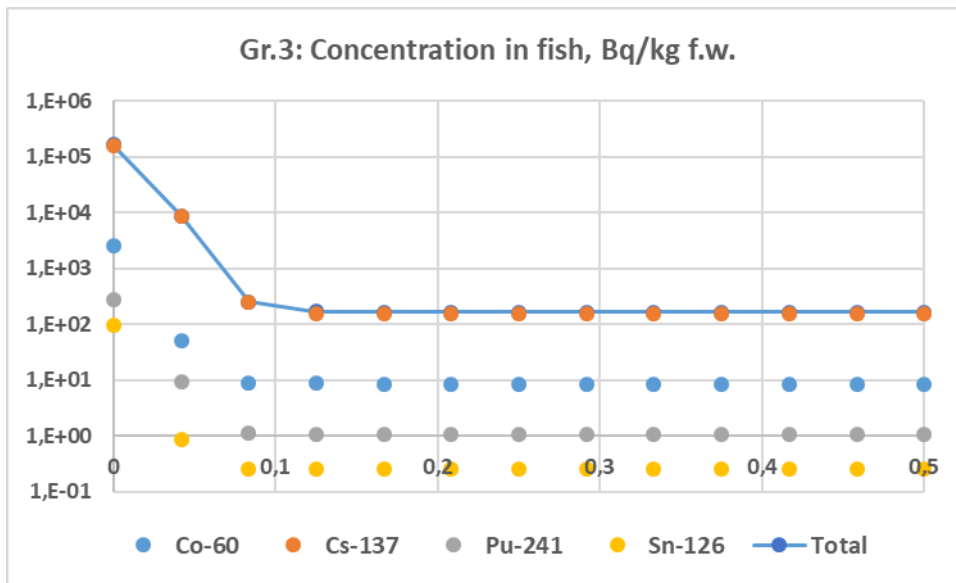
Figure 17. Concentration of radionuclides in biota (group 3). Simulations are presented within time interval [0, 0.5] year.
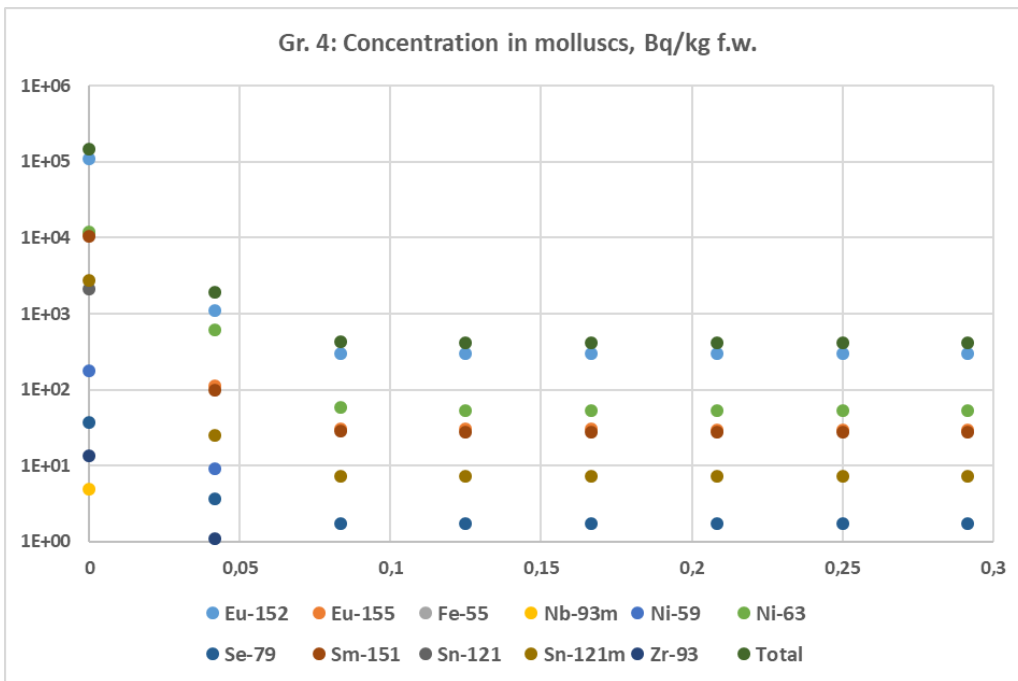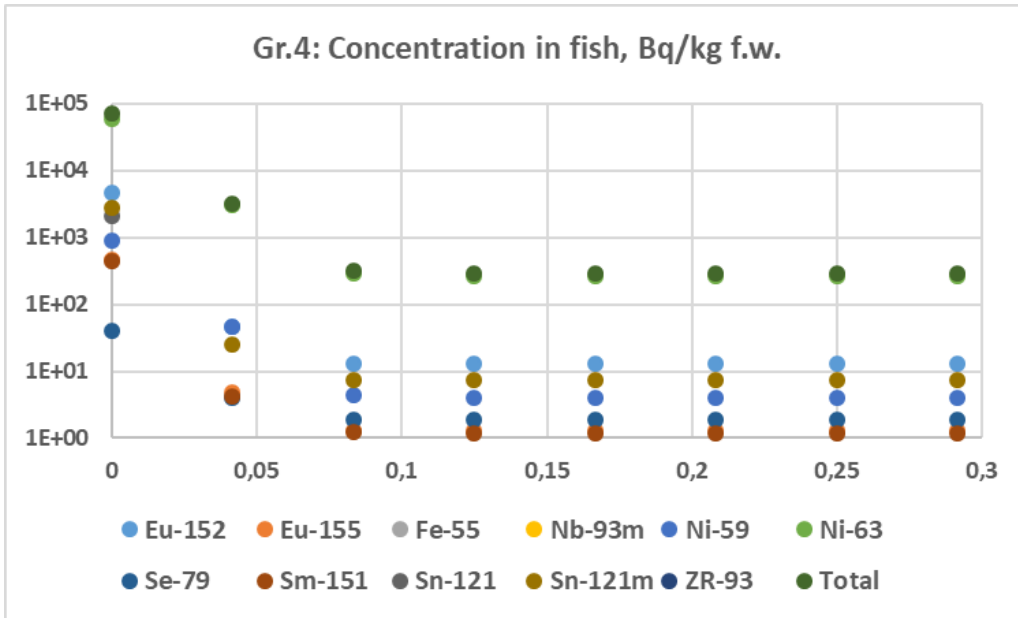
Figure 18. Concentration of radionuclides in biota (group 4). Simulations are presented within time interval [0, 0.3] year.

Simulations, based on assumptions about constant concentration factors/rates, indicate that concentrations of radionuclides in biota for Group 1 is higher than the FAO guideline levels throughout the 2-3 week period after the begining of radionuclide releases for fish, crustaceans, mammals and sea birds and for the entire simulation period (ten years) for molluscs. Further, results show that the concentration is dominated by isotopes of plutonium (Pu-238, Pu-239, Pu-240), mainly Pu-238. The impact of these isotopes to the concentration levels for Group 1 for all biota corresponds to 96-99% of the total concentration for group 1 radionuclides.

Similar to Group 1 radionuclides, the concentration of radionuclides in the biota for Group 2 radionuclides is higher than the guideline levels over a period of two - three weeks after the begining of radionuclide releases, approximately, for fish, crustaceans, mammals and sea birds and over the entire simulation period for molluscs. Concentrations are strongly dominated by Sr-90. The impact to concentration levels for Group 2 for all biota from Sr-90 corresponds to almost 100% of the total concentration for Group 2 radionuclides.

The concentration of radionuclides in the biota for Group 3 radionuclides is higher than the guideline levels over a period of one month after the begining of radionuclide releases, approximately, for all biota. The concentration for biota from Group 3 is dominated by Cs-137 and Co-60 (89-100% of the total concentrations).

The concentration of radionuclides in the biota for Group 4 radionuclides is higher than the guideline levels during one-two weeks, approximately, after the start of the releases. Concentrations are dominated by Ni-63 for fish, mammals and birds and Eu-152 for crustaceans and molluscs. The impact of radionuclides Ni-63, Eu-152 and Eu-155 corresponds to 87-99% of the total concentration for group 4 of radionuclides.

3.3.1.5.   Choosing of kinetic parameters based on available information and mathematical experiments

According to information from the previous section, radionuclides Pu-238, Pu-239, Pu-240 (Group 1), Sr-90 (Group 2), Cs-137 and Co-60 (Group 3) and Ni-63, Eu-152 and Eu-155 (Group 4) dominate the concentration in biota for the present release scenario.

In the present study, a kinetic modelling approach is based on Equation (5), which includes the following parameters for biota in different trophic levels: ingestion rates per unit mass, assimilation efficiency rates, rates of the direct uptake of activity from the water column and excretion rates.

It was assumed that different isotopes of the same radionuclide have the same physiology and metabolism. Therefore, all kinetic parameters are identical except excretion rates, which can be easily recalculated from isotope with the well-known biological half-life (derived from the basic isotope) according to the expression

$$k_{e,i} = k_{e,i}^{(0)} + \ln 2 \left[\frac{1}{T_{1/2,i}} - \frac{1}{T_{1/2,i}^{(0)}} \right] \tag{11}$$

where $k_{e,i}^{(0)}$ is an excretion rate of trophic level "i" for the basic isotope, $T_{1/2,i}$ and $T_{1/2,i}^{(0)}$ are radionuclide half-life for the considered isotope and for the basic isotope, correspondently.

Further, it is assumed that equilibrium state provided by equation (5), when $t \to \infty$ correspond to average concentration in biota, which can be defined due the concentration factor / ratio.

When $t \to \infty$ equation (5) for biota can be written as

$$0 = AE_i \cdot IR_i \cdot C_{i-1}^{(tl,eq)} + k_{u,i} \cdot C_w - C_i^{(tl,eq)} \tag{12}$$

where $C_{i-1}^{(tl,eq)}$ and $C_i^{(tl,eq)}$ are concentrations $C_{i-1}^{(tl)}$ and $C_i^{(tl)}$ of radionuclide in the marine organism as in equation (5), but under equilibrium conditions.

Expression (12) can be used for definition of unknown kinetic rates.

Some useful information concerning kinetic coefficients for the selected radionuclides and some of   reference organisms can be defined from Thomann (1981), Helling et al. (2002), Fievet and Plet (2003), Cazykina (2003), Brown et al. (2004), Beresford et al. (2015), Keum et al. (2015), PREPARE (2015), Iosjpe et al. (2016), Vives I Battle et al. (2016) and Hosseini et al. (2017).

Estimating kinetic coefficients can differ widly (inter-comparison of some selected parameters and radionuclides has been performed, for example, by Vives I Battle et al. (2016)).

Such uncertainties can be explained by definition of the reference organisms, where different species are described by the same reference biota. Further, great variability is associated with the dimensions, masses and habitats for different organisms of the same species. Because of this, the allometric approach is often used for the definition of kinetic parameters. This approach uses the following expression for definition of kinetic parameter P_k:

$$P_k = aM^b,\qquad\qquad(13)$$

where M is a mass of the organism and a and b are the parameters, which can be defined by statistical analysis. The construction of the expression (13) can easily contribute additional uncertainties into the definition of the kinetic parameters.

It is necessary to note that there are also differences in kinetic models to describe the bioaccumulation process in marine organisms that provide a different description of kinetic parameters.

Therefore, in the present study, the kinetic parameters for the selected radionuclides and marine organisms have been chosen as a result of a comparison of the concentrations in biota as calculated in: (i) the numerical simulations based on the published parameters and (ii) the information about concentration ratios/factors presented in the IAEA Technical reports 422 and 479 and the ERICA data base (IAEA, 2004; IAEA, 2014; ERICA, 2019). Figures 19 -23 provide a few examples of concentrations in biota for selected radionuclides and marine organisms after numerical simulations for 1Bq/l concentration in water.

Figures 19-21 show a comparison between the numerical simulation for kinetic and concentration ratio approaches for the 1 Bq / l concentration of Cs-137 in water. Figures 19 and 20 show concentrations for small fish (prey) and seabirds, respectively. Figures also show the minimum and maximum concentration of Cs-137 associated with 1 Bq / l water concentration according to the concentration ratio / factor approach. Figures 19-20 show an appropriate comparison between both approaches after some time after the release date. Figure 22 shows concentration dynamics for different marine organisms, where it is possible to follow the transfer of Cs-137 between different trophic levels.
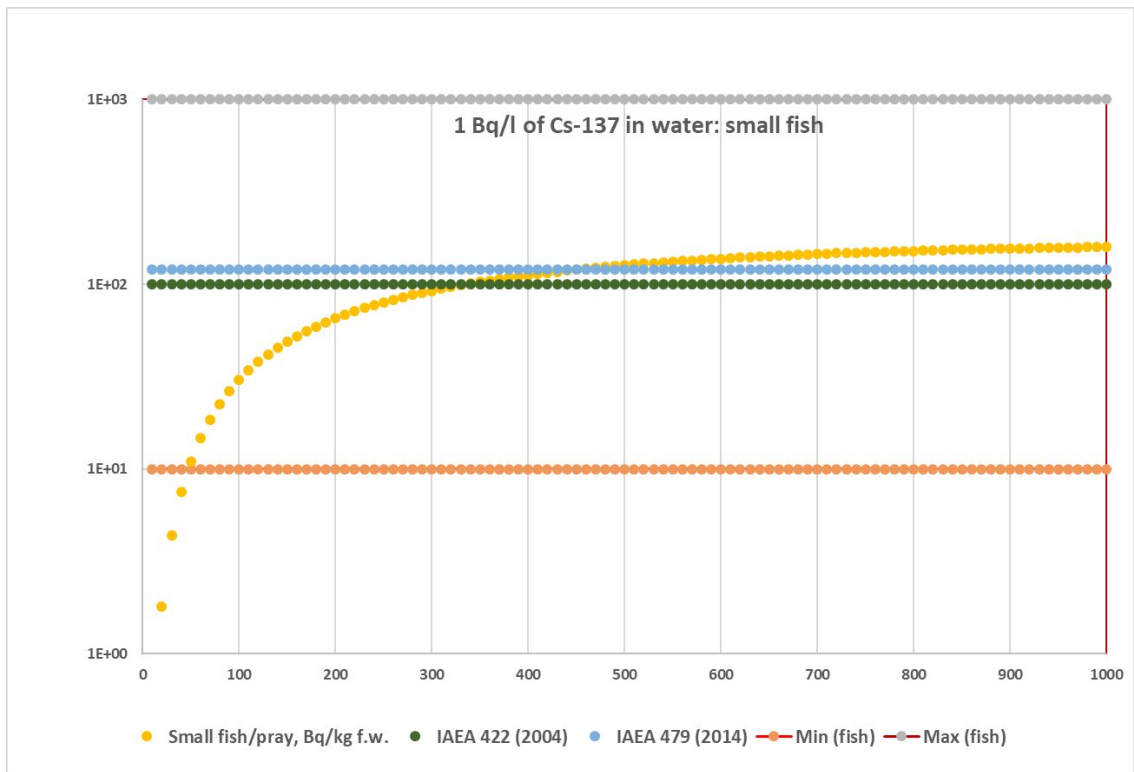
Figure 19. Concentrations of Cs-137 in sea water (1 Bq/l) and small fish /prey (Bq/kg f.w.). Simulations are presented within time interval [0, 1000] days.
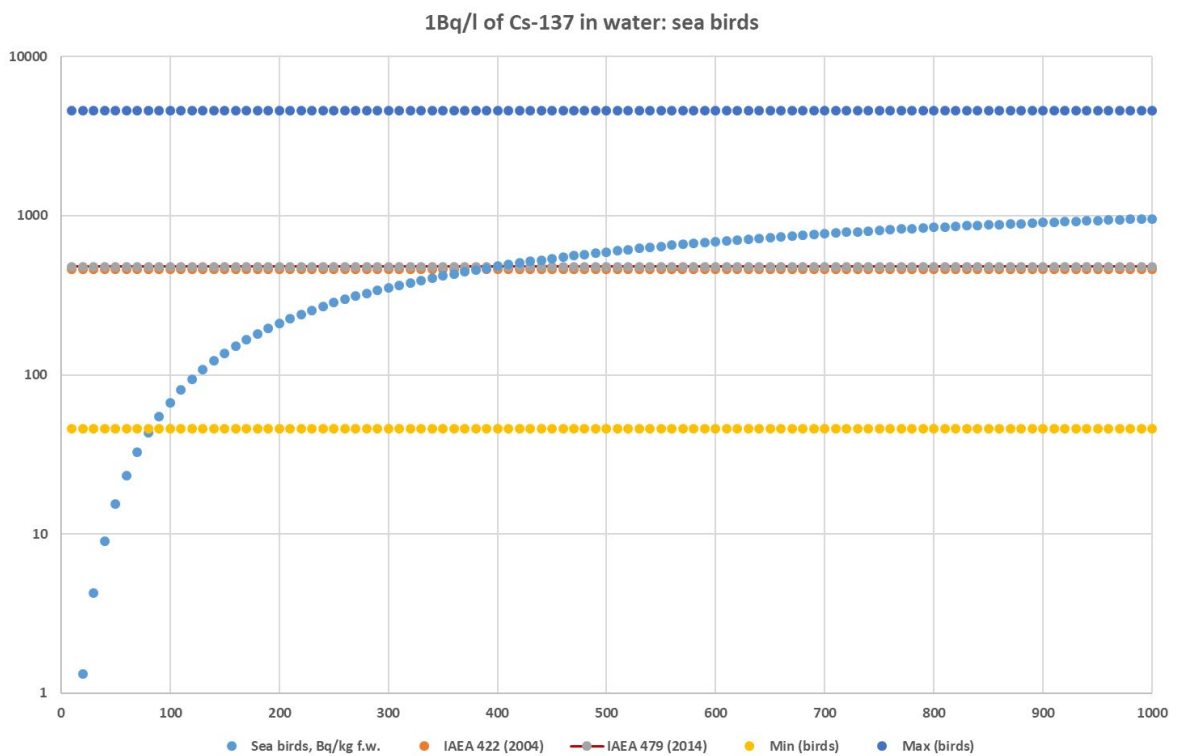

Figure 20. Concentrations of Cs-137 in sea water (1 Bq/l) and seabirds (Bq/kg f.w.). Simulations are presented in the range from 0 to 1000 days. Simulations are presented within time interval [0, 1000] days.
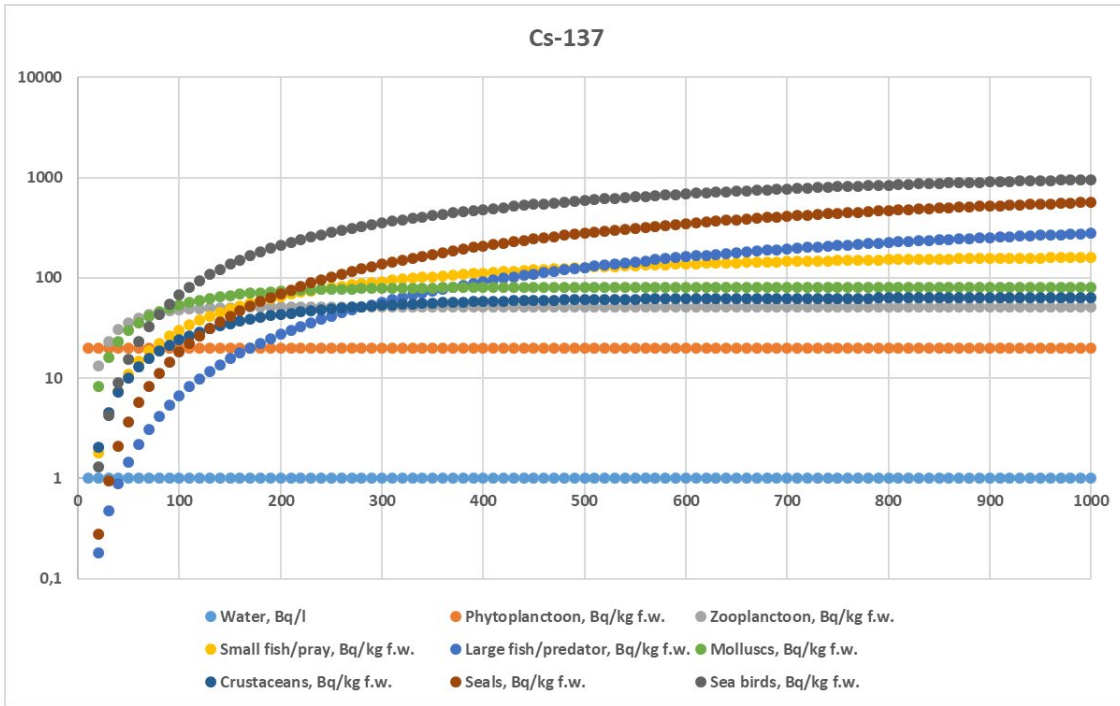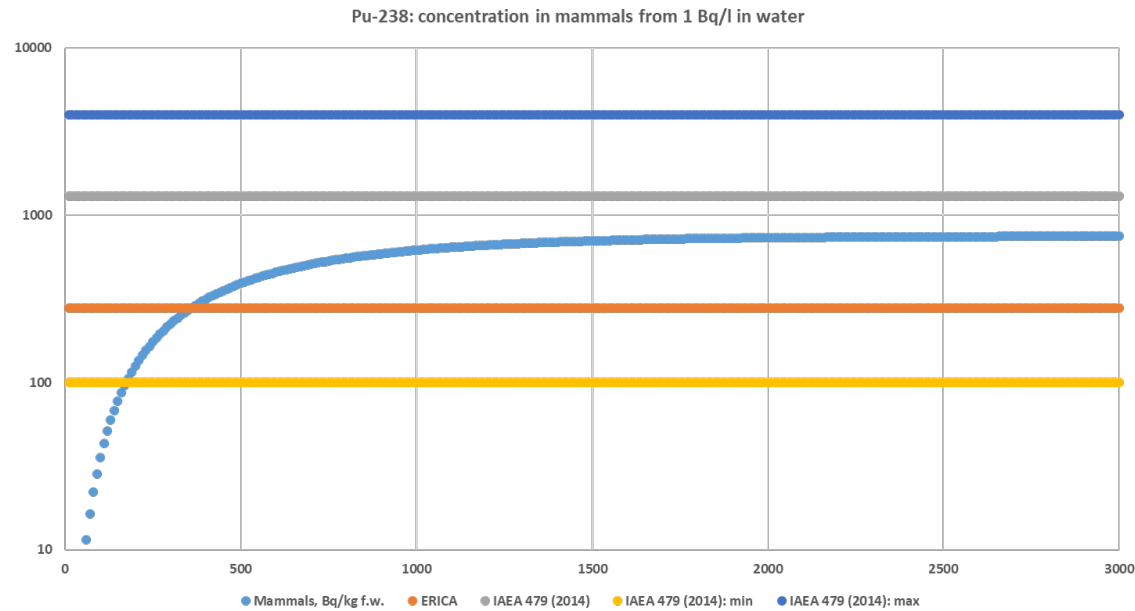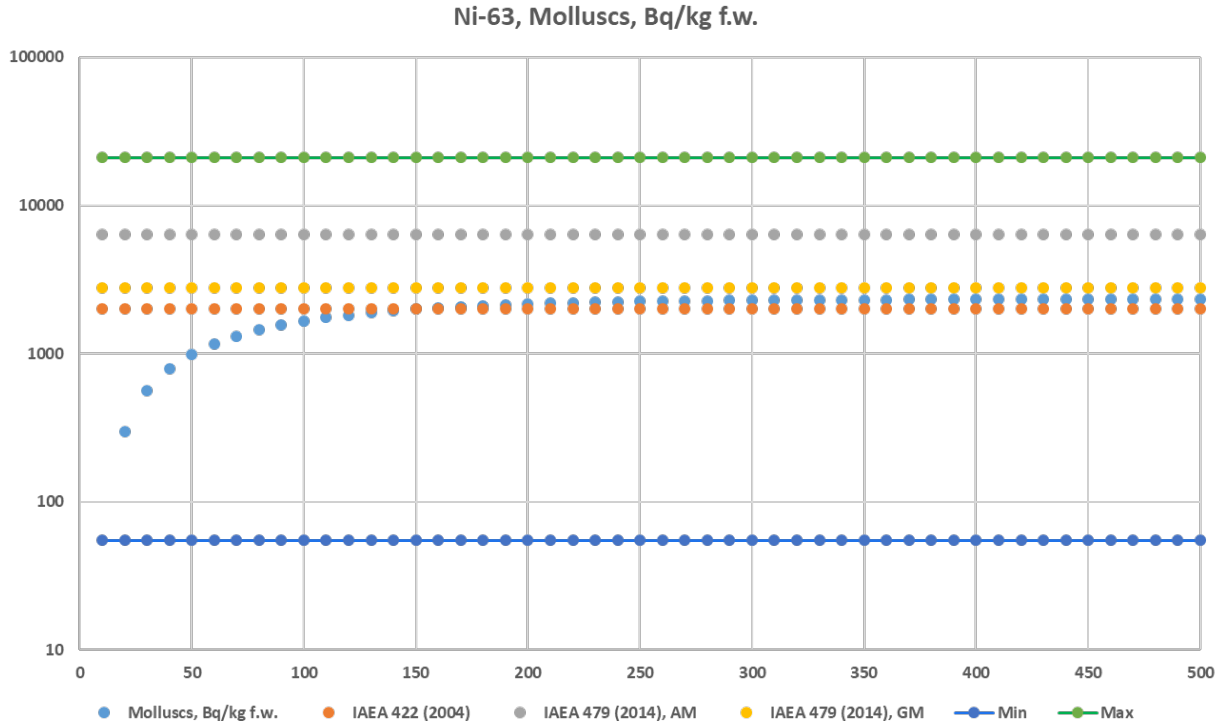
Figure 21. Concentrations of Cs-137 in sea water (1 Bq/l) and biota with different trophic levels (Bq/kg f.w.). Simulations are presented within time interval [0, 1000] days.

Figure 22 shows a comparison of concentration in mammals between the numerical simulation for kinetic and concentration ratio approaches (IAEA, 2014; ERICA, 2019) for the 1 Bq / l concentration of Pu-238 in water. Figure also show the minimum and maximum concentration of Pu-238 associated with 1 Bq/l water concentration according to the concentration ratio / factor.

Figure 22. Concentrations of Pu-238 in sea water (1 Bq/l) and mamals (Bq/kg f.w.). Simulations are presented within time interval [0, 3000] days.

Figure 23 shows a comparison of concentration in molluscs between the numerical simulation for kinetic and concentration ratio approaches (IAEA, 2014; IAEA, 2004) for the 1 Bq / l concentration of Ni-63 in water. The figure also shows arithmetic and geometric averages as well

as the minimum and maximum concentration of Ni-63 associated with 1 Bq / l water concentration according to the concentration ratio / factor. Figure 23 demonstrates that there is a significant difference between arithmetic and geometric averages of the concentration ratio for the same database (IAEA, 479). For the present study, a set of kinetic parameters was selected that provides a concentration in mollusks, which, after some initial time, is close to the IAEA (2004) concentration ratio and to the IAEA (2014) concentration ratio derived from the geometric average.

Figure 23. Concentrations of Ni-63 in sea water (1 Bq/l) and molluscs (Bq/kg f.w.). Simulations are presented in the range from 0 to 500 days.

3.3.1.6. Concentrations of radionuclides in marine biota

Following the FAO/WHO (CAC, 2006) recommendations, the model simulations for fish, crustaceans, molluscs, sea mammals and seabirds are provided separately for each group of radionuclides presented in Table 1.

It is necessary to note that during the human habit assessment for infants (Smith and Jones, 2003; US DoHHS, 1998), which was used for the FAO/WHO guideline (CAC, 2006) levels development, the consumption of fish was found to be very low, while consumption of crustaceans and molluscs was not found at all, probably because it is generally recommended to avoid feeding children seafood before the age of 12–36 months, due to allergy concerns (Fiocchi et al., 2006; Kullet al., 2006). Therefore, the results for crustaceans and molluscs have to be used without regards to the infant guideline levels.

Figures 24-27 shows that concentration in biota vary with time significantly for all goups of radionuclides. It is necessary to note that the calculations, presented in Figures 24 -27, correspond to the Stepovogo Bay of the Kara Sea (the compartment, where the accident location was chosen).
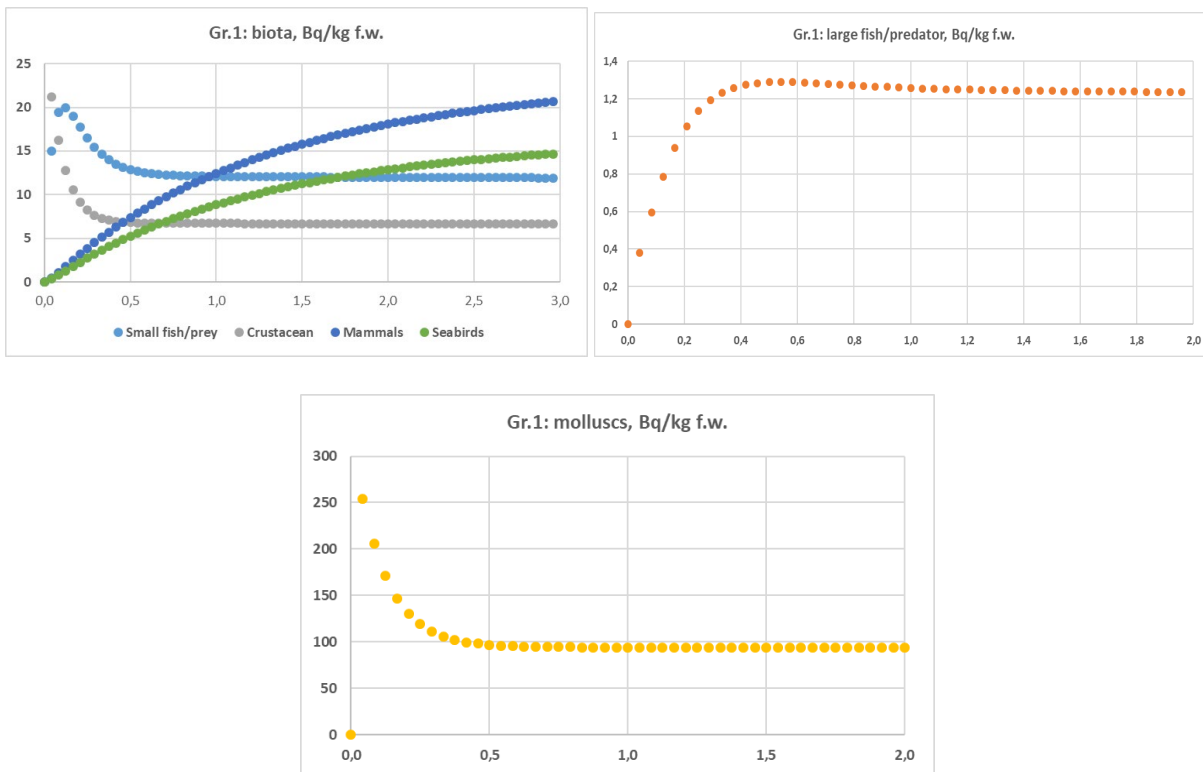
Figure 24. Concentration of radionuclides in biota for Group 1 (CAC, 2006). Simulations are presented within time intervals [0, 3] years (top) and [0,2] years (bottom).

Radionuclide concentrations from Group 1 exceed the Guidance levels values for all marine organisms during the entrie period of simulations (ten years) and, therefore, cannot be recommended as seafood without limitations (Figure 24). Nevertheless, some biota can be used as sea food with the following limitations: (i) large fish can be used for adults, (ii) crustacean can be also used as seafood for adults after initial time of releases of radionuclides (two months, approximately). A similar situation is shown in Figure 25 for radionuclides from Group 2, where marine organisms generally cannot be recommended as seafood, except for fish, which can be used without restrictions. Marine mammals and seabirds cannot be recommended as seafood for radionuclides from Group 3, but all other marine organisms, as well as all biota from Group 4, have no restrictions (Figures 26 and 27). The maximum values of the total concentration for marine organisms for all four groups are shown in Table 3. It is important to note that the concentration of radionuclides from Group 1 in biota (mainly Pu-238) is low compared to the concentration of radionuclides from Group 3 (mainly Cs-137). However, despite this, restrictions on the use of seafood is more significant for radionuclides from Group 1 due to dose conversion factors for alpha radiation-emitting radionuclides being much higher than for gamma and beta-emitting radionuclides.
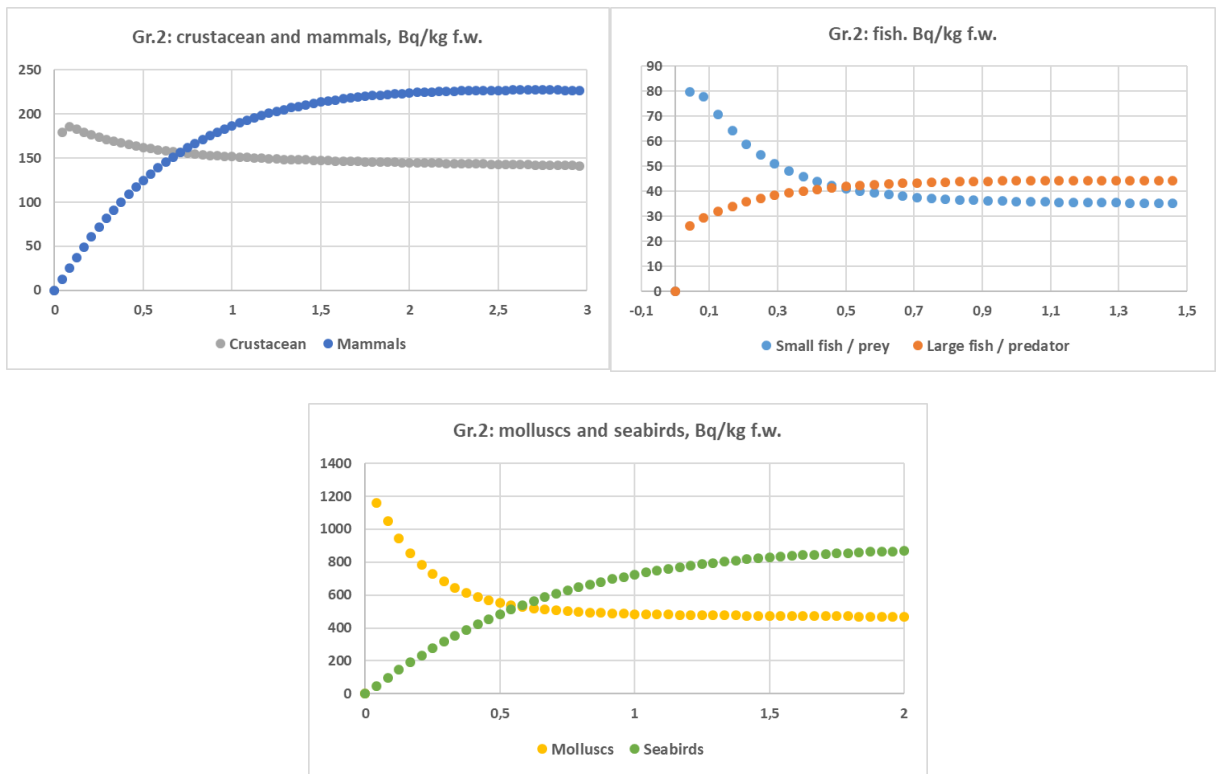
Figure 25. Concentration of radionuclides i biota for Group 2 (CAC, 2006). Simulations are presented within time intervals [0, 3] years (top left), [0, 1.5] year (top right) and [0, 2] years (bottom).
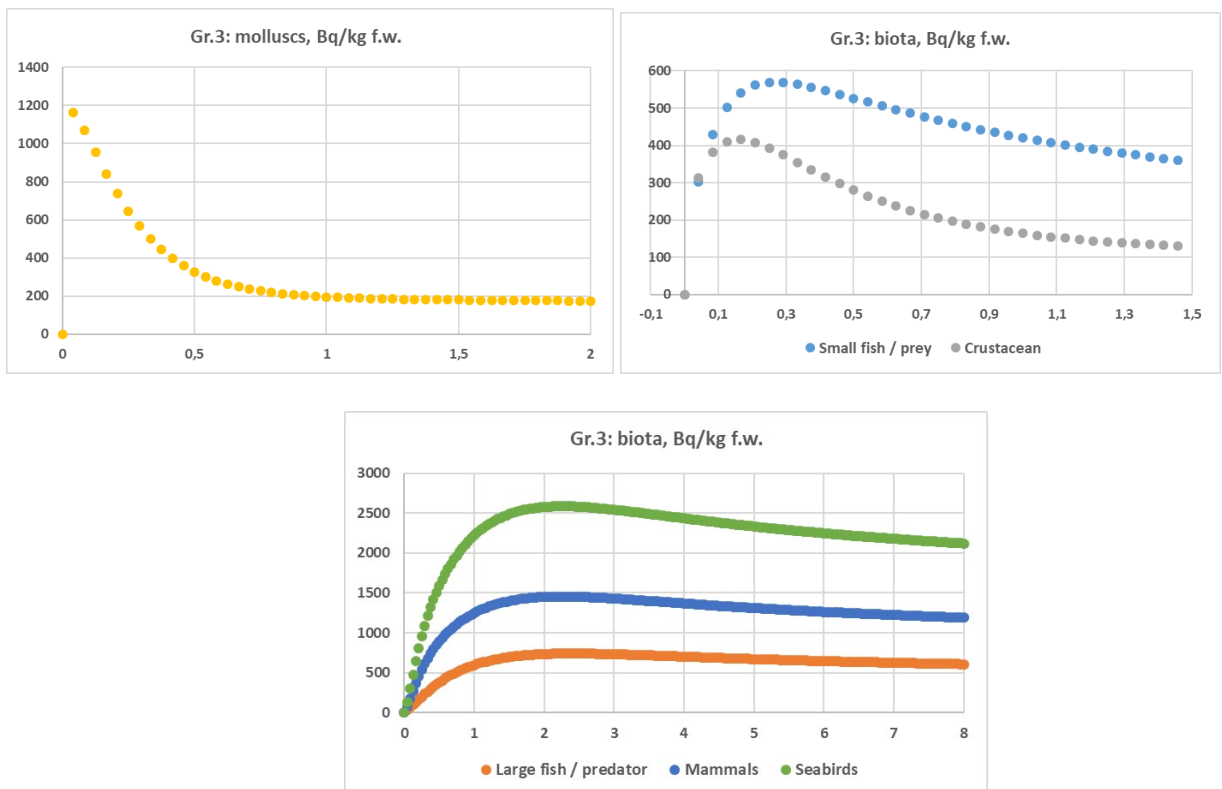

Figure 26. Concentration of radionuclides i biota for Group 3 (CAC, 2006). Simulations are presented within time intervals [0, 2] years (top left), [0, 1.5] year (top right) and [0, 8] years (bottom).
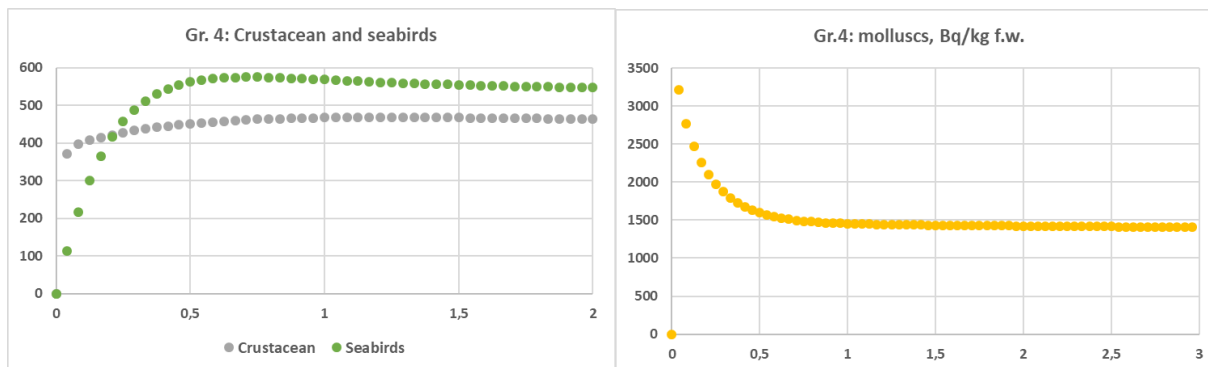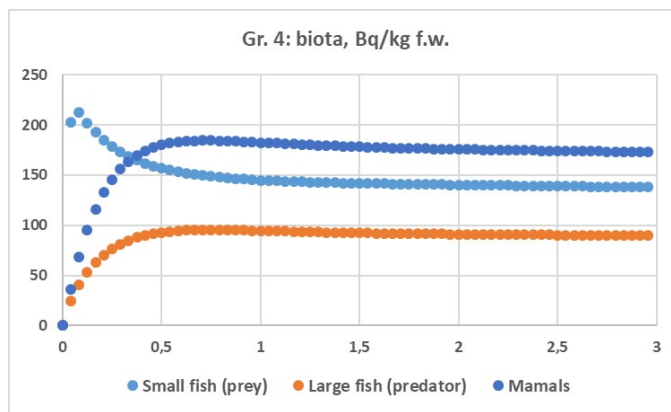
Figure 27. Concentration of radionuclides in biota for Group 4 (CAC, 2006). Simulations are presented within time intervals [0, 3] years (top), [0, 2] years (bottom left) and [0, 3] years (bottom right).

Table 3. The maximum levels of radionuclide concentration (Bq/kg, f.w.) in marine biota in the Stepovogo Bay for different groups of radionuclides.

	Group 1	Group 2	Group 3	Group 4
Fish (prey)	19.4	79.7	569	212
Fish (predator)	1.3	44.4	740	95.4
Crustacean	21.2	185	416	468
Molluscs	254	1159	1161	3212
Sea mammals	22.6	227	1454	184
Seabirds	16.1	881	2587	575

3.3.1.7. Doses to the critical group of humans

In the present report, the critical group of humans is defined as persons, which will use marine organisms from the Stepovogo Bay in spite of recommended restrictions from the previous section 3.3.1.6 with the following dietary data: (i) sea fish, 500 g/d; (ii) sea mammals, 80 g/d; (iii) sea birds, 20 g/d and (iv) seabirds eggs, 20g/d (IASAP, 2003; Hosseini et al., 2016). It is also assumed that concentration of radionuclides in seabirds eggs is the same as in seabirds.

Figures 28 and 29 show the dynamic of doses from different radionuclides and the total dose for the critical group, respectively. Figure 30 shows that the main impact to the maximal dose

for the critical group (3.8 mSv, the third year after start of radioactivity releases) corresponds to Cs-137 (73%). The dose of 3.8 mSv exceeds the dose from natural cases (2-4 mSv for this region (AMAP, 1998)) and can therefore not be ignored as consequences after the potential accident with NS K-27.
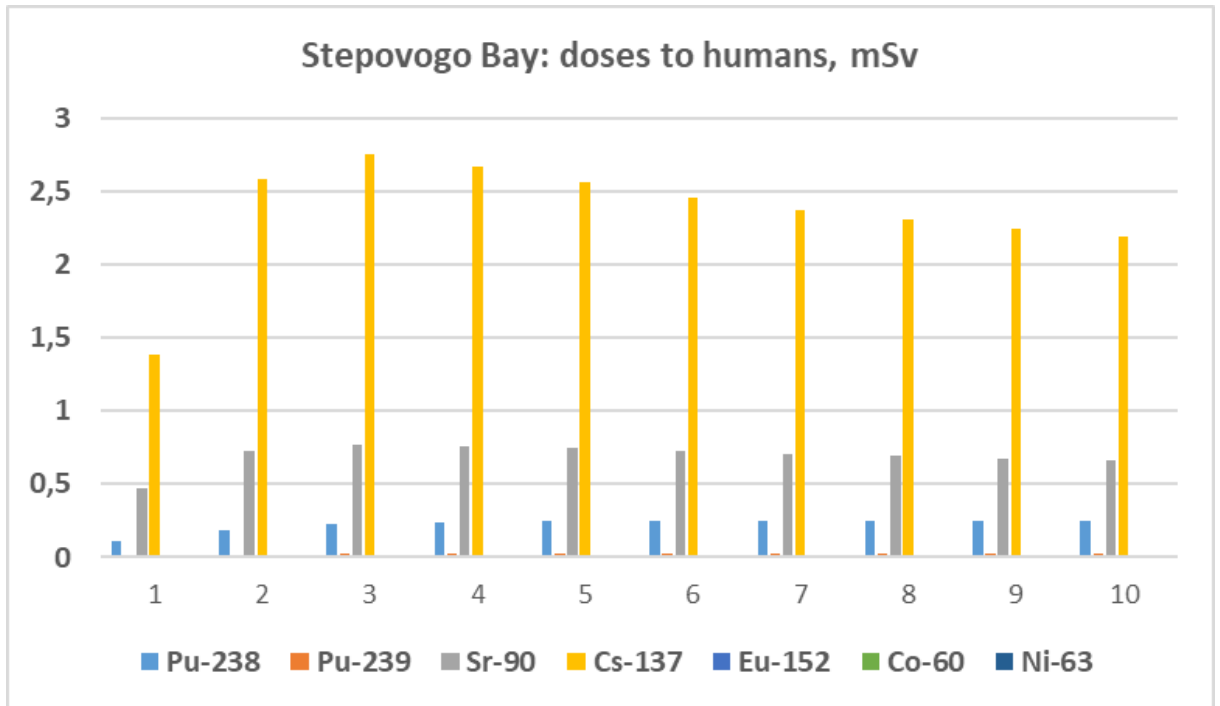

Figure 28. Dynamic of the impact of radionuclides in the effective dose to humans. Simulations are presented within time interval [0, 10] years.
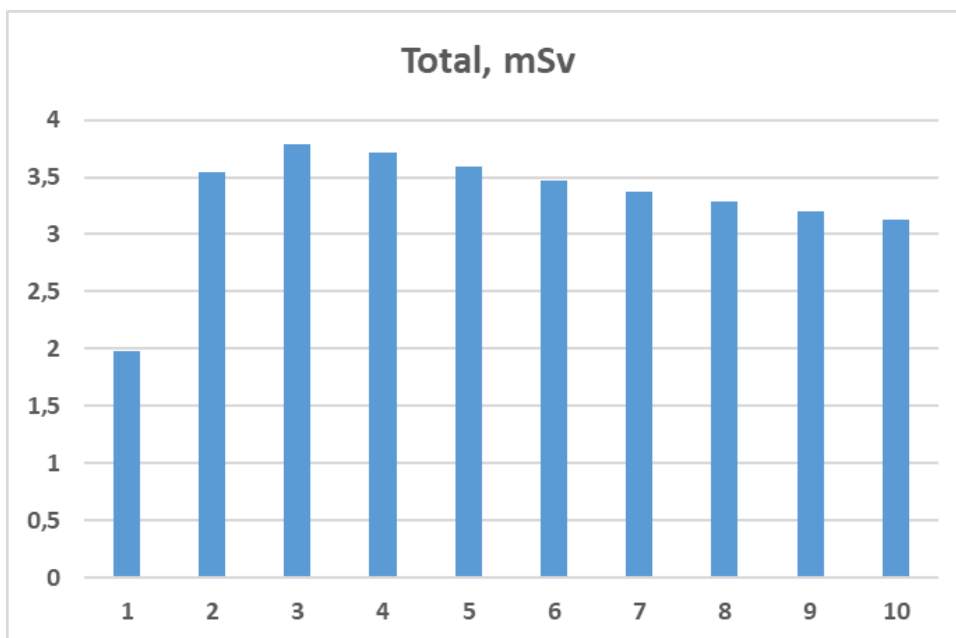

Figure 29. Dynamic of the total dose to the critical group of humans using marine organisms from the Stepovogo Bay. Simulations are presented within time interval [0, 10] years.
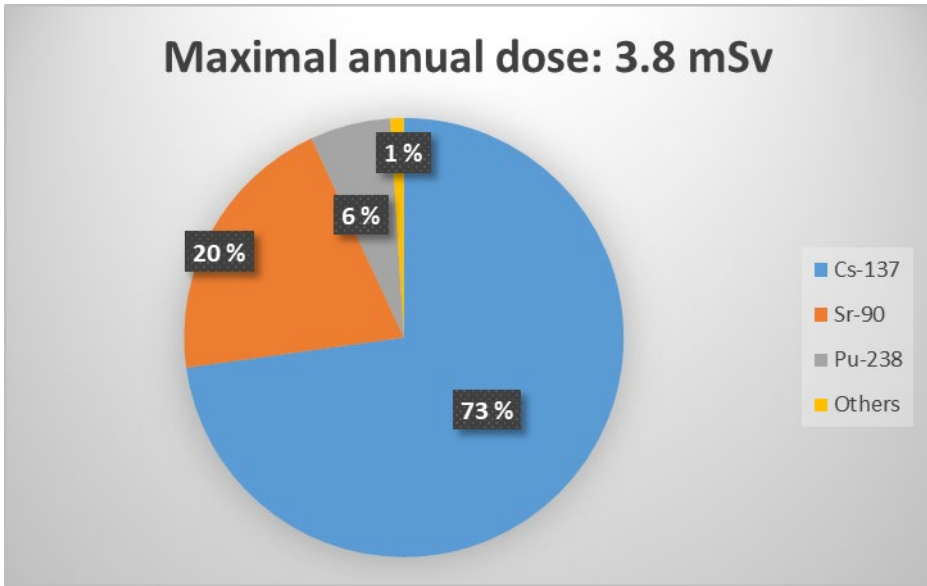
Figure 30. Impact of the radionuclides to the maximal dose to the critical group.

3.3.1.8 Dose rates to marine organisms

Dose rates calculated for different marine organisms in the Stepovogo Bay (the location for the hypothetical accident) are presented in Figures 31-42. Figure 31 shows the impact of different radionuclides on the dose rate (in units of µGy/h) for small fish (prey) at the onset of discharge. Figure 31 shows that the main impact to the dose rate corresponds to Cs-137 (81%) and Sr-90 (16%).
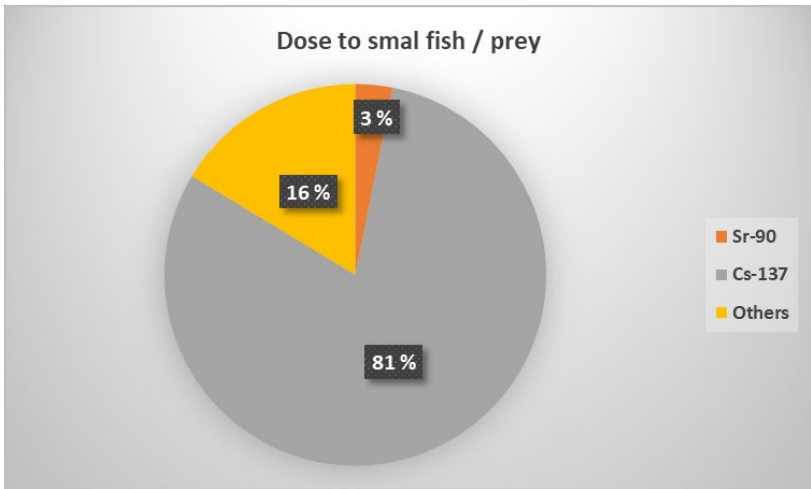

Figure 31. Contribution of various radionuclides to the dose rate for small fish (prey) at the onset of discharge.

Similarly, the effect of different radionuclides after 45 days after the release date is presented in Figure 32. Figure 31 shows that the main impact to the dose rate corresponds to Pu-238 (73%) and Cs-137 (12%).
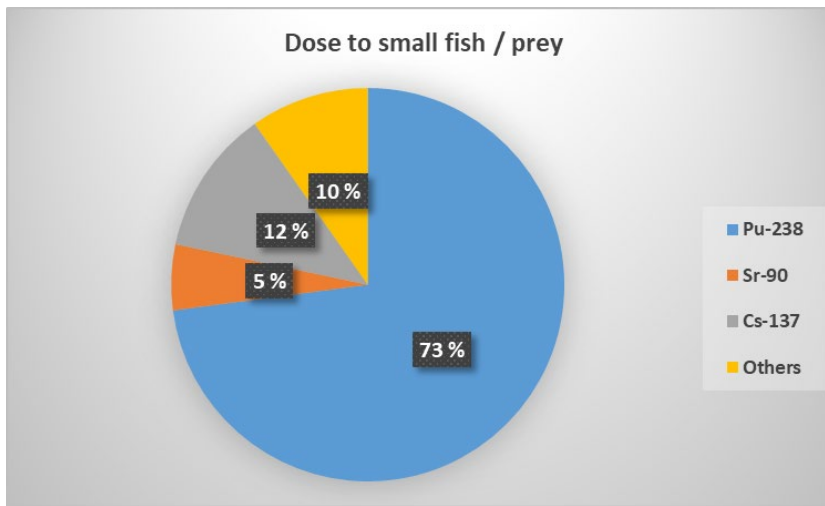
Figure 32. Contribution of various radionuclides to the dose rate for small fish (prey) the dose rate of small fish (prey) after 45 days from the onset of discharge.

Significant differences between results presented in Figures 31 and 32 are confirmed by the dose-rate dynamics over one year for small fish (prey) for Cs-137 and Pu-238, which are shown in Figure 33. Results of simulations in Figure 33 indicate that immediately after the start of releases, the dose-rate for small fish is dominated by external radiation, mainly from Cs-137 (and Sr-90, which is not shown in Figure 33). After some time (two weeks, approximately) internal radiation (mainly, Pu-238) dominates the dose-rate for small fish (prey) for the present release scenario because of relatively fast and high bioaccumulation presented in Figure 24 and the default radiation weighting factor of 10 for alpha radiation (see Section 2.3 of the present report).
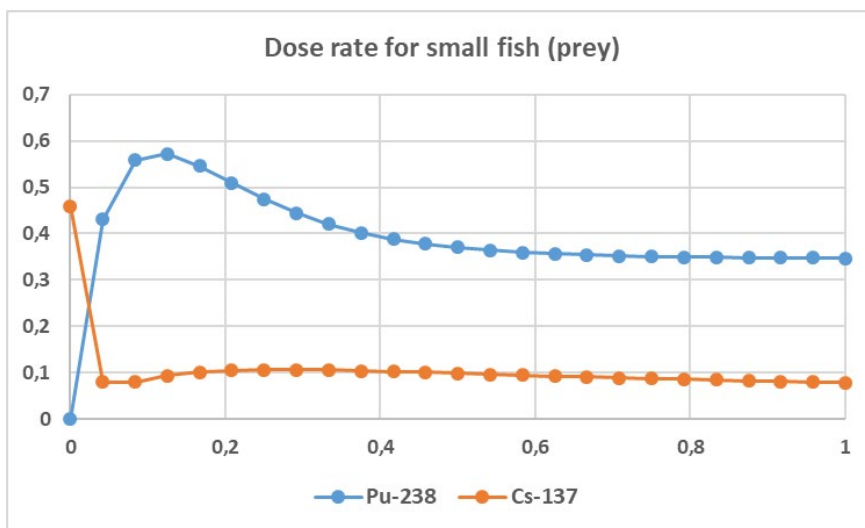

Figure 33. The dose-rates dynamic due one year for small fish (prey) for Cs-137 and Pu-238, µGy/h. Simulations are presented within time interval [0, 1] year.

For large fish (predators), Cs-137 dose rates dominate almost the entire time (Figure 34). It is interesting that, like the small fish, the effect of Pu-238 increases with time (Figure 35).
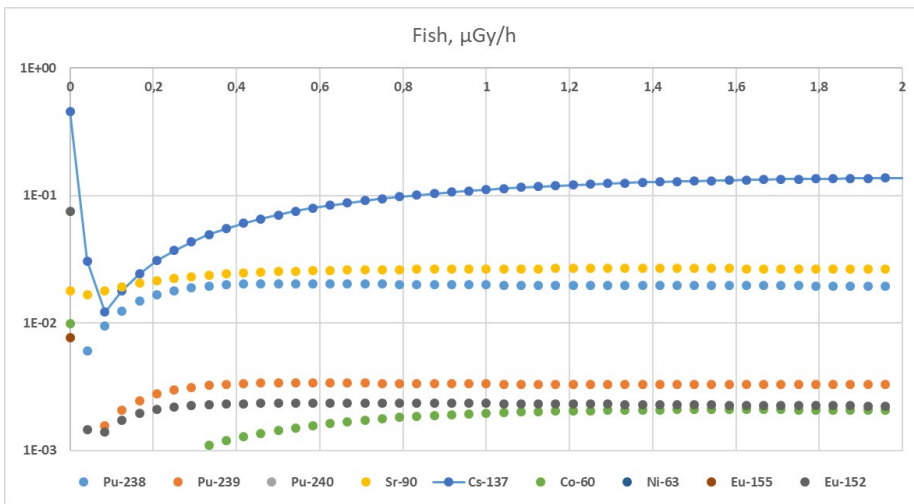
Figure 34. Dynamics of dose rates for large fish (predator) over two years, µGy/h. Simulations are presented within time interval [0, 1] year.
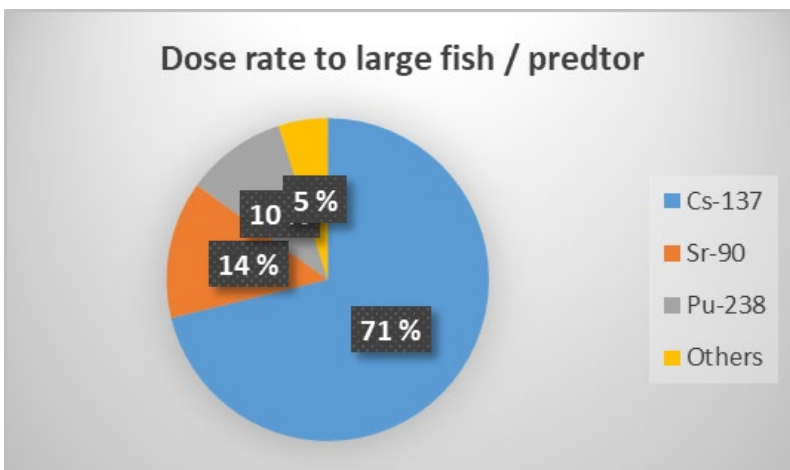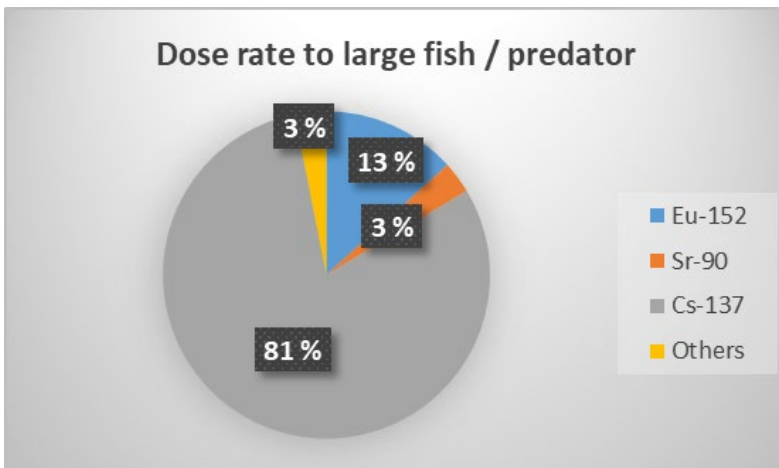

Figure 35. Contributions of different radionuclides on the dose rate of large fish (predator) at the onset of discharge (top) and after two years after the start of releases (bottom).

The dynamic of dose rates over one year for different radionuclides for crustaceans is shown in Figure 36, while the effect of different radionuclides on the crustacean dose rate (i) at initial time (immediately after the start of releases of radionuclides) and (ii) after 15 days from the start of radioactivity release, is shown in Figure 37. Figures 36-37 indicate that Eu-152

dominates the dose-rate, but at initial time the dose rate for crustaceans is dominated by Cs-137 because, similar to small fish, the dose rate is strongly dominated by external exposure.
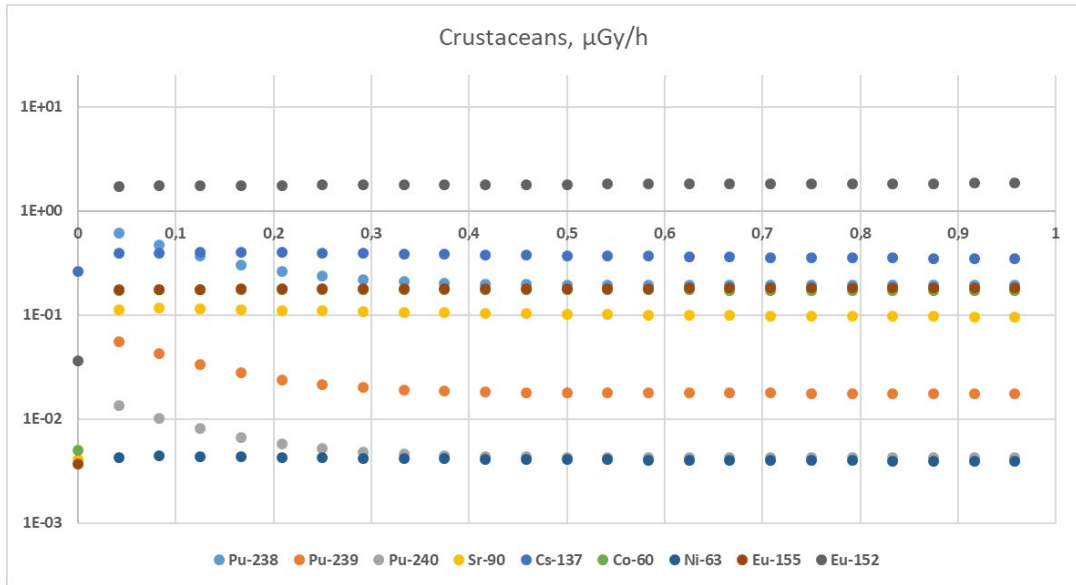

Figure 36. The dose-rates dynamic over one year for crustacean, µGy/h. Simulations are presented within time interval [0, 1] year.
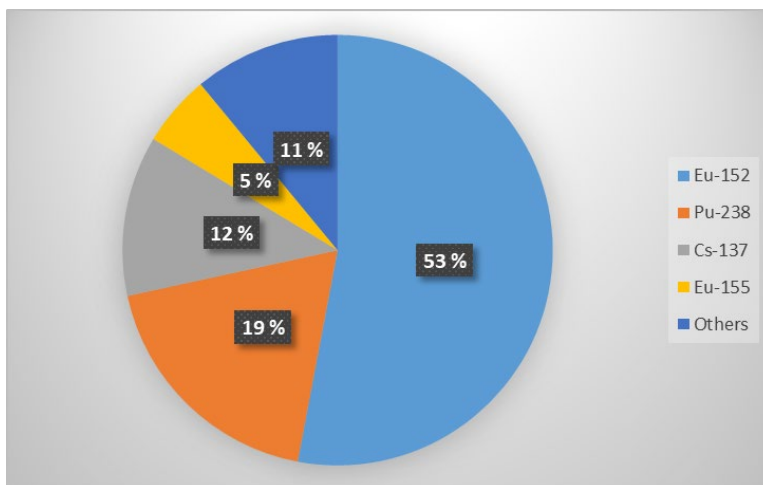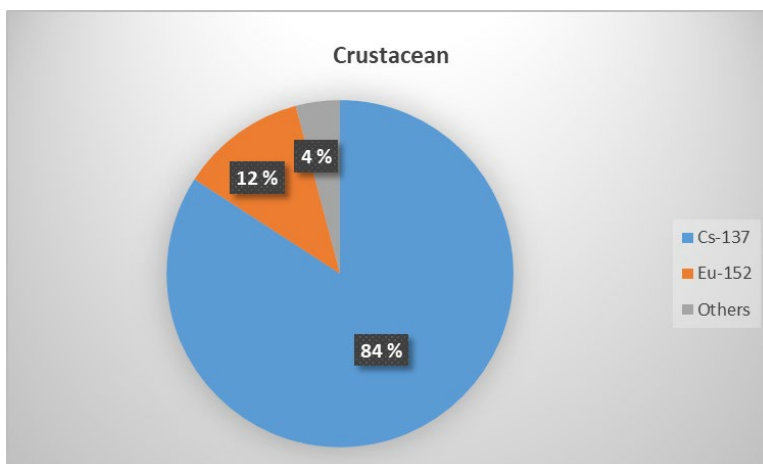

Figure 37. Effect of radionuclides on the dose rate of crustaceans at initial time (top) and after 15 days after the start of releases (bottom), µGy/h.

The effect of different radionuclides on the molluscs dose rate at initial time and after 15 days from the start of radioactivity release, is shown in Figure 38. Figure 38 shows that Pu-238 dominates the dose-rate for molluscs, but at initial time the dose rate is dominated by Cs-137, similar to the previous results.
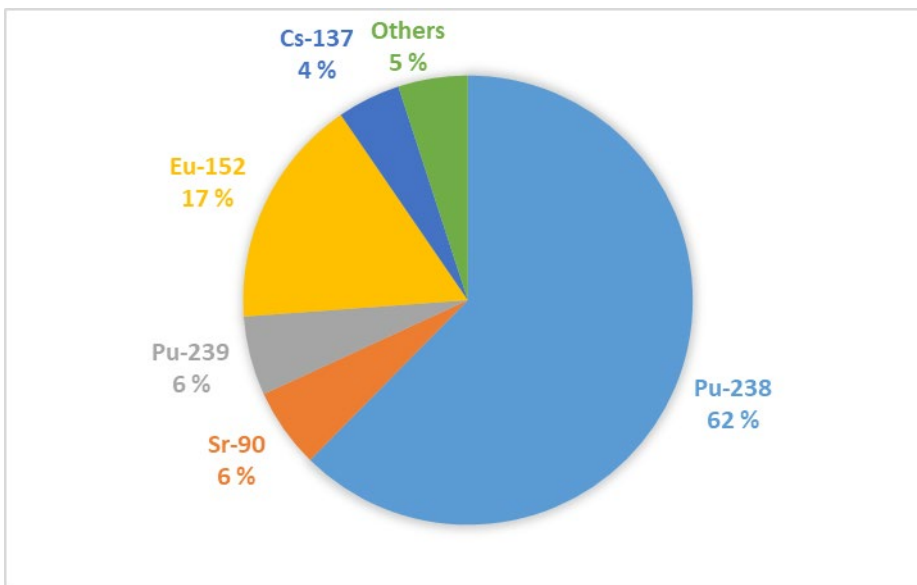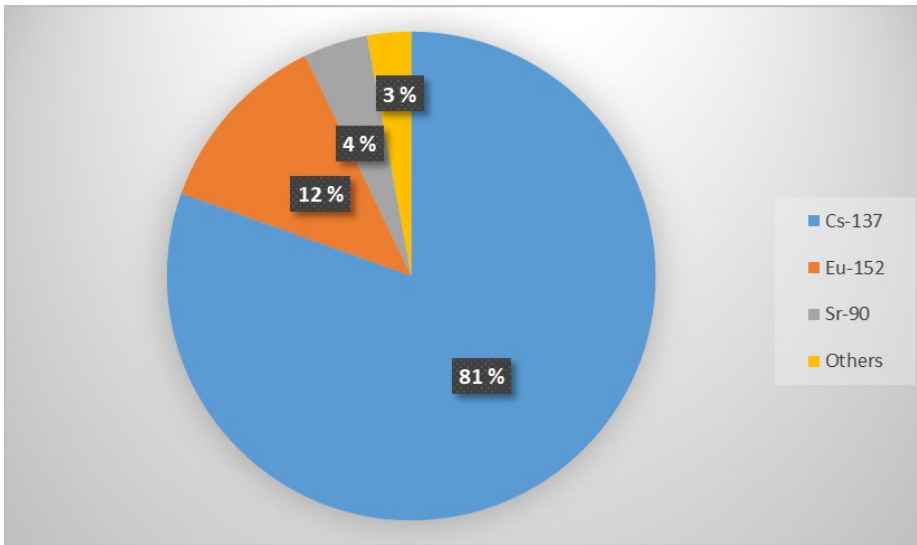

Figure 38. Effect of radionuclides on the dose rate of molluscs at initial time (top) and after 15 days after the start of releases (bottom)

Similar to the previous results, the dose rate for mammals is dominated by Cs-137 at initial time (Figure 39, top). The effect of different radionuclides after 4 years, approximately, is shown in Figure 39 (bottom) where the dose-rate for mammals is dominated by Pu-238 and Cs-137. The Figure 39 (bottom) corresponds to the maximal dose-rate for sea mammals according to dynamic of the dose rates, which is shown in Figure 40.
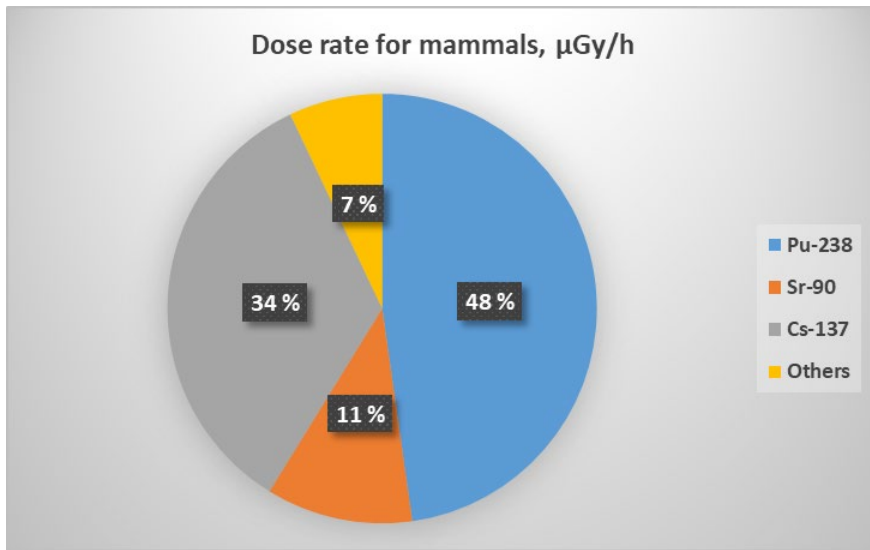
Figure 39. Effect of radionuclides on the dose rate of mammals at initial time (top) and after 4 years of releases of radioactivity
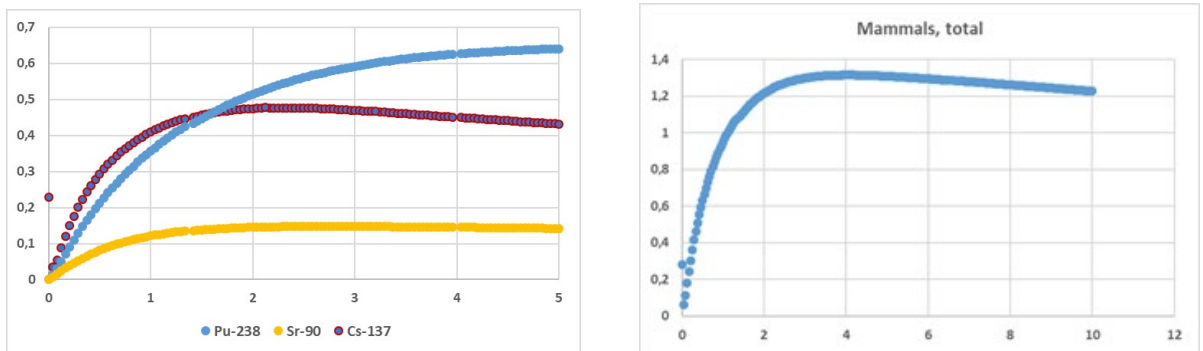
Figure 40. The dose-rates dynamic of Pu-238, Cs-137 and Sr-90 for mammals (left) and total dose-rate for sea mammals. Simulations are presented within time intervals [0, 5] years (left) and [0, 10] years (right).

The results for seabirds are similar to those for marine mammals (see Figure 41-42). Perhaps it should be noted that around the time when the dose rate for seabirds is maximal (3.5 years, approximately after the first release time), the effects of Cs-137, Pu-238 and Sr-90 are almost equal.
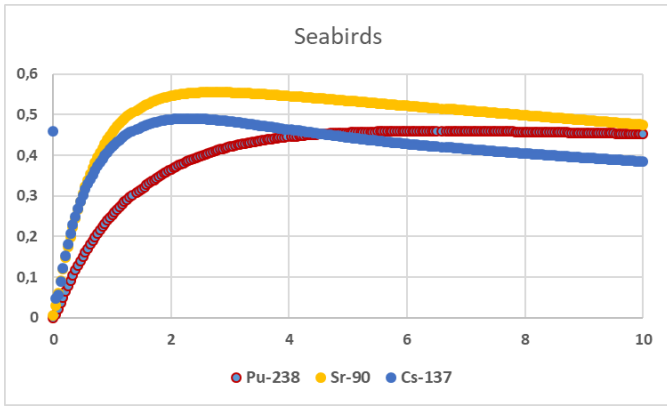
Figure 41. The dose-rates dynamic of Pu-238, Cs-137 and Sr-90 for seabirds, μGy/h. Simulations are presented within time interval [0, 10] years.
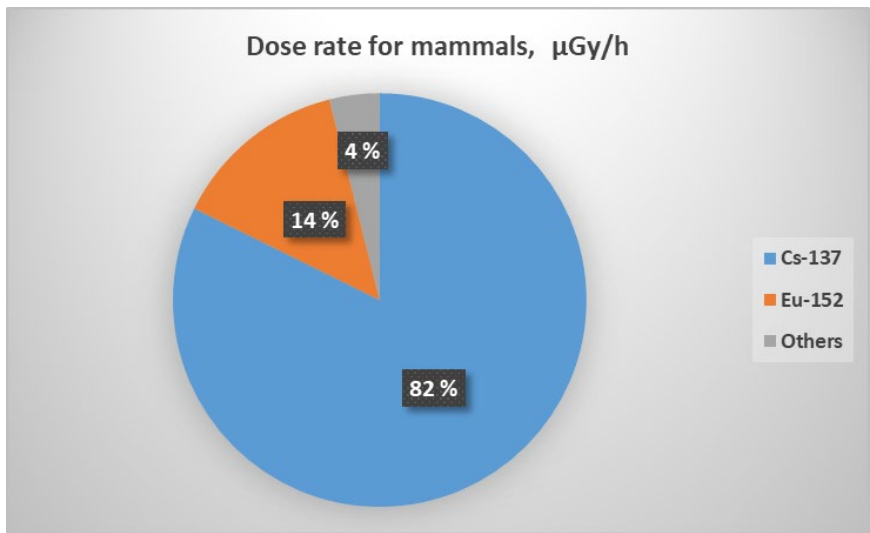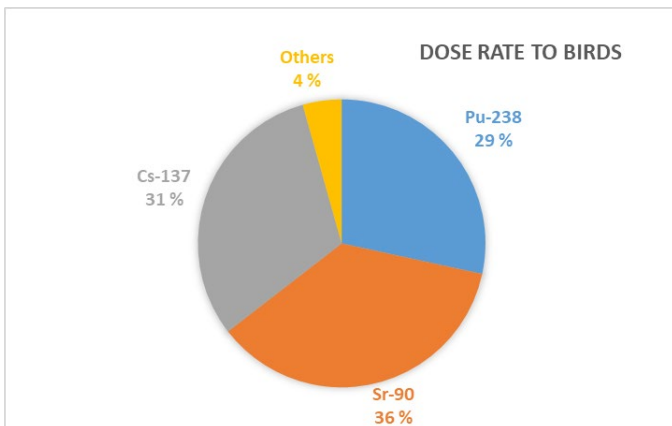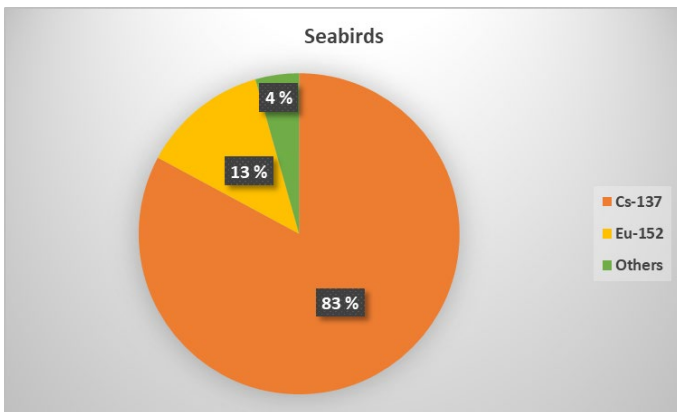

Figure 42. Effect of radionuclides on the dose rate of seabirds at initial time (top) and after 3.5 years of releases of radioactivity

The maximum values of the dose-rates for marine organisms are shown in Table 3. The calculations show that only for molluscs and only during one at initial time of releases the dose rate exceeds the screening dose (10 μGy/h), which can be considered as a safe level below which the potential for significant impacts on biota would be negligible.

Table 3. The maximum dose-rates (µGy/h) in marine biota.

Marine organisms	Dose-rate, µGy/h
Fish (prey)	0.79
Fish (predator)	0.57
Crustacean	3.3
Molluscs	11.7
Sea mammals	1.3
Seabirds	1.5

3.3.1.9 Consequences after additional scenarios for Cs-137

According to the present calculations, Cs-137 is an important radionuclide for radioecological analysis. Therefore, following the report (Brown & Hosseini, 2019) we will consider two additional scenarios for potential releases of Cs-137: 6 TBq instant and 0.8 TBq continuously.

Concentrations in water and sediment for the Stepovogo Bay are compared in Figure 43. Concentration after instantaneous release of 6 TBq of Cs-137 decreases for both water and sediment. Concentrations in water for the present approach and for the continuous release of 0.8 TBq per year are practically the same most of the time. Concentrations in sediment is more significant for the present approach in comparison with the continuous release of 0.8 TBq per year. This can be explained by (i) the current approach also includes instant releases and (ii) non-instantaneous radioactivity mixing for the current modeling. The combination of points (i) and (ii) provides high concentration in sediment in comparison with other approaches.
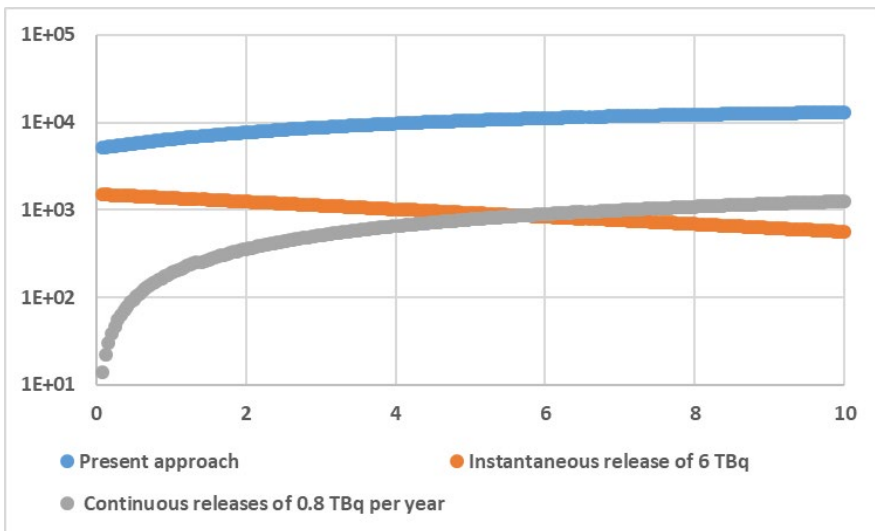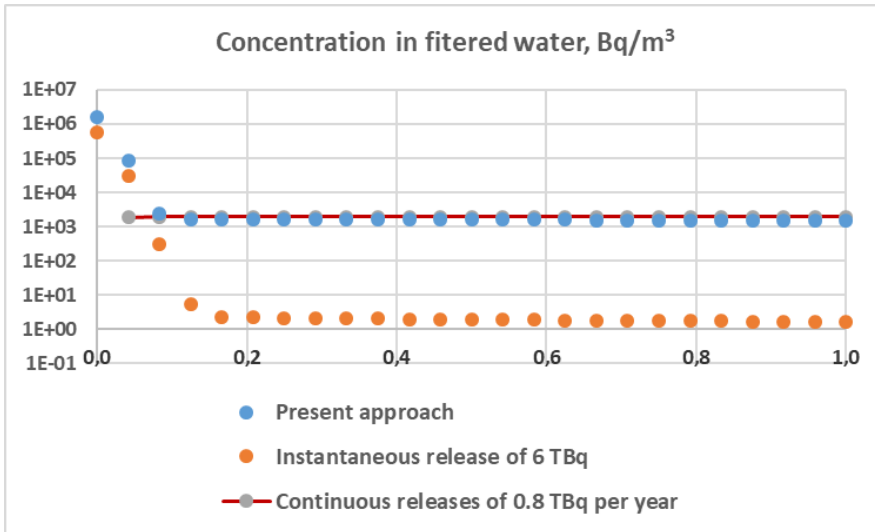
Figure 43. Concentrations in water, Bq/m³ (top) and sediment, Bq/kg d.w. (bottom) for the Stepovogo Bay Simulations are presented within time intervals [0, 1] year (top), and [0, 10] years (bottom).

Differences for concentrations in biota for the considered release scenarios depend only from differences of Cs-137 concentration in filtered water. Therefore, the shapes of differences for all marine organisms are, approximately, similar. Figure 44 shows comparison of the Cs-137 concentration in the considered marine organisms. Figure 44 shows that the present scenario provides the maximal concentration in biota at initial time, while the scenario with Cs-137 continuous releases of 0.8 TBq per year provides maximum concentration in biota after some time of exposure.

Maximal values of concentration in biota for all three scenarios are shown in Table 4.
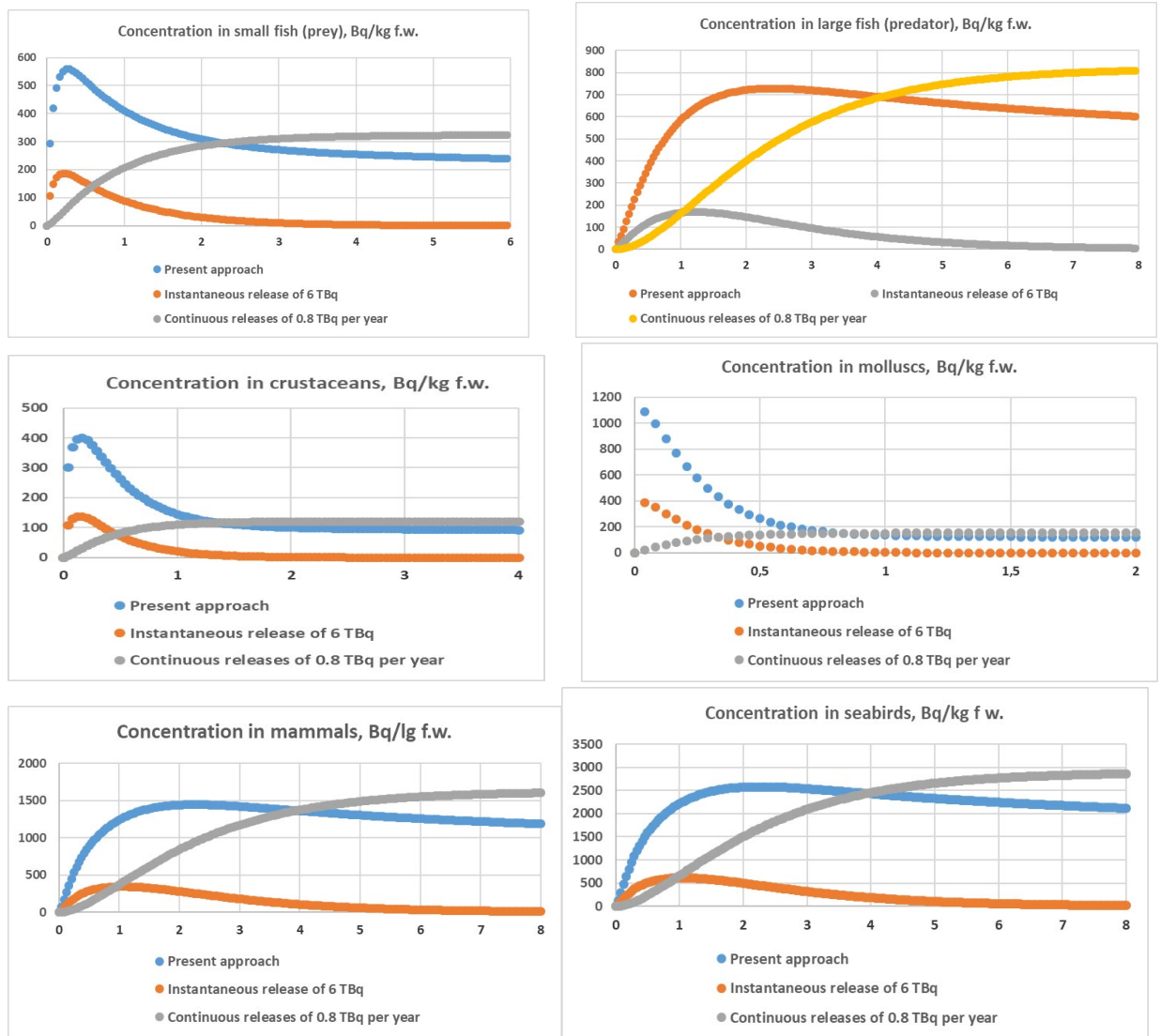
Figure 44. Comparison of the Cs-137 concentration in biota for all three scenarios. Simulations are presented within following time intervals: [0, 6] years for small fish; [0, 8] years for large fish, sea mammals and seabirds; [0, 4] years for crustaceans and [0, 2] years for molluscs.

Table 4. Maximum Cs-137 concentrations (Bq/kg f.w.) in marine biota.

	Concentration, Bq/kg f.w.		
Marine organisms	Present approach	Instantaneous release of 6 TBq	Continuous releases of 0.8 TBq per year
Fish (prey)	558	187	324
Fish (predator)	728	169	817
Crustacean	401	138	121
Molluscs	1087	391	154
Sea mammals	1445	343	1617
Seabirds	2580	613	2887

Figure 45 shows the dynamic of total doses from all three scenarios for the critical group. In addition, Figure 45 displays that the present scenario provides the maximal dose during the first four years, while the scenario with Cs-137 continuous releases of 0.8 TBq per year provides the maximum dose during the last six years of simulations (from year 5 to year 10 inclusive). Figure 45 shows also that doses from the scenario involving an instantaneous release of 6 TBq decreases dramatically with time because of strong currents, which flush out the contaminated water from the Stepovogo Bay.

Maximum values of doses for the critical group for all three scenarios are shown in Table 5.

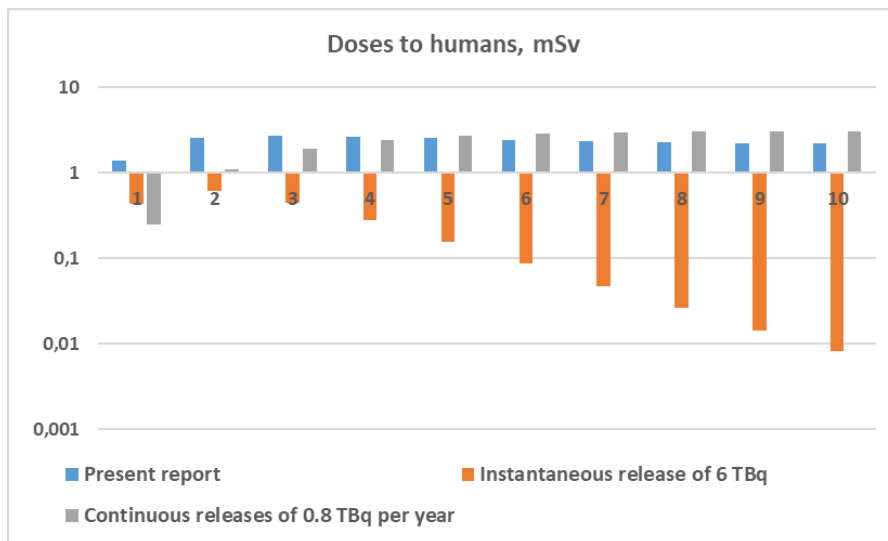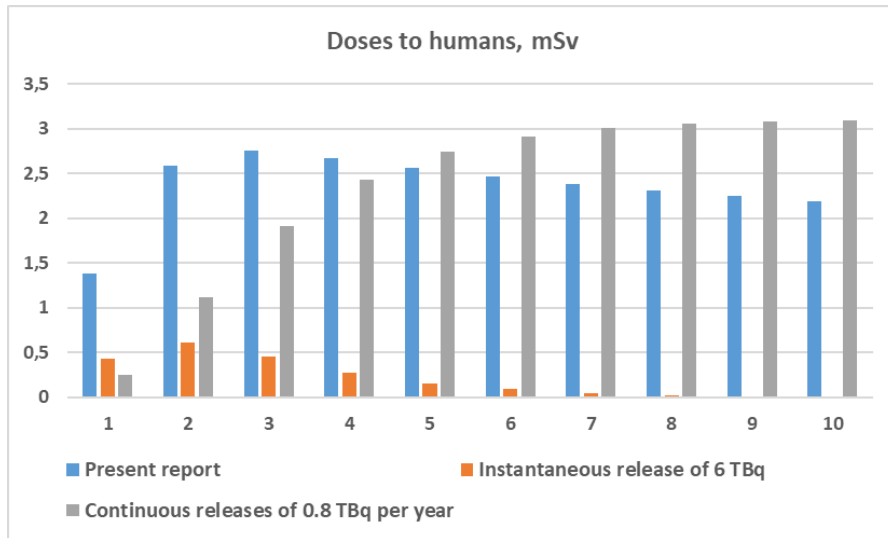Figure 45. The dynamic of total doses from all thre scenarios for the critical group during ten years with linear (top) and logarithmic (bottom) scales. Simulations are presented within time interval [0, 10] years.

Table 5. The maximum doses to humans (mSv per year)

Present approach	Instantaneous release of 6 TBq	Continuous releases of 0.8 TBq per year
2.67	0.62	3.10

Dynamic of dose-rates to biota is presented in Figure 46. Figure 46 shows that shapes of the dose-rates to crustaceans and molluscs are different in comparison with dose-rate shapes for fish, sea mammals and seabirds. These differences can be explained by the significant effects of external exposure from sediment for crustaceans and molluscs. Furthermore, Figure 46 shows that the present scenario provides the maximal concentration in fish, mammals and seabirds at initial time, while the scenario with Cs-137 continuous releases of 0.8 TBq per year provides maximum concentration in these biota after some time of exposure. Dose rates for crustaceans and molluscs are dominated by the results from the present scenario.

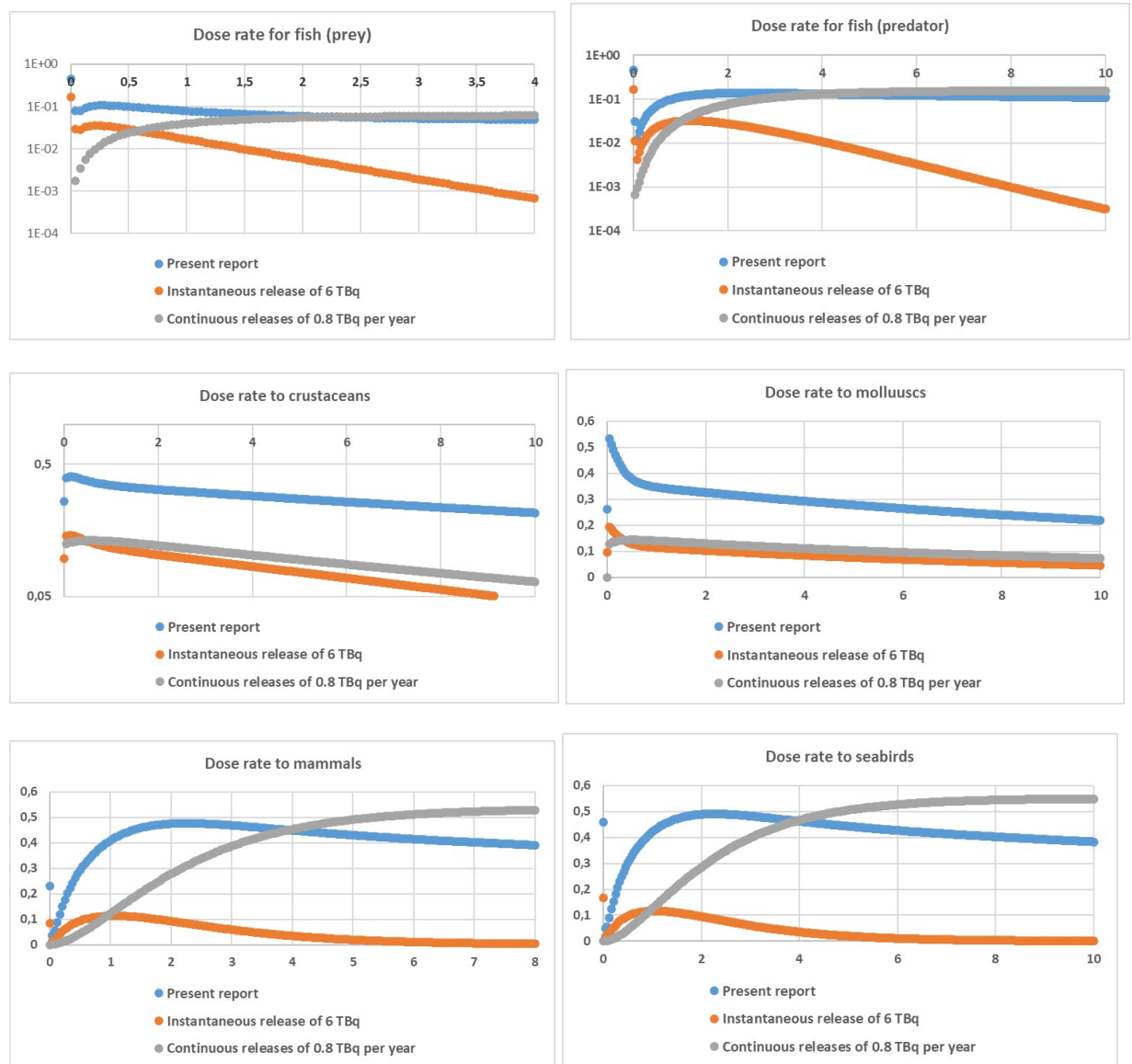

Figure 46. Dynamic of dose-rates to biota for all three scenarios, µGy/h. Simulations are presented within following time intervals: [0, 4] years for small fish (prey); [0, 10] years for large fish (predator), crustaceans, molluscs and seabirds; [0, 8] years for sea mammals.

Maximal values of concentration in biota for all three scenarios are shown in Table 6.

Table 6. The maximum Cs-137 dose-rates to biota (µGy/h).

Marine organisms	Dose-rates, µGy/h		
	Present approach	Instantaneous release of 6 TBq	Continuous releases of 0.8 TBq per year
Fish (prey)	0.46	0.17	0.16
Fish (predator)	0.46	0.17	0.16
Crustacean	0.40	0.14	0.13
Molluscs	0.53	0.19	0.14
Sea mammals	0.48	0.11	0.53
Seabirds	0.49	0.17	0.55

3.3.2   Consequences for the Gremikha Bay region

Parameters for the Stepovogo Bay are used here for as a generic local box due to the lack of information for local parameters for description of the Gremikha Bay.

Hence, all the above mentioned results for the Stepovogo Bay may be used for Gremikha Bay, except doses for human critical group due to different levels of sea food consumption across the two bays in question.

Comparison of the information concerninig the seafood consumption between the Stepovogo Bay and Gremikha Bay is shown in Table 7 (IASAP, 2003; Hosseini et al., 2016,2017).

Table 7. Seafood consumption, kg per year.

Seafood	The Stepovogo Bay	The Gremikha Bay
Fish	182.5	50
Crustacean	-	1
Molluscs	-	0.5
Sea mammals	29.2	-
Seabirds	7.3	-
Seabird eggs	7.3	-

Figure 47 and 48 show the dynamic of doses from different radionuclides and the total dose for the critical group, respectively.
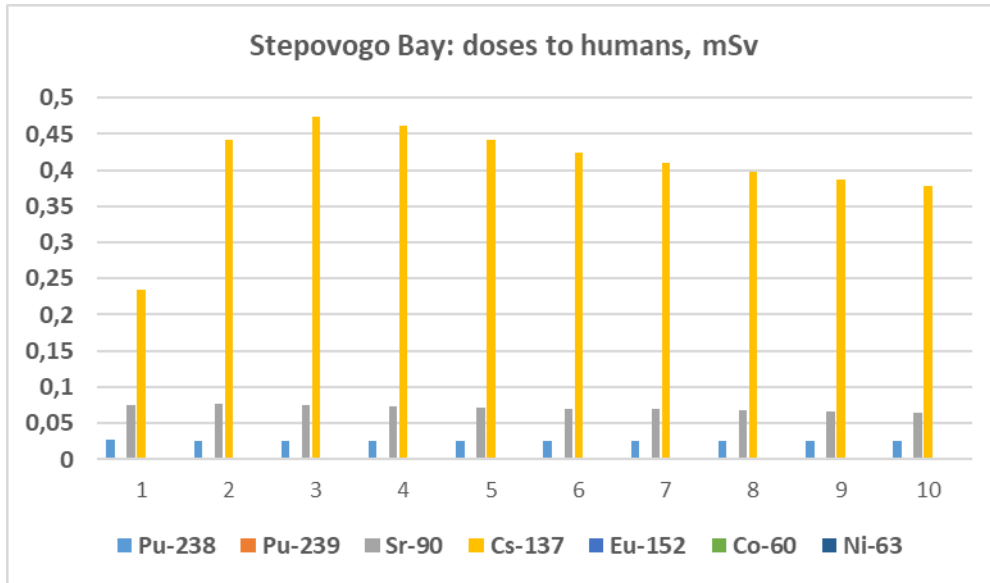
Figure 47. The dynamic of doses from different radionuclides for the critical group, mSv. Simulations are presented within time interval [0, 10] years.
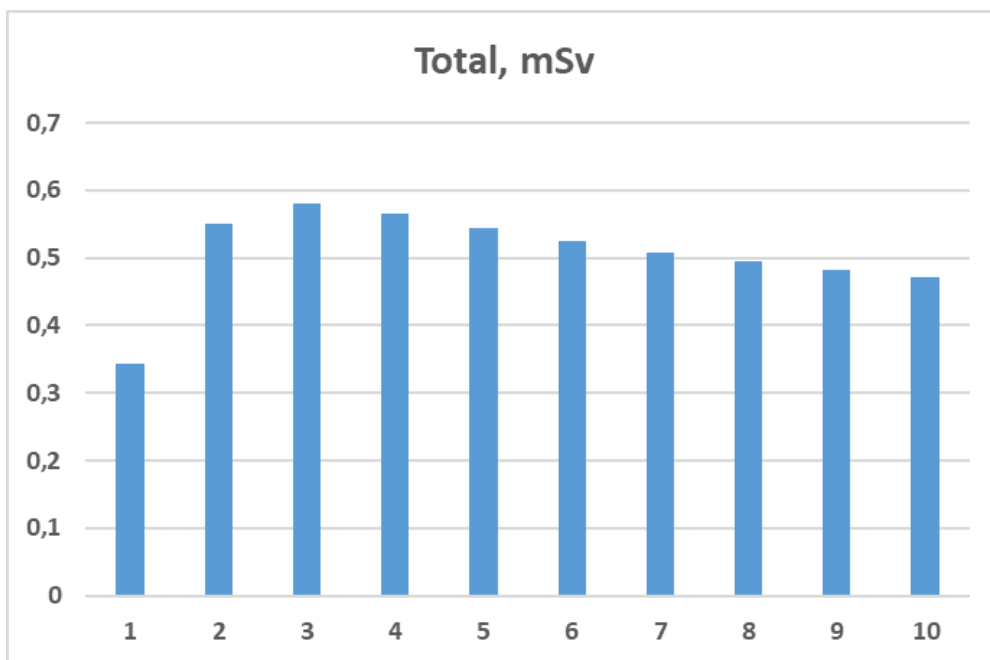
Figure 48. The dynamic of the total dose for the critical group, mSv. . Simulations are presented within time interval [0, 10] years.

Figure 49 shows that the main impact to the maximal dose for the critical group (0.58 mSv, the third year after start of radioactivity releases) corresponds to Cs-137 (82%). The dose of 0.58 mSv can be related to the dose from natural cases (2-4 mSv for this region (AMAP, 1998)), and, therefore, cannot be ignored as consequences after the potential accident with NS K-27.

Figure 49. The effects of different radionuclides to the maximal dose for the critical group at Gremikha Bay.

4 Radioecological assessment after potential accidents with the nuclear submarine K-159

4.1 Location of the potential accident with the NS K-159

Following previous reports (Hosseini et al., 2017; Brown and Hosseini, 2019), the southern part of the Barents Sea is chosen as a location for a potential accident involving NS K-159. The location is shown in Figure 50.

Figure 50. Location (a red spot) of the potential accident with the nuclear submarine K-159.
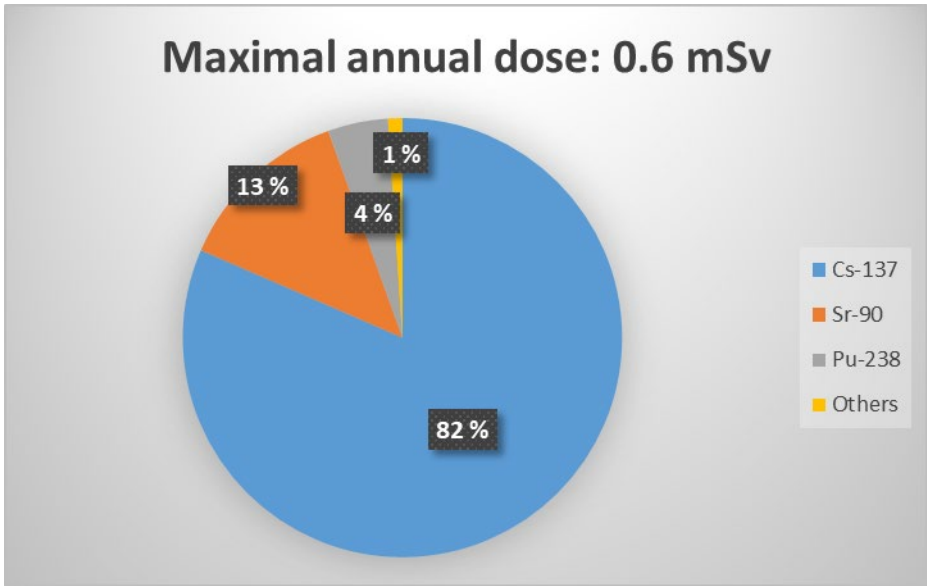
4.2 Inventory and release scenarios for NS K-159

The present study is based on the inventory of radionuclides and assumptions about radionuclide releases presented by Hosseini et al. (2017). Additionally, the two worst case scenarios for instantaneous and continuous releases of Cs-137 will be considered according to Brown and Hosseini (2019).

Similar to NS K-27, a release pattern, divided into two fractions, was assumed: (i) an instantaneous release of radionuclides and (ii) a slow long-term release similar to model the dissolution of the uranium oxide matrix. Unlike submarine K-27, NS K-159 has two reactors, which will be assumed to be identical with the same release dynamic.

Releases of radionuclides, which are chosen for the present simulations for submarine K-159 also stem from the conclusions from sections 3.3.1.4-3.3.1.5 are shown in Figure 51.
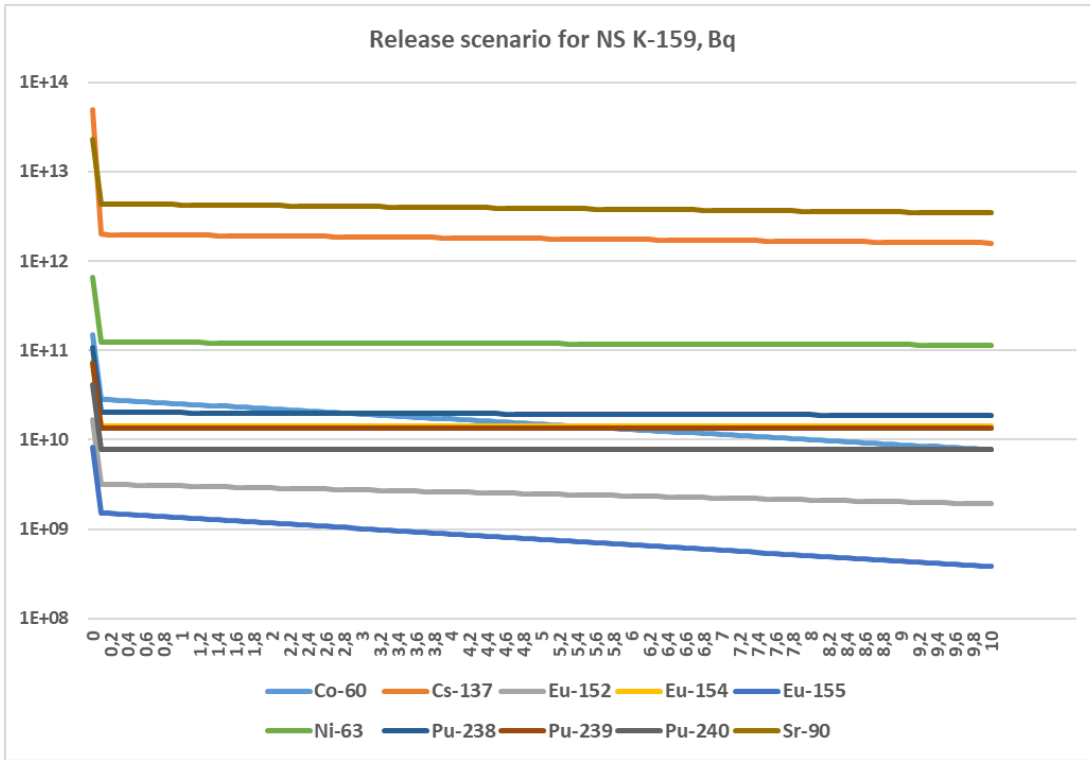
Figure 51. Instant plus continuous releases of radionuclides from NS K-159 after a potential accident.

Additionally, two release scenarios for Cs-137 will be considered (Brown & Hosseini (2019): (i) an instantaneous release of 100 TBq and (ii) continuous release of 12 TBq per year over 10 years.

4.3 Consequences after potential accident with the nuclear submarine K-159

4.3.1 Concentrations of radionuclides in water column

Results of calculations presented in Figure 52 show average concentrations of radionuclides in the filtered water of the Barents Sea (the South-East part) over one year. Simulations correspond to the five most significant radionuclides for contamination in this region. Total concentration is dominated by the Cs-137 and Sr-90.
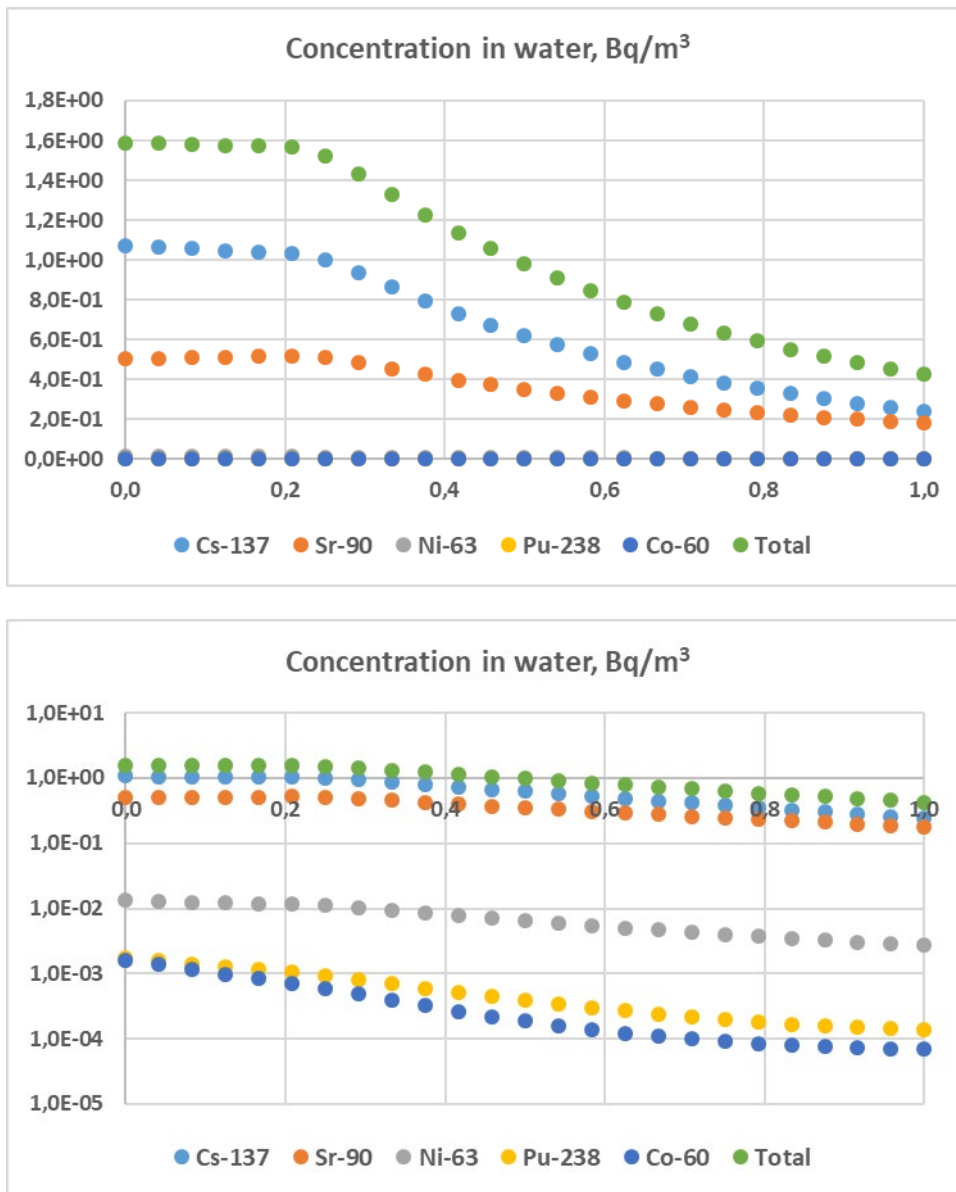
Figure 52. Dynamic of concentration in filtered water of radionuclides in the Barents Sea (the South-East part) during the first year. Results are presented in the linear (top) and logarithmic (bottom) scales. Release had started at time=zero. Simulations are presented within time interval [0, 1].

4.3.2 Concentrations of radionuclides in sediment

Results of calculations presented in Figure 53 demonstrate the five most significant radionuclides for the average contamination of the sediment in the Barents Sea (the South-East part). Total concentration is dominated by the Cs-137.
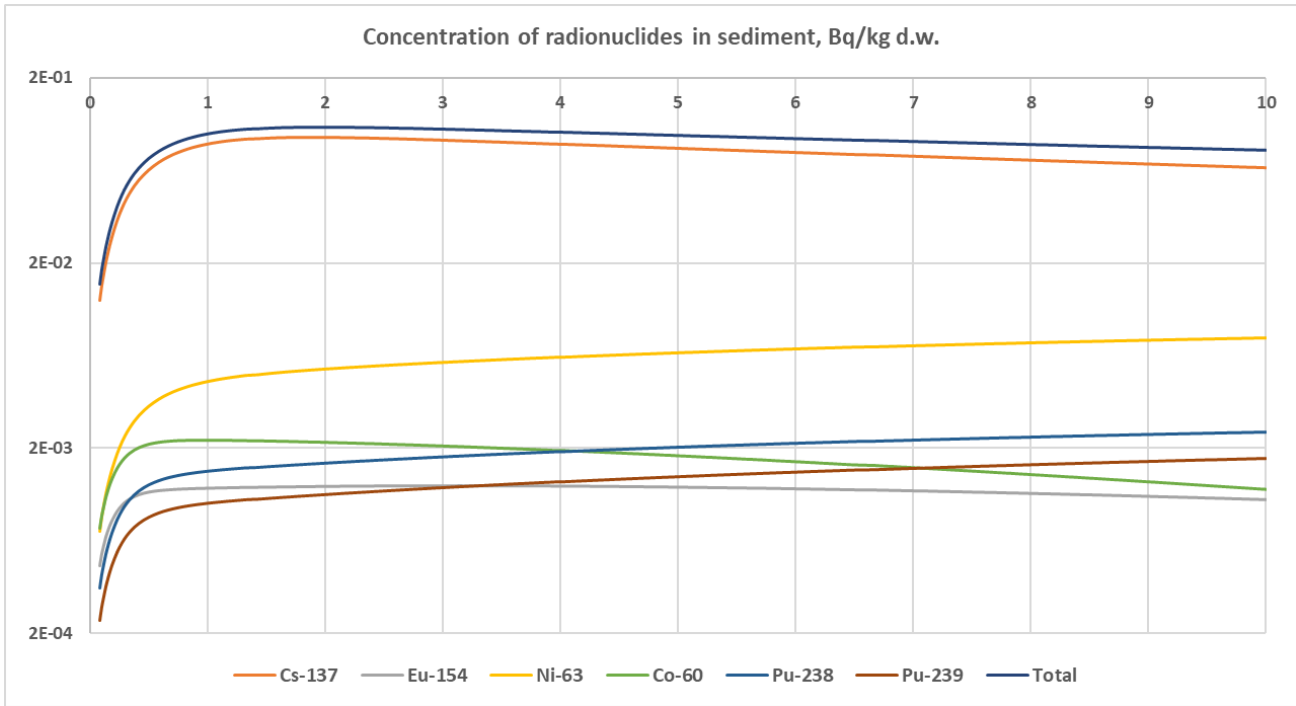
Figure 53. Dynamic of concentration of some radionuclides in sediment of the Barents Sea (the South-Eastern part). Simulations are presented within time interval [0, 10] years.

4.3.3 Concentrations of radionuclides in marine biota

Similar to section 3.3.1.6 of the present report, activity concentrations for marine organisms will be provided separately for each group of radionuclides presented in Table 1.

Figures 54-57 show that average concentration in biota for all four groups is much less than recommended guideline levels for sea food, mainly because of relatively fast mixing of the radionuclides in an open sea region (the South-East part of the Barents Sea). Low concentrations in biota means that seafood from this region can be used without any limitations, but additional monitoring of the radionuclide concentrations in biota can be provided for the local regions for control of potential uncertainties for site-specific conditions.
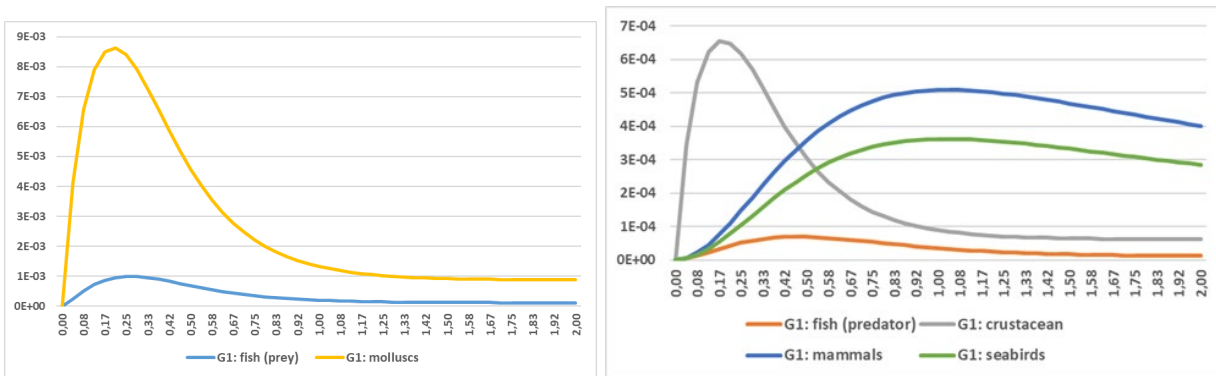
Figure 54. Concentration of radionuclides i biota for Group 1, Bq/kg f.w. Simulations are presented within time interval [0, 2] years.
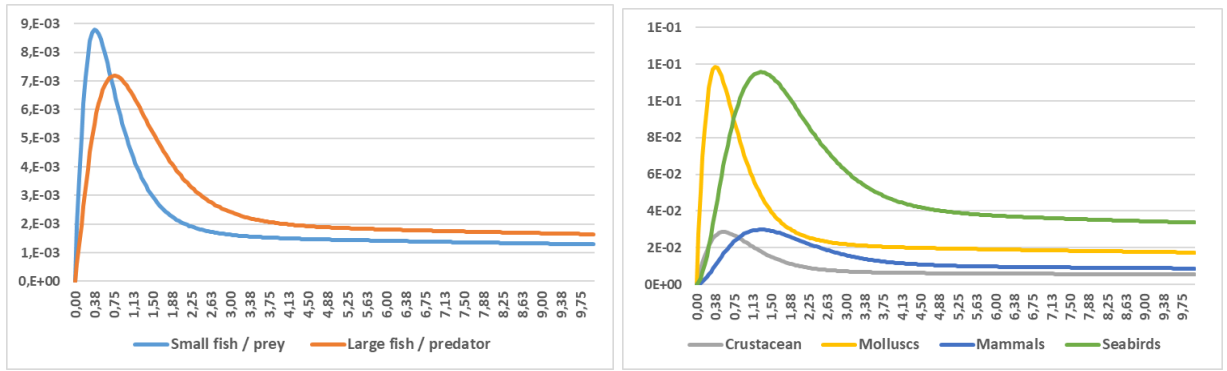
Figure 55. Concentration of radionuclides i biota for Group 2, Bq/kg f.w. Simulations are presented within time interval [0, 10] years.
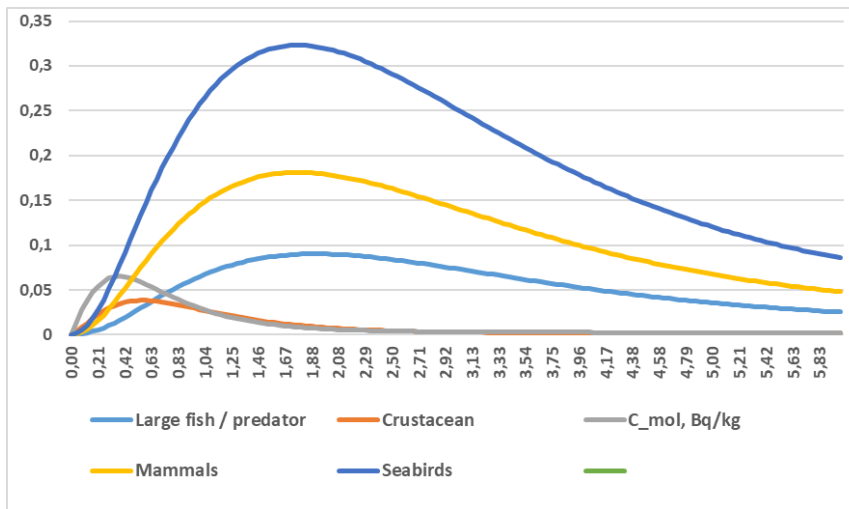
Figure 56. Concentration of radionuclides in biota for Group 3, Bq/kg f.w. Simulations are presented within time interval [0, 6] years.
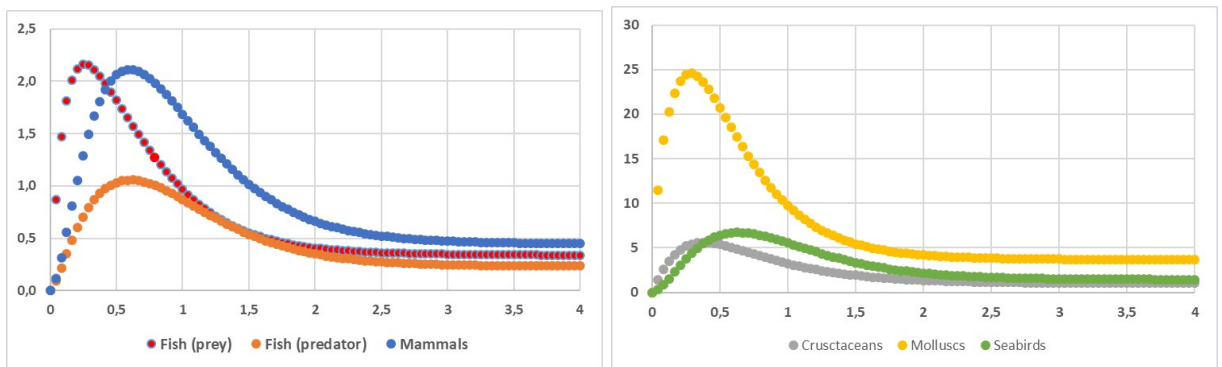
Figure 57. Concentration of radionuclides in biota for Group 4, mBq/kg f w. Simulations are presented within time interval [0, 4] years.

4.3.4 Dose estimates for the critical group of humans

For the South-Eastern part of the Barents Sea region, two critical groups will be considered: (i) the group located on the Kola Peninsula and (ii) Norwegian population located on the sea coastline with high seafood consumption. Seafood consumption for both groups is presented in Table 8.

Table 8. Seafood consumption, kg per year (IASAP, 2003; Hosseini et al., 2017, Bergsten, 2003; Iosjpe et al., 2009).

Seafood	The group located on the Kola Peninsula	The Norwegian group with a high rate consumer of seafood
Fish	50	73
Crustaceans	1	14.6
Molluscs	0.5	1.46

Figure 58 shows the dynamic of the total dose for both critical groups. Figure 59 shows that the main impact to the maximal dose for the critical group (0.06 and 0.1 μSv for groups (i) and (ii), respectively), corresponds to Cs-137 (86 and 81%, respectively).
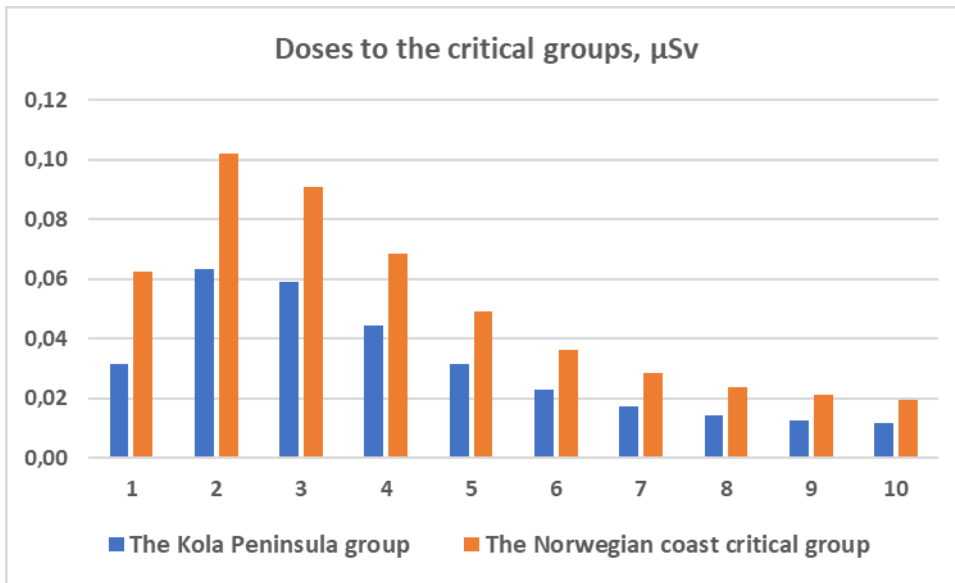
Figure 58. The dynamic of the total dose for critical groups of humans located on the Kola Peninsula and on the Norwegian coastline. Simulations are presented within time interval [0, 10] years.
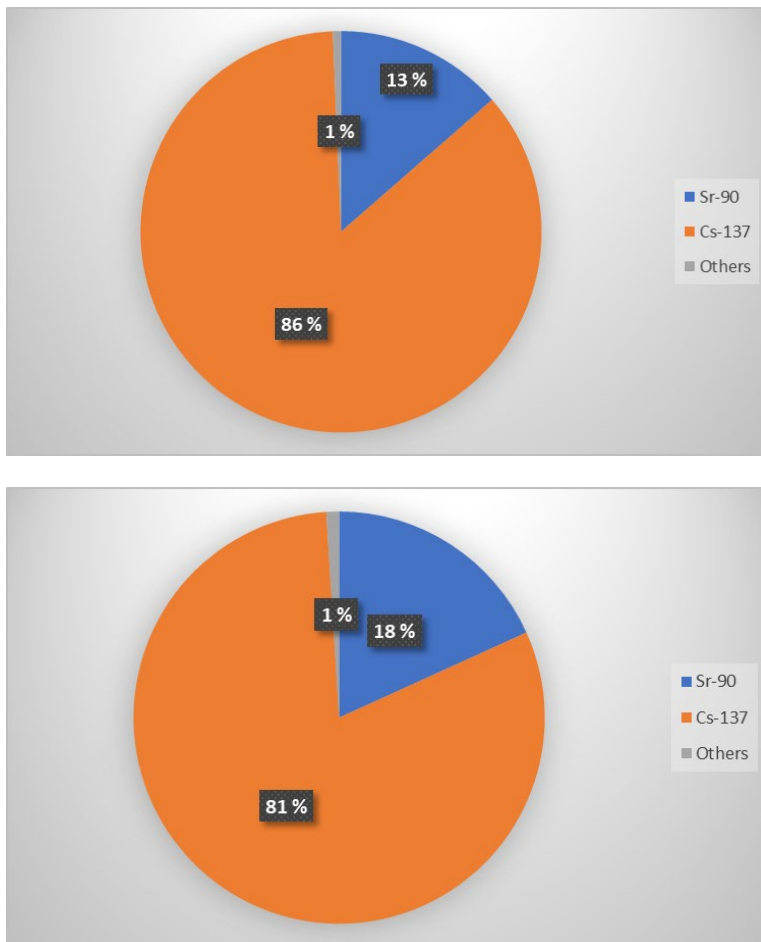
Figure 59. The impact of different radionuclides to the maximal dose for the critical groups of humans located on the Kola Peninsula (top) and on the Norwegian coastline (bottom).

4.3.5   Dose rates to marine organisms

Dose rates calculated for different marine organisms in the south part of the Barents Sea are presented in Figures 60-70. Figure 60 shows the dynamic of the dose rate (in units of μGy/h) for small fish (prey) with most significant contributions of radionuclides.

The effects of different radionuclides immediately after the accident and at a time point 106 days after the release date are presented in Figure 61. Figure 61 shows that the main effect on the dose rate immediately after the accident corresponds to Cs-137 (91%), while after some time the main effect on the dose rate is distributed between isotopes of plutonium (Pu-238, Pu-239 and Pu-240), Cs-137 and Sr-90. Differences between different impact of radionuclides in Figure 61 can be explained in the same way as in section 3.3.1.8, namely (i) dominant influence of external radiation at short times after the accident and (ii) specifics of bioaccumulation and exposure from isotopes of plutonium.
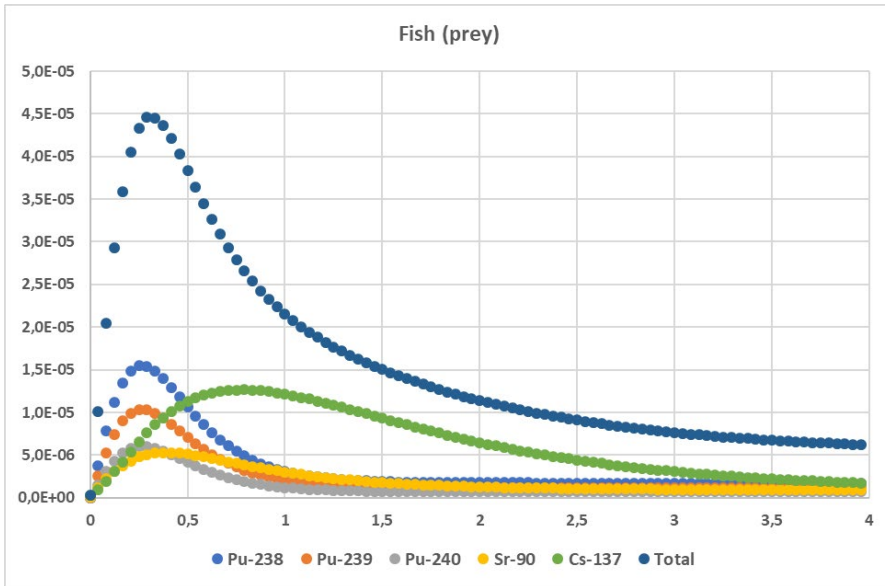
Figure 60. The dynamic of the total dose rate (in units of μGy/h) for small fish (prey) with contributions of some radionuclides, μGy/h. Simulations are presented within time interval [0, 4] years.
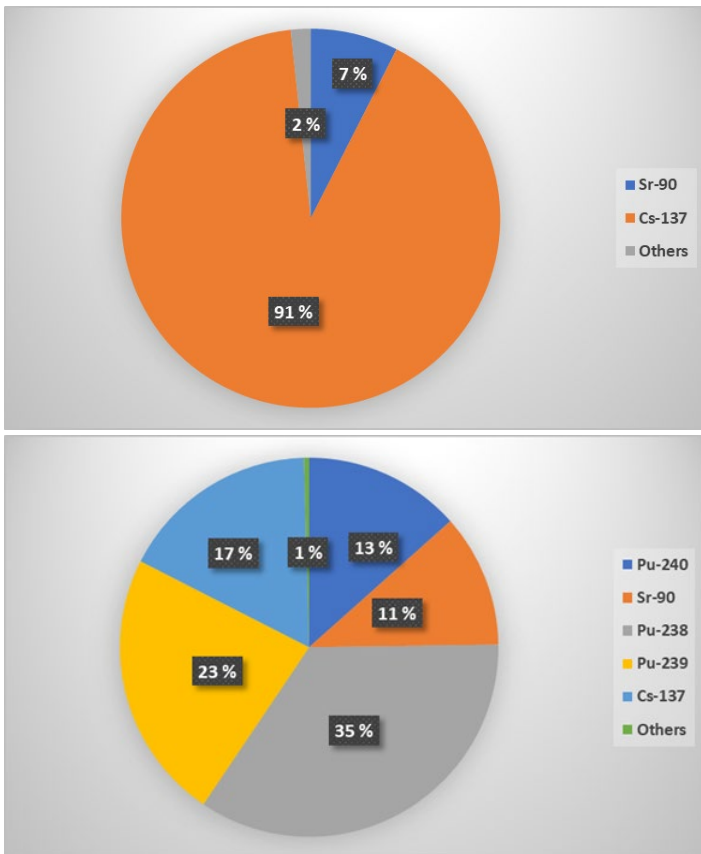
Figure 61. The effect of radionuclides on the dose rate immediately after the accident (top) and after 106 days of exposure (bottom), μGy/h .

Figure 62 shows that the dose rate from Cs-137 dominates the total dose rate over almost the entrie simulation period. At the same time, radionuclides Sr-90 and Pu-238 must also be considered.
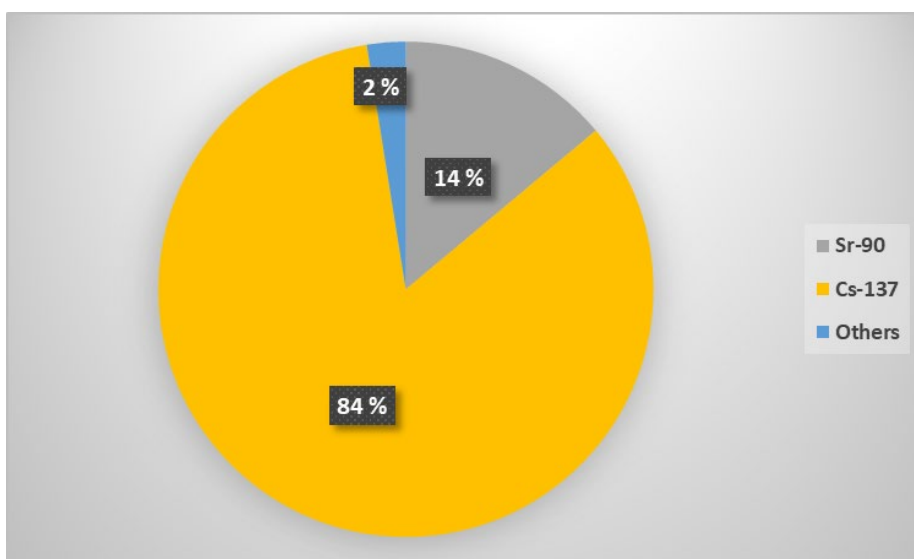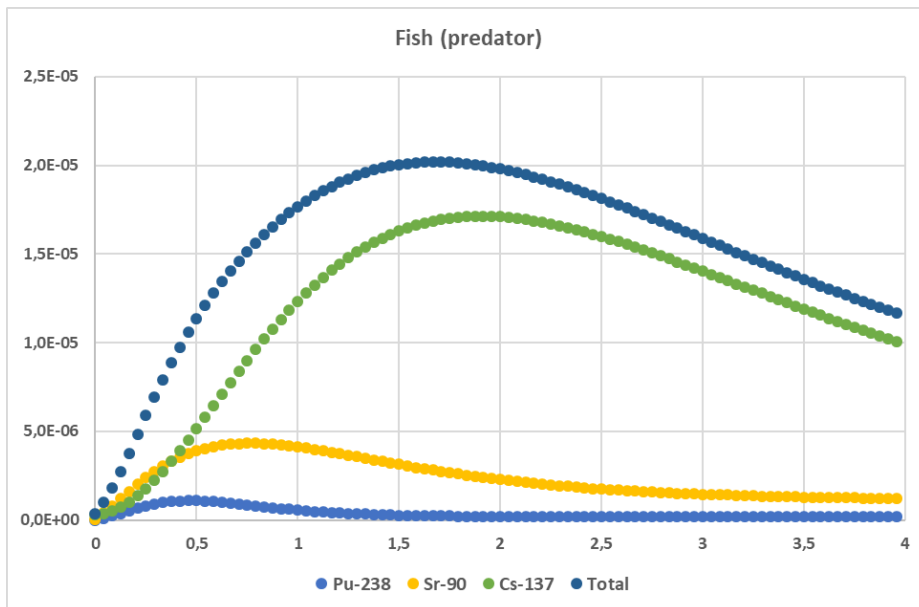
Figure 62. The dynamic of the total dose rate (in units of µGy/h) for large fish (predator) with contributions of some radionuclides (top), where simulations are presented within time interval [0, 4] years, and the effect of radionuclides on the dose rate and after 608 days of exposure (bottom).

The dynamic of total dose rates and dose rates for some radionuclides over four years for crustaceans is shown in Figure 63. The effect of different radionuclides on the crustacean (i) at initial time (immediately after the start of releases of radionuclides) and (ii) after 122 days from the start of radioactivity release, are shown in Figure 64. Figures 63-64 indicate that Cs-137 and Sr-90 dominate dose rates for crustaceans for the present release scenario. This effect is especially strong at initial time because of external exposure, which dominates completely the dose rate at this time. Figures 63-64 show that the impact from isotopes of plutonium has to be also considered.
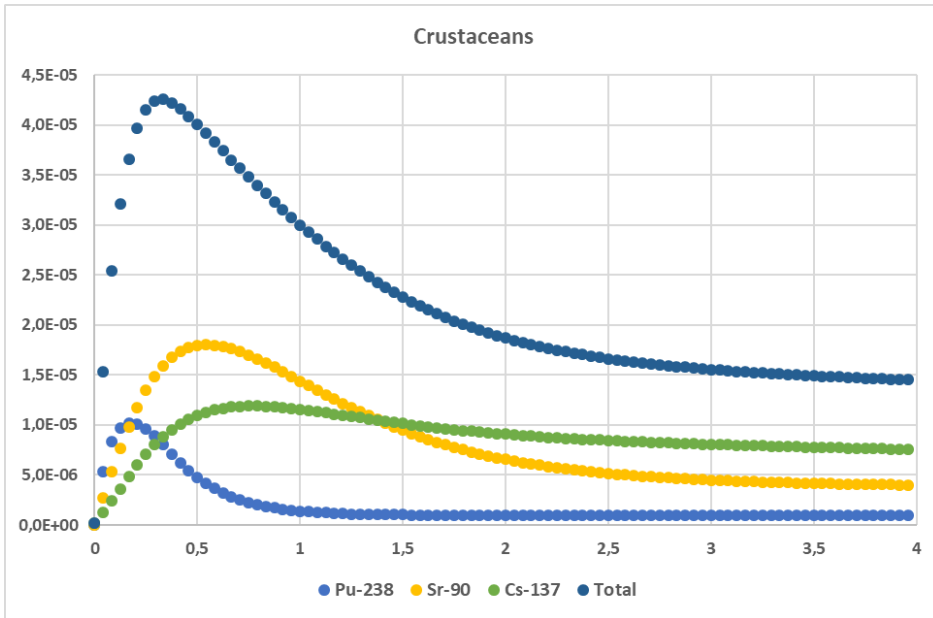
Figure 63. The dynamic of total dose rates and dose rates for some radionuclides over four years for crustaceans, μGy/h.

Figure 64. The effect of different radionuclides on the crustacean immediately after the start of releases of radionuclides (top) and after 122 days from the start of radioactivity release (bottom), μGy/h.

Figures 65-66 demonstrate that isotopes of plutonium (mainly, Pu-238) dominate dose rates for molluscs, but at initial time the dose rate is dominated by Cs-137, similar to previous results.
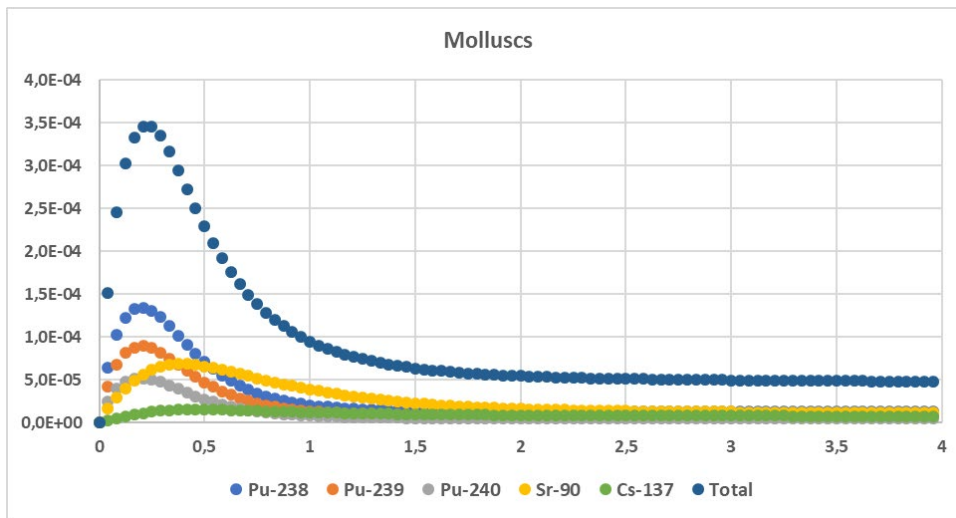
Figure 65. The dynamic of total dose rates and dose rates for some radionuclides over four years for molluscs, µGy/h.
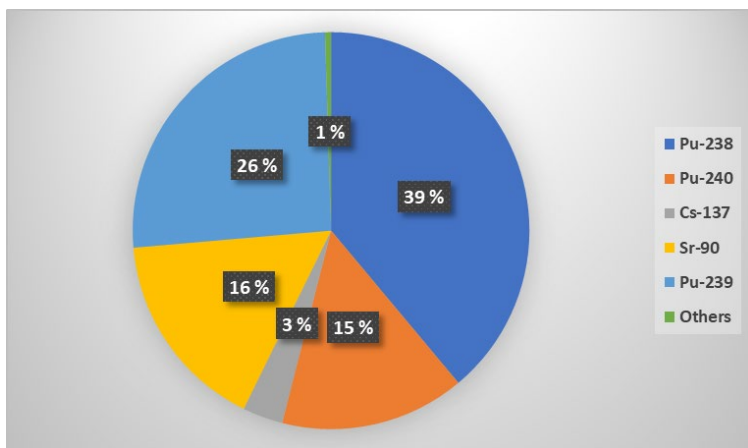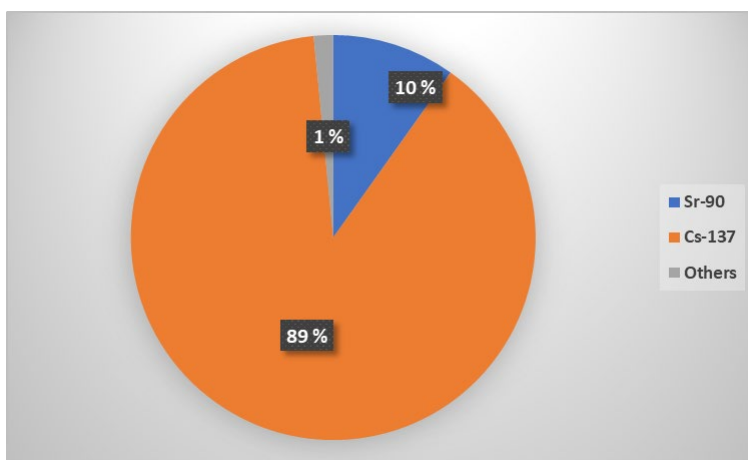
Figure 66. The effect of different radionuclides on the dose-rates for molluscs immediately after the start of releases of radionuclides (top) and after 76 days from the start of radioactivity release (bottom), µGy/h .

Figures 67-68 show that the dose rate for mammals is dominated by Cs-137 (especially at initial time). Dose-rate for mammals peaks at 1.5 years, approximately. Cs-137 dominates the dose-rate at this time, but other radionuclides such as Sr-90 and Pu-238 have to be also considered.
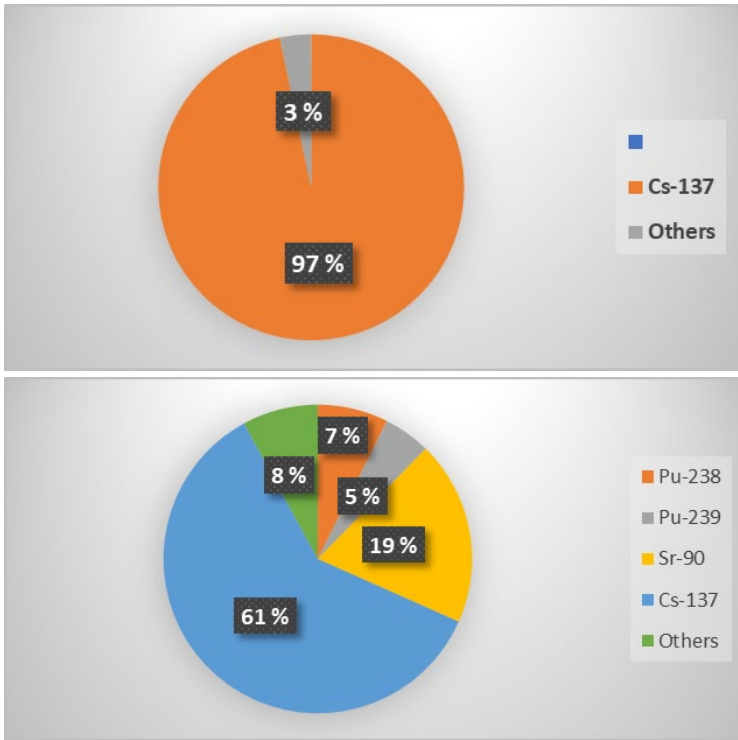
Figure 67. The effect of different radionuclides on the dose rate for mammals immediately after the start of releases of radionuclides (top) and after 562 days from the start of radioactivity release (bottom), µGy/h .
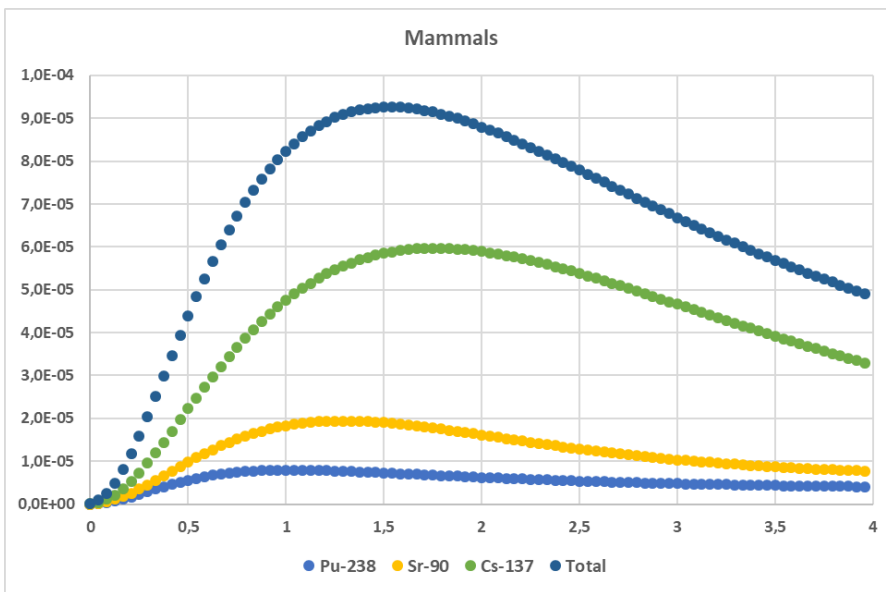
Figure 68. The dynamic of total dose rates with effect of most significantradionuclides for mammals, µGy/h. Simulations are presented within time interval [0, 4] years.

Figures 69-70 show that the dose rate for seabirds is dominated by Cs-137 and Sr-90. Cs-137 dominates the dose rate immediately after the start of release, then Sr-90 dominates dose rate for birds during the first two years, approximately, and finally, Cs-137 dominates the dose rate until the end of the simulations (ten years).
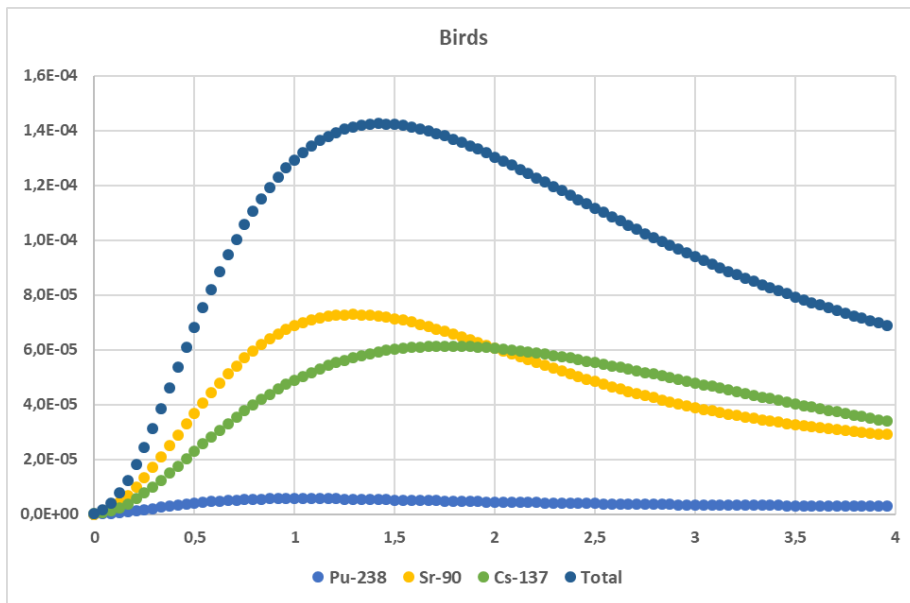
Figure 69. The dynamic of total dose rates with effect of most significant radionuclides for seabirds, µGy/h. Simulations are presented within time interval [0, 4] years.
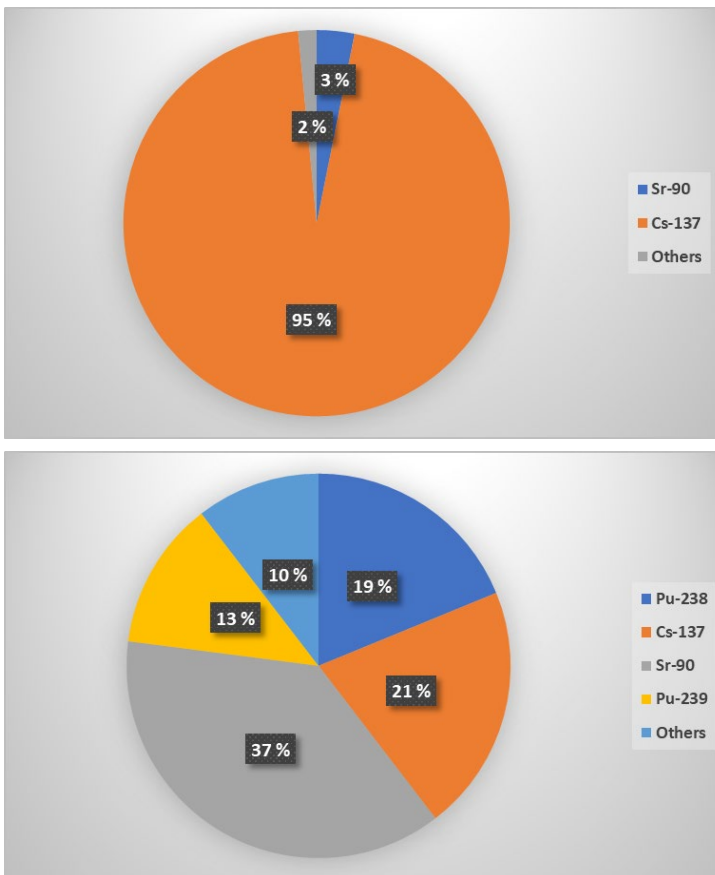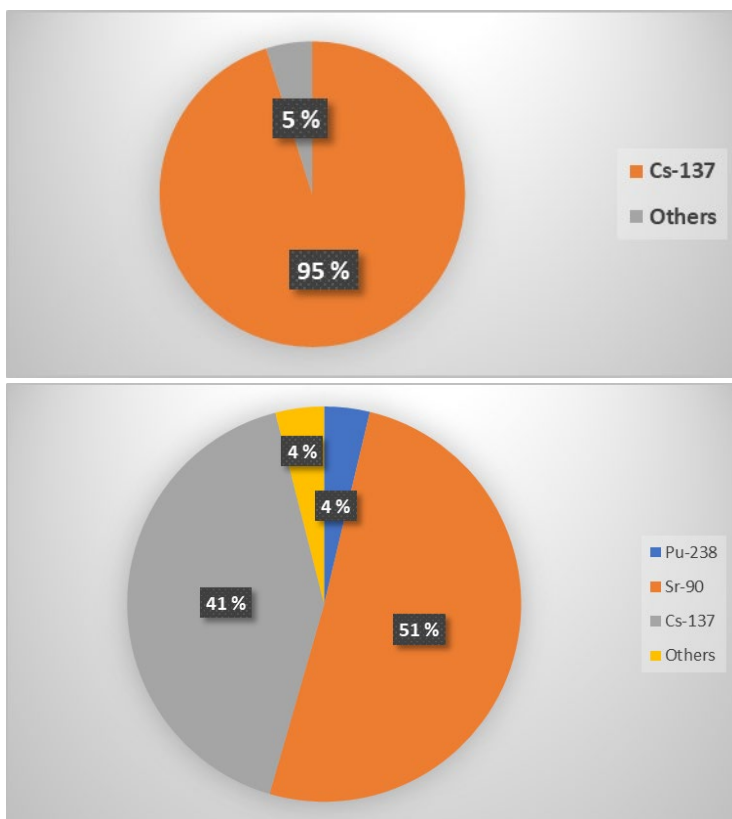

Figure 70. The effect of different radionuclides on the dose rate for seabirds immediately after the start of releases of radionuclides (top) and after 1.5 year of simulations (bottom), approximately, µGy/h .

The maximum values of the dose-rates for marine organisms are shown in Table 9. The calculations show that dose rates for all marine organisms do not exceed the screening dose (10 µGy/h), which is considered as safety level for potential damages for biota.

Table 9. The maximum dose-rates (µGy/h) in marine biota.

Marine organisms	Dose-rate, µGy/h
Fish (prey)	4.5E-5
Fish (predator)	2.0E-5
Crustacean	4.3E-5
Molluscs	3.5E-4
Sea mammals	9.3E-5
Seabirds	1.4E-4

4.3.6 Consequences after additional scenarios for Cs-137

Two additional scenarios for potential releases of Cs-137 (100 TBq instantaneous and 12 TBq continuous) will be evaluated in this section. Scenarios are selected from the report (Brown & Hosseini, 2019).

Concentrations in water and sediment for the south part of the Barents Sea are compared in Figure 71 for all three scenarios. Concentration after instantaneous release of 100 TBq of Cs-137 decreases for both water and compartments, but at the same time this scenario gives the highest values of Cs-137 concentrations at the initial time of simulation for water and at all time-points for simulations pertaining to sediment. The scenario with continuous releases dominates the contamination in the water column after three years of exposure, approximately. The main reason for this dominance of the selected scenarios is the fact that they correspond to the very high release of Cs-137 into the marine environment.
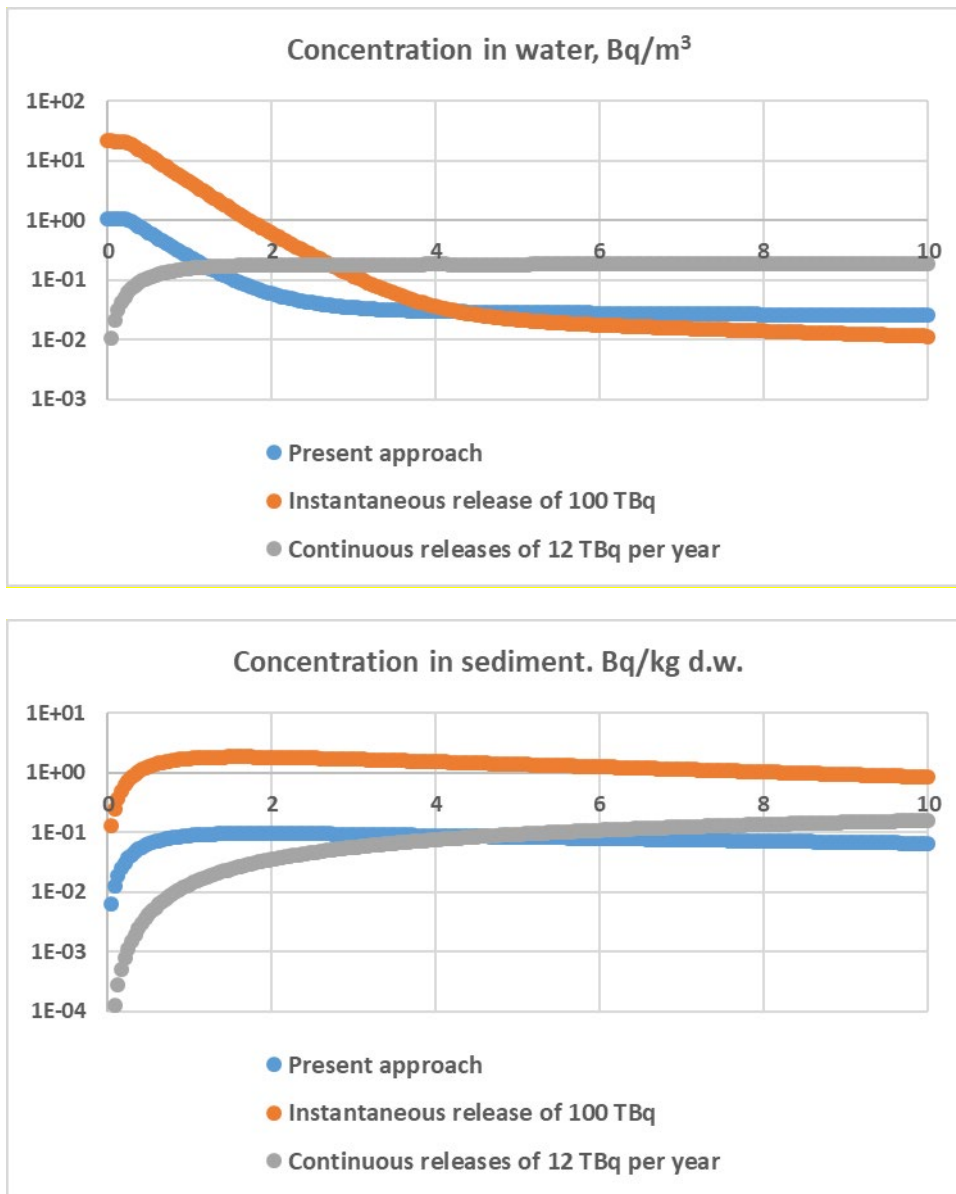
Figure 71. Concentrations in water (top) and sediment (bottom) for the considered region (the south part of the Barents Sea). Simulations are presented within time interval [0, 10] years.

Differences for concentrations in marine organisms for the considered release scenarios depend only on differences of Cs-137 concentration in filtered water. Therefore the shapes of differences for all marine organisms are, approximately, similar. Figure 72 shows comparison of the Cs-137 concentration in considered marine organisms. Figure 72 shows that the scenario with instantaneous release of 100 TBq of Cs-137 provides the maximal concentration in biota during first 3-8 years of exposure, approximately, while the scenario with Cs-137 continuous releases of 12 TBq per year provides maximum concentration in biota after this time.

Maximal values of concentration in biota for all three scenarios are shown in Table 10.
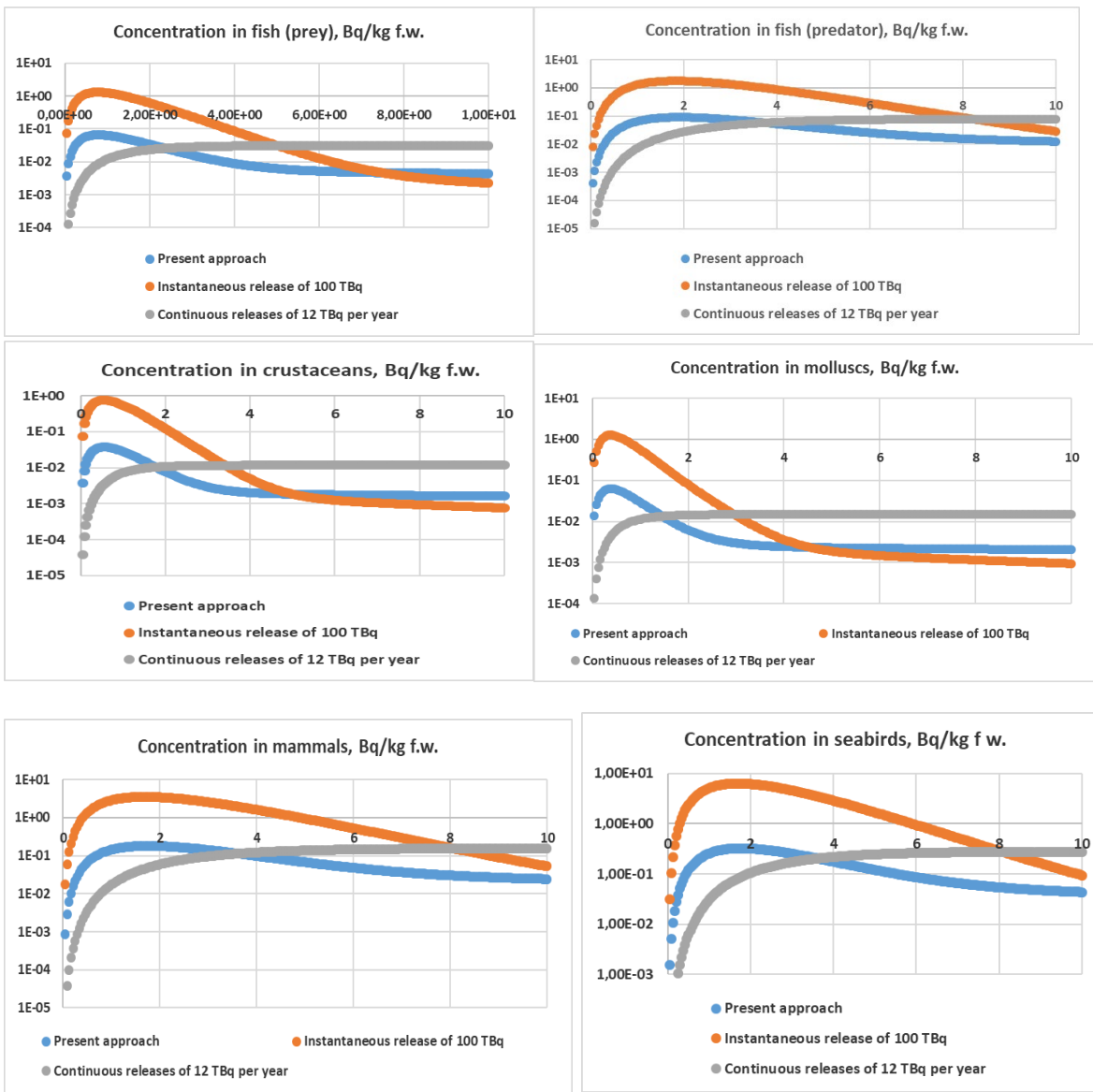
Figure 72. Comparison of the Cs-137 concentrations in biota for all three scenarios. Simulations are presented within time interval [0, 10] years.

Table 10. The maximum Cs-137 concentrations (Bq/kg f.w.) in marine biota.

Marine organisms	Concentration, Bq/kg f.w.		
	Present approach	Instantaneous release of 100 TBq	Continuous releases of 12 TBq per year
Fish (prey)	6.6E-2	1.3	3.1E-2
Fish (predator)	9.0E-2	1.8	7.9E-2
Crustacean	3.8E-2	7.8E-1	1.2E-2
Molluscs	6.3E-2	1.3	1.5E-2
Sea mammals	1.8E-1	3.5	1.6E-1
Seabirds	3.2E-1	6.3	2.8E-1

Figures 73-74 show the dynamic of total doses from all three scenarios for the critical groups located on the Kola Peninsula and on the Norwegian coastal line. Figures 73-74 display that the scenario with instantaneous release of 100 TBq of Cs-137 provides the maximal dose during first eight years, while the scenario with Cs-137 continuous releases of 12 TBq per year provides the maximum dose during the last two years of simulations. These results can be easily expanded by combination of two factors: (i) dynamic of the large fish (predator) contamination, presented in Figure 72, where we have dominance of the instantaneous scenario of 100 TBq in comparison with other scenarios during the first eight years and (ii) the large fish is main source for human doses.

Maximum values of doses for the critical group for all three scenarios are shown in Table 11.
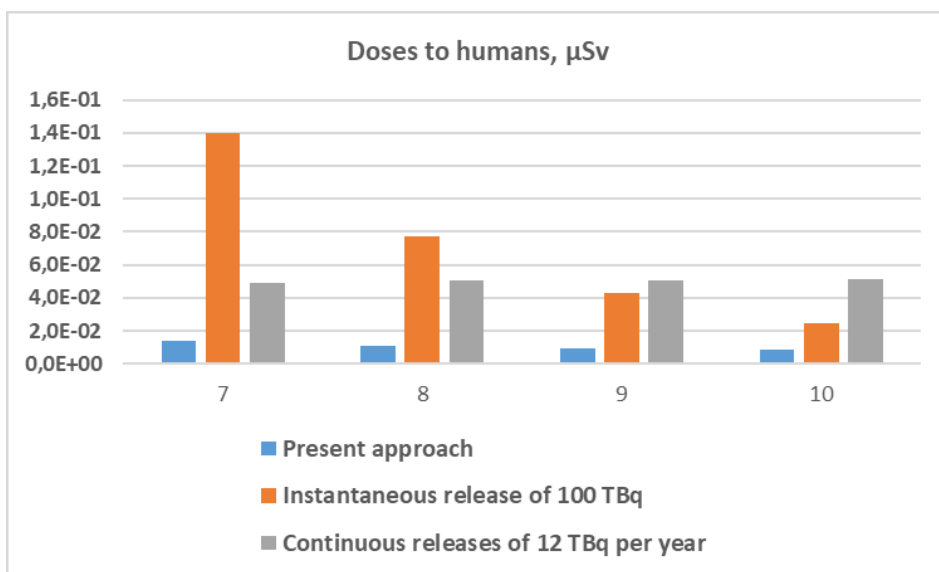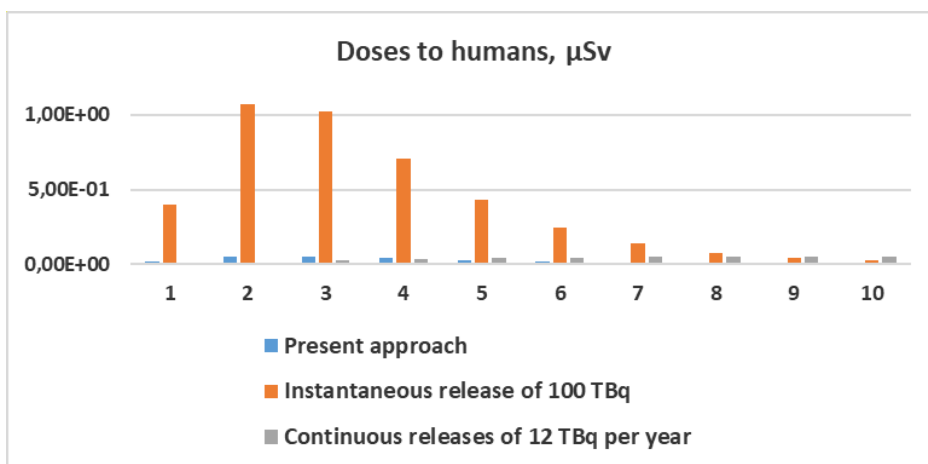
Figure 73. The dynamic of total doses from all three scenarios for the critical group located on the Kola Peninsula during ten years (top) and last four years (bottom), μSv per year.
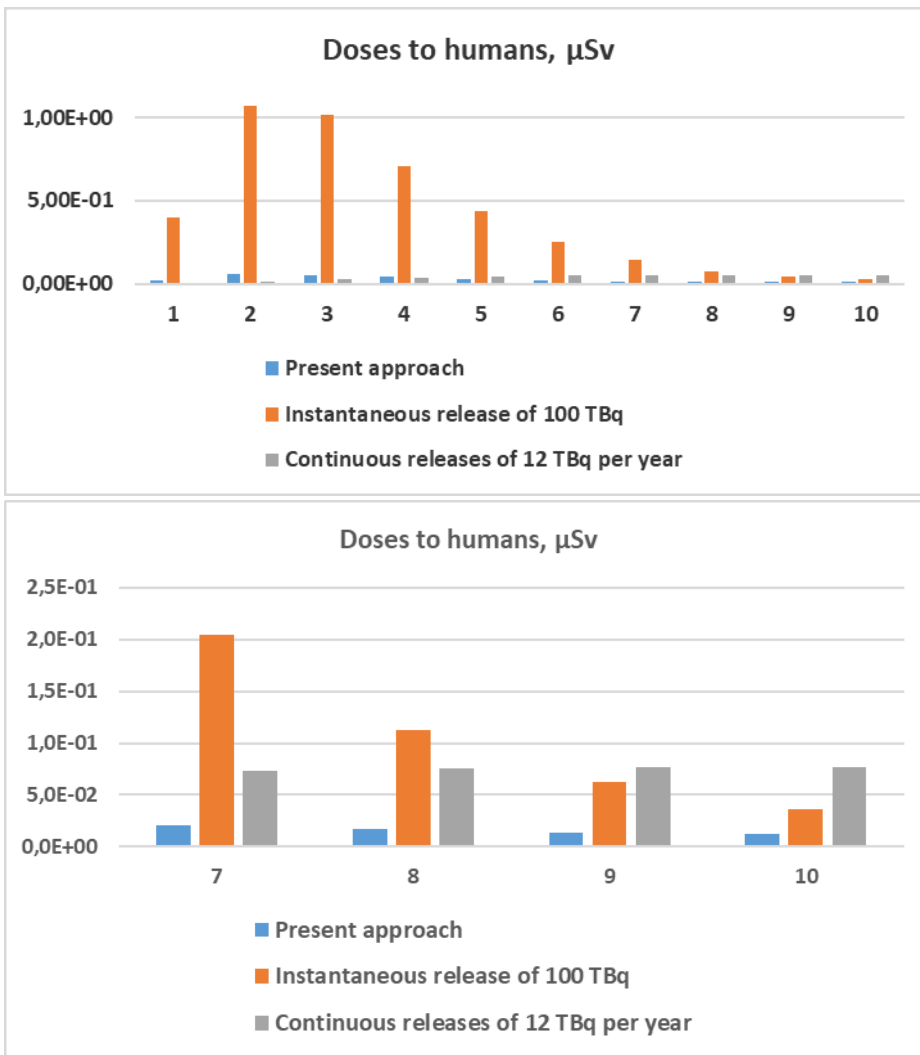
Figure 74. The dynamic of total doses from all three scenarios for the critical group located in Norway during ten years (top) and last four years (bottom), µSv per year.

Table 11. The maximum doses to humans (µSv per year)

Present approach	Instantaneous release of 100 TBq	Continuous releases of 12 TBq per year	Location
5.45E-2	1.07	5.13E-2	The Kola Peninsula
8.24E-2	1.62	7.71E-2	The Norwegian coastal line

Dynamic of dose-rates to biota is presented in Figure 75. Figure 75 shows that the scenario with instantaneous release of 100 TBq of Cs-137 provides the maximal dose-rates to biota during first 5-8 years of exposure to fish, all time of simulations (10 years) for crustaceans and mollusks and 8 years for sea mammals and seabirds. The scenario with Cs-137 continuous releases of 12 TBq per year provides maximum dose-rates to fish, sea mammals and seabirds after this time.
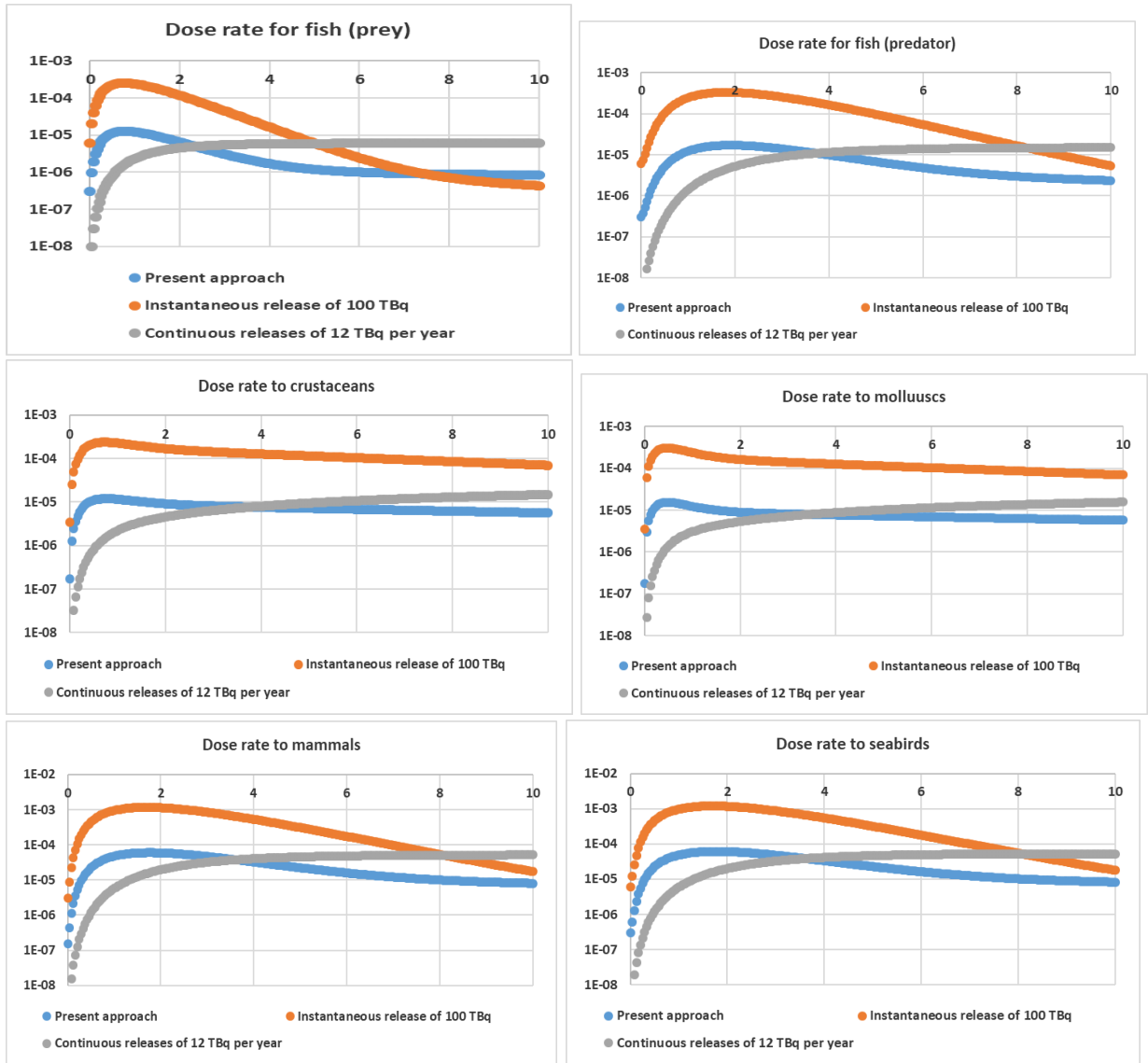
Figure 75. Dynamic of dose-rates to biota for all three scenarios, µGy/h. Simulations are presented within time interval [0, 10] years.

Maximal values of concentration in biota for all three scenarios are shown in Table 12.

Table 12. The maximum Cs-137 dose-rates to biota (µGy/h).

Marine organisms	Dose-rates, µGy/h		
	Present approach	Instantaneous release of 100 TBq	Continuous releases of 12 TBq per year
Fish (prey)	1.3E-5	2.5E-4	6.6E-6
Fish (predator)	1.7E-5	3.4E-4	1.5E-5
Crustacean	1.2E-5	2.4E-4	1.5E-5
Molluscs	1.6E-5	3.1E-4	1.6E-5
Sea mammals	6.0E-5	1.2E-3	5.1E-5
Seabirds	6.1E-5	1.2E-3	5.3E-5

4.3.7   Notes about different modelling approaches for radioelogical assessment

As previously described, this report provides additional information on radioecological assessment following potential releases of radionuclides in the marine environment, which is a supplement to previous results presented in (Brown & Hosseini, 2019; Hosseini et al., 2016, 2017).

Contrary to results for Stepovogo and Gremikha Bays, simulations for the Barents Sea are significantly different from the results presented in (Brown & Hossein, 2019; Hosseini et al., 2017).

These differenses can be mainly explained by the diferent modelling approaches, which have been used in this report and reports published by Brown & Hosseini (2019) and Hosseini et al. (2017). Therefore, a number of points should be noted for better understanding of the source for differences between these results.

As mentioned above, radioecological assessment includes the following aspects: (i) dispersion of radionuclides in the marine environment; (ii) concentration of radionuclides in marine organisms based on point (i). (iii) dose assessment for humans based here on (ii) and (iv) dose assessment for biota based on points (i) and (ii).

The methodology for the calculation of the points (ii), (iii) and (iv) in the present report and reports (Brown & Hosseini 2019) and (Hosseini et al., 2017) are the same or closely related, while modelling approaches for the description of the dispersion of radionuclides are significantly different.

The results presented in reports (Brown & Hosseini 2019) and (Hosseini et al., 2017) are based on the propagation of radionuclides in the ocean space in accordance with a high-resolution hydrodynamic model. The results of this report are based on the propagation of radionuclides in the oceanic space, divided into boxes.

We will briefly examine the differences between the two model approaches. Hydrodynamic models provide modeling based on the fine resolution of the ocean space and supplement information regarding currents, heat fluxes, winds, ice cover, etc. Box modelling uses more or less not so fine (or 'low resolution') compartments in the oceanic space and average advection of the water masses. It is obvious that hydrodynamic modeling can provide more accurate results for the dispersion of radionuclides compared to box modeling provided the necessary information. On the other hand, it is impossible to have satisfactory information on, for example, winds and currents for prediction of dispersion radionuclides in the future. For such predictions, box modeling can provide more accurate and robust simulations. During the IAEA MODARIA program, radionuclide scattering simulations from the hydrodynamic models (Eulerian and Lagrangian) and box models were tested and compared with monitoring data (Periáñez et al., 2016; Periáñez et al., 2016a). It was noted that an "ideal" model that can be used on all spatial-temporal scales does not exist (Periáñez et al., 2016).

Let us now consider some special features of the high-resolution hydrodynamic model (Antipov et al., 2015; Sarkisyan, et al., 2010; Ibraev et al., 2012), which is the basic model for results of radionuclide dispersion in reports (Brown & Hosseini 2019) and (Hosseini et al. 2017).

The model has a resolution of about 3 km on a horizontal grid and the vertical resolution of the grid is 49 levels with a variable step (6 m in the upper layer. If the volume of $3 \cdot 3 \cdot 6 \cdot 10^9$ m^3 will be used as the starting volume for the release of 50 TBq Cs-137, the initial concentration in this

volume will be equal to $9.26 \cdot 10^5$ Bq/m³ at time 0 (beginning of dispersal process). In about a month the concentration of Cs-137 will be in range of 100-1000 Bq/m³ in the larger area (20 × 180 km) with volume of $5 \cdot 10^{10} - 5 \cdot 10^{11}$ m³. This estimate corresponds to the results in Figure 76, adopted from the report (Brown & Hosseini 2019). It is necessary to note that this region of high concentration of radionuclides is a relatively small part of the actual part of the Barents Sea (10%, approximately). The other parts of the Barents Sea have much lower concentration of Cs-137 (up to zero). In contrast to the fine resolution hydrodynamic model described by Antipov et al. (2015), the box for radionuclide releases for the simulations in this report (the southeastern part of the Barents Sea) has volume $4.59 \cdot 10^{13}$ m³. And since box modeling uses a uniform distribution of radionuclides in the boxes, the initial radionuclide concentration in the box will be 2-3 orders of magnitude lower than the concentration predicted by the hydrodynamic model under the initial phase of radionuclide dispersion. At the same time, the average concentration of radioactivity in the region must be much better matched between the models due to (i) a relatively small part of the Barents Sea with a high radioactivity concentration predicted by the hydrodynamic model and (ii) non-instantaneous mixing in the oceanic space of the present the box modeling approach, where the concentration of radionuclides exhibits practically no reduction in the box during the first 100 days, approximately, as shown in Figure 52 (time for propagation of radioactivity within the initial box). It is also noticeable that Figures 52 and 76 show similar results for the Cs-137 concentration after 100 days, approximately.
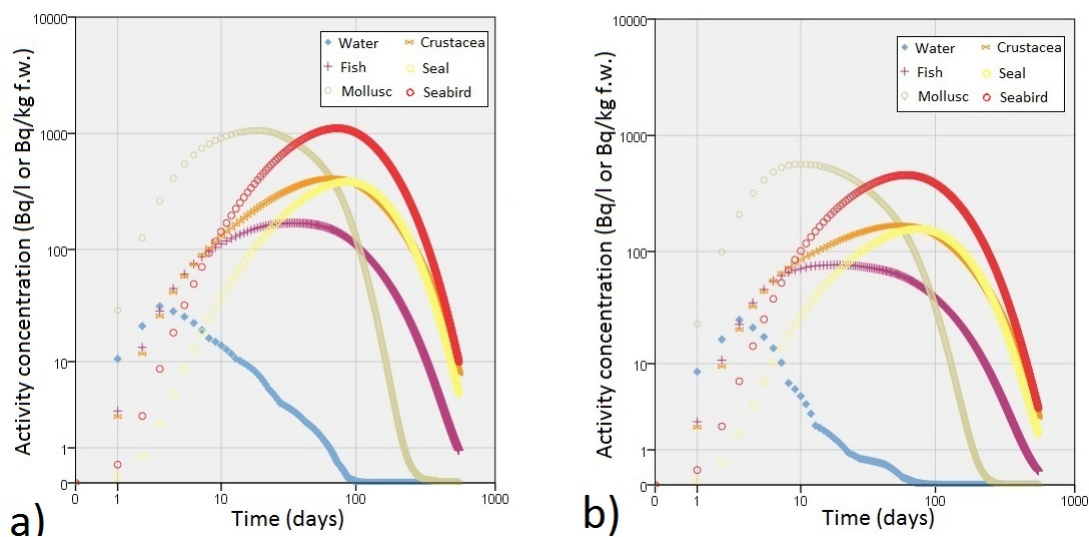
Figure 76. Maximum activity concentrations of Cs-137 in sea water (Bq/l), fish, molluscs, crustaceans, seals and seabirds (Bq/kg f.w.) associated with instantaneous releases to the marine environment at a) the seabed (NS K-159 burst at the bottom) and b) the surface (NS K-159 burst at the surface).

Therefore, it is possible to made a statement about compatible average concentration between both modelling approaches, while the hydrodynamic model describe propagation of radioactivity in the sea in a much more detailed way than the box modelling during the initial time after potential accident. It is interesting to note that this statement supports one of the recommendations from Periáñez et al. (2016) to use the different dispersion modes: For estimating radioactivity propagation in hours, days and months, it is better to use Lagrangian and Eulerian hydrodynamic models, but to estimate the spread of radioactivity over time for years, it is better to use box modeling.

Furthermore, spatial distributions of biota in the Barents Sea are presented, for example, in (Ingvaldsen & Gjøsæter, 2013; Eriksen et al., 2012; Fall et al., 2018). Radioecological assessment is based on evaluation of concentration of radionuclides in biota. It is difficult to associate a concentration of radionuclides in different marine organisms with the concentration of

radioactivity in a water column without averaging over significant sea regions in the absence of natural boundaries (for example, bays and fjords). Perhaps that is why concentrations in marine organisms in (Antipov et al. 2015) may only be presented in comparison with the parts of an ocean with different concentrations of Cs-137, because it will otherwise be necessary to use additional assumptions about potential movement and residence time for marine organisms in different parts of the Barents Sea.

Finally, the reports (Brown & Hosseini 2019) and (Hosseini et al., 2017) as well as the current report use a conservative estimate of potential release scenarios for radionuclides. From this point of view, the results of the potential accident with the K-159 submarine in the Barents Sea presented in this report, correspond to the average concentrations in marine environment and biota for the conservative scenarios, while the high concentration values in the water column and biota presented in (Brown & Hosseini 2019) and (Hosseini et al., 2017) corresponds to the maximum potential constraints for these endpoints. It is also important that the results presented in (Antipov et al., 2017; Brown & Hosseini 2019 and Hosseini et al., 2017) can be used concurrently with monitoring for estimating real releases of radionuclides from submarine K-159 in the event of an actual accidental release.

5   Conclusions

The present report can be viewed as a supplement to the previously published results (Hosseini et al., 2015, 2016, 2017; Brown and Hosseini, 2019), and provides additional information concerning radioecological assessment after potential releases of radionuclides into marine environment following a possible accident involving a Russian nuclear submarine of the types K-27 and K-159.

As an addition to the previous studies (Hosseini et al., 2015, 2016, 2017; Brown and Hosseini, 2019), the present simulations were carried out with two factors: (i) the water-sediment interactions into the process of distribution of radionuclides in the marine environment and (ii) a wide set of radionuclides. This radioecological assessment was done in part to allow for a comparison with the previous studies.

Present simulations have been carried out using the modified approach for compartmental modelling, which uses the non-instantaneous dispersion of radioactivity in the marine environment.

These simulations demonstrate that there are two factors particularly important for radioecological assessment: (i) selection of release scenarios and (ii) initial location for potential releases including geographical positions, water exchange between surrounding sea regions and biota close to the source of contamination. For instance, results for the same release scenarios for small locations such as bays are very different than in open sea regions.

The results of the present study also show that the inclusion of a wide set of radionuclides can be very important for the radioecological assessment in comparison with using only Cs-137. For instance, isotopes of plutonium can dominate the doses to biota.

Simulations demonstrate that for some marine organisms (for example crustaceans and mollusks), the concentration of radionuclides in sediment can provide a significant part of the external exposure.

It is also shown that it is impossible to use two approaches for the bio accumulation process at the same time: (i) bio accumulation based on the concentration factor/rate approach and (ii) kinetic modelling of the bioaccumulation process. Simultaneous use of these two approaches provides a wrong description of the bioaccumulation process and concentration of radionuclides in biota, especially during the first period of exposure. In this connection, the correct definition of the kinetic parameters for bioaccumulation process for different radionuclides and biota becomes one of the most important tasks for improvement of the radioecological risk assessment methodology.

6   References

AMAP, 1998. AMAP Assessment Report: Arctic Pollution Issues. Arctic Monitoring and Assessment Programme (AMAP), Oslo, Norway. xii+859 pp.

Antipov S. V., Bilashenko V. P., Vysotskii V. L., Kalantarov V. E., Kobrinskii M. N., Sarkisov A. A., Sotnikov V. A., Shvedov P. A., Ibraev R. A., and Sarkisyan A. S., 2015. Prediction and evaluation of the radioecological consequences of a hypothetical accident on the sunken nuclear submarine b-159 in the Barents Sea. Translated from Atomnaya Énergiya, Vol. 119, No. 2, pp. 106–113, August, 2015. DOI 10.1007/s10512-015-0039-x.

Beresford, N.A., Beaugelin-Seiller, K., Wells, C., Vives-Lynch, S., Vives i Batlle, J., Wood, M.D., Tagami, K., Real, A., Burgos, J., Fesenko, S., Cujic, M., Kryshev, A., Pachal, N., Su, B.S., Barnett, C.L., Uchida, S., Hinton, T., Mihalík, J., Stark, K., Willrodt, C., Chaplow, J., 2015. A Database of Radionuclide Biological Half-life Values for Wildlife. NERC-Environmental Information Data Centre. http://doi.org/10.5285/b95c2ea7-47d2-4816-b942-68779c59bc4d.

Bergsten, C., 2003. Fish and Game Study, Part B. The Consumption of Foodsthat may be Important when Assessing the Dietary Intake of Mercury, Cadmium and PCB/ dioxins, with a Focus on Population Groups Living on the Coast and in the Inland of Norway. Norwegian Food Safety Authority, Oslo (in Norwegian).

Bezhenar R., Jung K. T., Maderich V., Willemsen S., Govert de With, F. Qiao (2016). Transfer of radiocaesium from contaminated bottom sediments to marine organisms through benthic food chain in post-Fukushima and post-Chernobyl periods. Biogeosciences, 13, 3021-3034, 2016, http://www.biogeosciences.net/13/3021/2016/, doi:10.5194/bg-13-3021-2016

Brown J., Børretzen P., Dowdall M., Sazykina T., and Kryshev I., 2004. The derivation of transfer parameters in the assessment of radiological impacts on Arctic marine biota. Arctic, 57, No. 3, 279-289.

Brown, J.E. & Hosseini, A., 2019. 'Task 3.3 - Prioritization based on radiological hazards'. Feasibility study INSC/2013/ MC.04/13 Report for Feasibility Study and Preparation for the Implementation of an Action Plan Concerning the Safe and Secure Management/Disposal of Sunken Radioactive Objects in the Arctic Sea; Report to: Directorate General for International Cooperation and Development – Europeaid.

CAC, 2006. Codex Alimentarius Commission: Joint FAO/WHO Food Standards Programme. Appendix XXXI. ftp://ftp.fao.org/codex/Alinorm06/al29_41e.pdf (09.01.07)

CEC, 1990. The Radiological Exposure of the Population of the European Community from Radioactivity in North European Marine Waters. Project 'Marina'. Commission of the European Communities, Bruxelles. EUR 12483.

EC, 2000. The radiological exposure of the population of the European Community to radioactivity in the Baltic Sea, Marina-Balt Project. European Commission, Luxembourg, EUR 19200.

EC, 1994. The Radiological Exposure of the Population of the European Community from Radioactivity in the Mediterranean Sea. Project ''MARINA-Med''. In: Radiation Protection Series 69, EC XI-094/93.

ERICA assessment tools, 2019, http://erica-tool.com/erica/

Eriksen E, Prozorkevich D, Trofimov A, Howell D, 2012. Biomass of Scyphozoan Jellyfish, and Its Spatial Association with 0-Group Fish in the Barents Sea. PLoS ONE 7(3): e33050. doi:10.1371/journal.pone.0033050.

Fall J., Ciannelli L., Skaret G., Johannesen E., 2018. Seasonal dynamics of spatial distributions and overlap between Northeast Arctic cod (Gadus morhua) and capelin (Mallotus villosus) in the Barents Sea. PLOS ONE, https://doi.org/10.1371/journal.pone.0205921 October 16, 2018

Fievet B., Plet D., 2003.Estimating biologicalhalf-lifes of radionuclides in marine compartments from environmental time-series measurements. Journal of Environmental Radioactivity, 65, 91–107.

Fiocchi, A., Assa'ad, A., Bahna, S., 2006. Food allergy and the introduction of solid foods to infants: a consensus document. Adverse Reactions to Foods Committee, American College of Allergy, Asthma and Immunology. Annals of Allergy, Asthma and Immunology, 2006 Jul; 97(1):10–20; quiz 21, 77.

HELCOM, 1995. Radioactivity in the Baltic Sea 1984-1991. Baltic Sea Environment Proceedings 61, 182 pp.

Heling R., Koziy I., Bulgakov V., 2002. On the dynamic uptake model developed for the uptake of radionuclides in marine organisms for the POSEIDON-R model system. Radioprotection 37 (C1), 833-838.

Hosseini, A., Amundsen, I., Bartnicki, J., Brown, J.E., Dowdall, M., Dyve, J.E., Karcher, M., Kauker, F., Klein, H., Lind, O.C., Salbu, B., Schnur, R., Standring, W., (2016). Environmental Modelling and Radiological Impact Assessment Associated with Hypothetical Accident Scenarios for the Nuclear Submarine K-27. StrålevernRapport 2016:8. Statens strålevern, Østerås, Norway.

Hosseini, A., Amundsen, I., Brown, J.E., Dowdall, M., Dyve, J.E., Klein H. (2017). Radiological impact assessment for hypothetical accident scenarios involving the Russian nuclear submarine K-159. StrålevernRapport 2017:12. Østerås: Statens strålevern, 2017.

Hosseini, A., Amundsen, I., Brown, J.E., Dowdall, M., Standring W. (2015). Inventory and source term evaluation on the dumped nuclear submarine K-27. StrålevernRapport 2015:06. Østerås: Statens strålevern, 2015.

IAEA, 2014. Handbook of parameter values for the prediction of radionuclide transfer to wildlife. Technical report series 479. Vienna: IAEA, 2014.

IAEA (1998). Radiological conditions of the Western Kara Sea: assessment of the radiological impact of the dumping of radioactive waste ion the Arctic Seas. Radiological assessment reports series 4. Vienna: IAEA, 1998.

IAEA, 2004. Sediment Distribution Coefficients and Concentration Factors for Biota in the Marine Environment. In: IAEA Technical Reports Series No. 422. International Atomic Energy Agency, IAEA, Vienna.

IASAP, 2003. Modelling of the radiological impact of radioactive waste dumping in the Arctic Seas. IAEA-TECDOC-1330. Vienna: International Atomic Energy Agency, IAEA.

Ibraev R. A., Khabeev R. N., and Ushakov K. V., 2012. Eddy-resolving 1/10° model of the oceans, Izv. Ross. Akad. Nauk, Fiz. Atm. Okeana, No. 48(1), 45–55.

ICRP (2008). Environmental protection: the concept and use of reference animals and plants. ICRP publication 108. Annals of the ICRP 2008; 38(4-6).

Ingvaldsen R. B. & Gjøsæter H., 2013. Responses in spatial distribution of Barents Sea capelin to changes in stock size, ocean temperature and ice cover, Marine Biology Research, 9:9, 867-877, DOI: 10.1080/17451000.2013.775450, https://doi.org/10.1080/17451000.2013.775450.

Iosjpe M., 2006. Environmental Modelling: Modified Approach for Compartmental Models. In: Radionuclides in the Environment. Edd. P.P. Povinec, J.A. Sanchez-Cabeza. Radioactivity in the Environment, vol. 8, Series Editor: M.S. Baxter, 2006, 463-476.

Iosjpe M., 2011. A sensitivity analysis of the parameters controlling water-sediment interactions in the coastal zone: Consequences to man and environment, Journal of Marine Systems 88 (2011), 82-89.

Iosjpe M., Brown J. & Strand P.. 2002. Modified Approach for Box Modelling of Radiological Consequences from Releases into Marine Environment, Journal of Environmental Radioactivity, Vol. 60, No 1-2, 91-103.

Iosjpe M., Isaksson M., Joensen H.P., Jonsson G., Logemann K., Roos P., Suolanen V., Thomas R., 2016. Effects of dynamic behaviour of Nordic marine environment to radioecological assessments, 15 Febr 2016, ISBN: ISBN 978-87-7893-442-0, http://www.nks.org/en/nks_reports/view_document.htm?id=111010213400466

Iosjpe M., M. Karcher, J. Gwynn, I. Harms, R. Gerdes and F. Kauker, 2009. Improvement of the dose assessment tools on the basis of dispersion of the 99Tc in the Nordic Seas and the Arctic Ocean. Radioprotection, vol. 44, no 5, 531-536.

Iosjpe M., O. Reistad, I.B. Amundsen, 2009. Radioecological consequences of a potential accident during transport of spent nuclear fuel along an Arctic coastline. Journal of Environmental Radioactivity 100 (2009) 184–191.

Iosjpe M. and Liland A., 2012. Evaluation of environmental sensitivity of the marine regions. Journal of Environmental Radioactivity 108 (2012) 2-8.

Karcher M.J. and Harms I.H., 2000. Estimation of water and ice fluxes in the Arctic for an improved box structure of the NRPA box model. In: Iosjpe M. (Ed.): Transport and fate of contaminants in the Northern Seas, NRPA, 2000.

Karcher, M., Hosseini, A., Schnur, R., Kauker, F., Brown, J.E., Dowdall, M., Strand, P. (2017). Modelling dispersal of radioactive contaminants in Arctic waters as a result of potential recovery operations on the dumped submarine K-27. Marine Pollution Bulletin 116 (1-2), 385-394.

Keum D.-K., Jin L., Kim B.-H., Lim K.-M., Choi Y.-H., 2015. A dynamic model to estimate the activity concentration and whole body dose rate of marine biota as conswquences of a nuclear accident. . Journal of Environmental Radioactivity, 140, 84-94.

Kull, I., Bergstroöm, A., Lilja, G., Pershagen, G., Wickman, M., 2006. Fish consumption during the first year of life and development of allergic diseases during childhood. Allergy 61 (8), 1009–1015.

Maderch V., Bezhenar R., Heling R., G. de With, Jung K.T., Myoung J.G., Cho Y.-K., Qiao F., Robertson L., 2013. Regional long-term model of radioactivity dispersion and fate in the Fukushima Dai-ichi accident. Journal of Environmental Radioactivity 2013, www.elsevier.com/locate/jenvrad

Periánez R., Bezhenar R., Brovchenko I., Duffa C., Iosjpe M., Jung K.T., Kobayashi T., Lamego F., Maderich V., Min B.I., Nies H., Osvath I., Outola I., Psaltaki M., Suh K.S., G. de With, 2016. Modelling of marine radionuclide dispersion in IAEA MODARIA program: lessons learnt from the Baltic Sea and Fukushima scenarios. The science of the total environment, vol. 569-570, 594-602.

Periáñez R., Bezhenar R., Brovchenko I., Cuffa C., Iosjpe M., Jung K.T., Kobayashi T., Lamego F., Maderich V., Min B.I., Nies H., Osvath I., Outola I., Psaltaki M., Suh K.S. and G. de With, 2016a. A comparison of radionuclide dispersion model performances for the Baltic Sea and Fukushima releases in the Pacific Ocean. Radioprotection, 51 (HS2), S149-S151

PREPARE, 2015. Design document for POSEIDON model integration. Deliverable D 5.2, PREPARE(WP5)-(1)-01.

Reistad O., 2008. Analyzing Russian naval nuclear safety and security by measuring and modeling reactor and fuel inventory and accidental releases. Doctoral thesis at NTNU, 2008:14.

Sarkisyan A. S., Ibrayev R. A., and. Iakovlev N. G, 2010. High resolution and four-dimensional analysis as a prospect for ocean Modeling, Rus. J. Numer. Anal. Math. Model., No. 25(5), 477–496.

Cazykina T., 2003. Radioactivity in aquatic biota. Chapter 7. In: Scott, E.M. (Ed.), Modelling Radioactivity in the Environment, 201-219.

Thomann R.V., 1981. Equilibrium model of fate of microcontaminants in diverse aquatic food-chains. Canadian Journal of Fisheries and Aquatic Sciences 38:280-296.

UNSCEAR, 2008. United Nations Scientific Committee on the Effects of Atomic Energy. Sources and Effects of Ionizing Radiation. 2008 Report to the General Assembly, with Scientific Annexes. Volume I. New York: United Nations, 2010. Available from: http://www.unscear.org/docs/reports/2008/09-86753_Report_2008_GA_Report_corr2.pdf

Vives i Batlle J., Beresford N.A., Beaugelin-Seiller K., Bezhenar R., Brown J., Cheng J.-J., Ćujić M., Dragović S., Duffa C., Fiévet B., K.T., Kamboj S., Keum D.-K., Kryshev A., LePoire D., Maderich V., Min B.-I., Periáñez R., Sazykina T., Suh K.-S., Yu C., Wang C., Helling R. 2016. Inter-comparison of dynamic models for radionuclide transfer to marine biota in a Fokushima accident scenario. Journal of Environmental Radioactivity 153, 31-50.

Vives i Batlle J., Wilson R.C., Watts S.J., Jones S.R., McDonald P., Vives-Lynch S., 2008. Dynamic model for assessment of radiological exposure to marine biota. Journal of Environmental Radioactivity 99, 1711-1730.

White Book-2000, 2005. Technological radionuclides in the seas surrounding Russia, IzdAT, Moscow, p. 624.

Yefimov E., 1994. Radionuclides composition, characteristics of shielding barriers and analysis of week points of the dumped reactors of nuclear submarine N 601, Working material of the International Arctic Seas assessment project IASAP, IAEA-IASAP-6, Vienna.

IIIIIII DSA

Norwegian Radiation and
Nuclear Safety Authority